Binaural Sound Reproduction via Distributed Loudspeaker Systems

Diplomarbeit

durchgeführt von

Martin TESCHL

Institut für Elektronische Musik

der Universität für Musik und darstellende Kunst Graz

durchgeführt am

Institute of Sound and Vibration Research

University of Southampton, UK

Betreuer:
Prof. Philip A. Nelson
Takashi Takeuchi
Prof. Robert Höldrich

Graz, im Dezember 2000

Diese Diplomarbeit ist meinen Eltern, Franz und Maria Teschl, gewidmet.

This thesis is dedicated to my parents.

Abstract

The basic principle of binaural sound reproduction technique is to reconstruct the same sound pressures at a listener's eardrums that would have caused there by a real sound source to be simulated. Consequently, the listener cannot distinguish between the real sound source and the generated virtual sound source. If a pair of loudspeakers is used, the appropriate ear signals are delivered to the listener by inverting the transmission paths between the two loudspeakers and the two ears. This process, known as "crosstalk cancellation", can be considered as an inversion of a $[2 \times 2]$ matrix of transfer functions.

Previous work undertaken in this area was concentrated on the use of a conventional stereo set-up where the loudspeakers span an angle of 60° as seen from the listener. As opposed to a stereo set-up, by using two closely spaced loudspeakers, the performance had proven more robust with respect to misalignment or movement of the listener's head. However, one disadvantage of this approach is the source strengths required for the crosstalk cancellation at low frequencies. In terms of matrix algebra, the crosstalk cancellation problem is said to be "ill-conditioned" at these frequencies.

Based on a free-field model of the problem, it can be shown that ill-conditioning depends on frequency and the loudspeaker span of the system, respectively. For instance, for a smaller span the system inversion is ill-conditioned at low frequencies, whereas for larger source spans the conditioning is worse at higher frequencies. This connection resulted in the idea to vary the source span as a function of frequency in order to maintain the best possible conditioning over the whole frequency range. A practical solution of this new approach is to use multiple pairs of loudspeakers for each frequency range with corresponding source spans in order to eventually cover the whole audible frequency range.

This diploma thesis will discuss the potential for such an approach. Theory, practical implementation, and testing of such systems will be described in detail. Many sound localisation experiments were conducted in order to subjectively validate the system's performance. Results show a significant improvement, in particular with respect to azimuth localisation for virtual images well to the sides.

Zusammenfassung

Das Grundprinzip binauraler Schallwiedergabetechnik ist, denselben Schalldruck am Trommelfell eines Hörers zu rekonstruieren, der dort von einer realen Schallquelle verursacht werden würde. Als Folge kann der Hörer nicht mehr zwischen der realen und der simulierten, virtuellen Schallquelle unterscheiden. Bei der Verwendung von zwei Lautsprechern, müssen die Übertragungsfunktionen zwischen den beiden Lautsprechern und den beiden Ohren invertiert werden, um die entsprechenden Signale korrekt an die Ohren des Hörers zu liefern. Dieser Vorgang, der allgemein als Übersprechkompensation bezeichnet wird, kann als eine Inversion einer $[2 \times 2]$ Matrix von Übertragungsfunktionen betrachtet werden.
Frühere Arbeiten auf diesem Gebiet haben sich auf die Verwendung eines konventionellen Stereo Systems konzentriert, wo die beiden Lautsprecher einen Winkel von 60° aufspannen. Im Vergleich dazu hat sich eine Anordnung der beiden Lautsprecher sehr nahe aneinander als robuster in Bezug auf Kopfbewegung des Hörers bzw. auf ungenaue Positionierung herausgestellt. Ein Nachteil dieser Methode ist jedoch, dass die Übersprechkompensation sehr hohe Lautsprechersignale im Niederfrequenzbereich erfordert. Inverse Probleme dieser Art werden in der Matrixalgebra als eine "schlecht gestellte Aufgabe" bezeichnet, oder man sagt, die Aufgabe ist "schlecht konditioniert".
Anhand eines Freifeldmodells des Kompensationsproblems kann gezeigt werden, dass schlechte Konditionierung neben der Frequenz auch von der Geometrie der Lautsprecheranordnung (vom aufgespannten Winkel) abhängig ist. So ist die Systeminversion mit kleineren Winkeln im Niederfrequenzbereich schlecht konditioniert, wohingegen größere Aufspannwinkel schlechtere Konditionierung für hohe Frequenzen ergeben. Dieser Zusammenhang hat zur Idee geführt, den Aufspannwinkel abhängig von der Frequenz zu variieren um so die bestmögliche Konditionierung über den gesamten Frequenzbereich zu sichern. Eine praktische Lösung dafür ist die Verwendung mehrerer Lautsprecherpaare für verschiedene Frequenzbereiche, die jeweils unter entsprechenden Winkeln angeordnet werden um letztlich den gesamten hörbaren Frequenzbereich abzudecken.
Diese Diplomarbeit diskutiert die generelle Machbarkeit und Möglichkeiten einer derartigen Methode. Die zugrundeliegende Theorie, die praktische Umsetzung sowie die Erprobung solcher Systeme wird im Detail beschrieben. Resultate von umfassenden Schallokalisierungs-experimenten zeigen eindeutig signifikante Verbesserung, im speziellen hinsichtlich der Azimutlokalisierung für stark seitlich präsentierte virtuelle Schallquellen.

Acknowledgements:

First and foremost, I would like to thank Professor Philip Nelson and Mr. Takashi Takeuchi, my supervisors at the ISVR in Southampton, for their constant encouragement, guidance, enthusiasm, vital help, patience and kindness throughout the progress of this project. I would also like to thank Professor Robert Höldrich, my supervisor in Graz, especially for the helpful discussions concerning the data analysis of the subjective experiments.

I am most grateful to my parents who gave me all the wonderful opportunities in my life and who always support me in everything I do.

Contents

Chapter 1
Introduction

1.1 Introduction and Literature Review

Basically, any 3D sound reproduction system attempts to give a listener a sense of ”space”, and hence must somehow make the listener believe that sound is coming from a position where no real sound source exists in fact. This approach is usually referred to as *virtual source imaging*.

A considerable part of current research into virtual source imaging systems relies heavily on *binaural technology*. This technique can be considered as the art of ”fooling” the human auditory mechanism for sound localization. It is based on the sensible engineering principle that if a sound reproduction system is able to generate the same sound pressures at the listener’s eardrums as would have been reproduced there by a real sound source, then the listener should not be able to tell the difference between the virtual image and the real sound source. In order to determine these *binaural signals*, or *”target” signals*, it is necessary to know how the listener’s *torso* (upper body), head and *pinnae* (outer ears) modify the incoming sound waves according to a specific position of the sound source. This information can be obtained by means of measurements on “*dummy heads*” or human subjects [Kleiner, 1978; Møller *et al*. 1997]. The results of such measurements are usually called *Head-Related Transfer Functions*, or just *HRTFs*. Any synthetic binaural signal can be created by convolving (filtering) a monophonic sound signal with the appropriate pair of HRTFs, a procedure referred to as *binaural synthesis*.

In order to correctly deliver the binaural signal to a listener using transducers, the signal must be equalized to compensate for the transmission paths from the transducers to the

eardrums. In terms of control theory, these transmission paths are usually referred to as the *"plant"*, which denotes the physical system to be controlled.

Headphones are often used for binaural audio because they ensure excellent channel separation, they can isolate the listener from external sounds and room reverberation, and the transmission paths from the transducers to the ears are easily equalized. An alternative to headphones is the use of conventional stereo loudspeakers placed in front of the listener. In this case, the transmission path equalization is accomplished by inverting the [2 × 2] matrix of transfer functions between the two loudspeakers and the two ears. This procedure is called *crosstalk cancellation* since it involves the acoustical cancellation of the unwanted crosstalk from each speaker to the opposite ear. Usually, the term *"generalized"* is added to characterize crosstalk cancellation systems that account for the influence of the listener's head by allowing realistic HRTFs to be included. Thus, the purpose of *generalized crosstalk cancellation* is to be able to produce a specified desired signal very accurately at one ear of the listener, while nothing is heard at the other ear. Once this can be achieved, any pair of binaural signals can be produced at the ears of a listener.

The technique of crosstalk cancellation was first introduced by Bauer [1961], and put into practice by Schroeder and Atal [1963; Atal *et al*., 1966]. Later, it was subjectively verified by Damaske [1971] and Schroeder [1975] with good results even for phantom images positioned outside the angle spanned by the loudspeakers. The method, using analog techniques, was based on a free-field model that did not account for the presence of the listener in the sound field. Since then, more sophisticated methods, some based on digital signal processing techniques, have been developed for generalized crosstalk cancellation, such as by Cooper and Bauck [1989]; Bauck and Cooper [1996], Kirkeby *et al*. [1996a], Nelson *et al.* [1992, 1995], Nelson and Orduña-Bustamente [1996], Griesinger [1989], and Møller [1989].

With a few notable exceptions [Bauck and Cooper, 1996; Heegaard, 1992], most researchers have concentrated on systems using the traditional stereo loudspeaker arrangements spanning an angle of typically 60 degrees as seen by the listener. A fundamental problem that one faces when using relatively widely spaced loudspeakers is that the listener's ears are required to be within a rather small region (*"equalization zone"*) which is under the control of the system. Misalignment of the head results in a change of the HRTFs and thus in an inaccurate synthesis of the binaural signals. Consequently, the directional

information associated with the acoustic signals is inaccurately reproduced. In addition, the digital signal processing tends to give the reproduced sound an unpleasant *"coloration"*.

However, a system using two closely spaced loudspeakers turned out to be surprisingly robust with respect to head movement [Takeuchi *et al*., 1997], and it also avoids coloration of the reproduced sound. The size of the *equalization zone* around the listener's head is increased significantly without any noticeable reduction in performance. Kirkeby *et al.* [1996b; 1997] use the term *"Stereo Dipole"* to describe such a virtual source imaging system since the inputs to the two closely spaced loudspeakers are close to being exactly out of phase over a wide frequency range [Kirkeby and Nelson, 1997]. Consequently, they reproduce a sound field very similar to that generated by a point dipole source. Strictly speaking, the reproduced field rather approximates that field generated by a combination of a point dipole and a point monopole source at the same position [Nelson *et al*., 1997; Bauck and Cooper, 1996]. Thus, it would be more accurate to use the term "stereo monopole-dipole".

1.2 Objectives

In practice, crosstalk-cancelling systems suffer from a variety of problems apart from the fact that they are fairly sensitive to the position of the listener's head. First of all is that the *multi-channel system inversion* involved with crosstalk-cancellation requires amplification of the signal at certain frequencies and attenuation of the signal at other frequencies. The maximum required amplification yields the maximum output signal of the system, which must be within the range of the overall system in order to avoid clipping of the signals. Thus, the maximum amplification due to the system inversion directly results in *loss of dynamic range*.

The *stability* or *robustness* of the system inversion is another important problem. The electro-acoustic transfer functions of the transmission path between loudspeakers and the listener's ears show very small magnitudes at certain frequencies. These frequencies are usually referred as being *"ill-conditioned"* because the inversion of their magnitudes results in very high values [Wilkinson, 1965]. Thus, a small change (a small error) in the transfer

function (e.g. due to a slight movement of the listener) causes a large change in the solution for the inverse filter around ill-conditioned frequencies. In order to avoid this, "*regularisation*" is often used in the design of practical filters for multi-channel system inversion [Press *et al*., 1992; Kirkeby *et al*., 1996a]. In principle, the technique of regularisation allows to reduce both dynamic range loss caused by the system inversion, and sensitivity to small changes around ill-conditioned frequencies. This is done by means of penalising the excess amplification due to the inversion, but this in turn results in poor control performance around ill-conditioned frequencies. In other words, regularisation is a matter of finding an appropriate trade-off between allowed dynamic range loss, limiting large output magnitudes around ill-conditioned frequencies, and obtaining a desired control performance in terms of crosstalk cancellation.

In general, the problems of dynamic range loss and ill-conditioning depend on frequency and on the positions of the reproduction loudspeakers relative to the ears. For instance, as the loudspeaker span is reduced, it is much harder to achieve efficient crosstalk cancellation at low frequencies, and, in addition, an increasing amount of low-frequency energy is required in order to create a virtual source image at a position well outside the angles spanned by the two loudspeakers [Kirkeby *et al*., 1997; 1998].

More specified investigations show that a small loudspeaker span creates a system that is "well-behaving" within a wide region in the middle-band frequencies, whereas a large loudspeaker span works better at low frequencies [Takeuchi and Nelson, 2000a; 2000b]. In fact, these results represent the main feature as well as the main drawback of the "Stereo-Dipole" system. Though, using closely spaced loudspeakers greatly widens the equalisation zone in the middle-band frequencies, it compromises the performance at low frequencies considerably. Without any precautions, the inverse filters tend to excessively amplify the ill-conditioned low frequencies, which likely leads to saturation of the audio amplifiers and/or damage of the loudspeakers.

However, if one were able to continuously vary the loudspeaker span as a function of frequency, this problems could be ideally solved. A practical solution for this is to divide the audible frequency range into two or more bands, and hence "discretise" the loudspeaker span. The low frequency band is reproduced through widely spaced loudspeakers while the loudspeakers for the high frequency band are spaced closer together. Although this arrangement uses four or more loudspeakers, it still has to be considered as a two-channel

loudspeaker system. Following this idea, Takeuchi and Nelson [2000a; 2000b] accomplished extensive investigations, based on a free-field model of the problem, in order to find optimal solutions of how to dicretise the audible frequency range and how to distribute the loudspeakers. Eventually, these investigations resulted in the proposal of a new virtual acoustic system, referred to as *"Optimal Source Distribution"* or "*OSD"* system. Thereby, the word "optimal" indicates that the system has to be designed to ensure as well behaviour of the system as possible over a frequency range that is as wide as possible.

The main objective of the present work is to put such a system into practice and investigate its performance. Cross-over filters (low pass, high pass, or band pass) are used in order to distribute the signals of the appropriate frequency range to the appropriate pair of driver units. Other than for the ideal case of theoretical simulations, there are transition regions around the cross-over frequencies where multiple pairs of loudspeakers are contributing significantly to the synthesis of the reproduced binaural signals. This is obvious because an ideal cross-over filter which gives a rectangular window in the frequency domain cannot be realised in practice. Therefore, it is important to ensure the transition regions of the cross-over filters are also within the "well-behaving" range of the applied principle.

If the matrix of transmission paths (the plant matrix) is measured when including the cross-over network, it contains the responses of the cross-over network as well as the interaction between different pairs of loudspeakers. Designing the inverse filter matrix from this plant matrix is obviously the most straightforward among other options, since it automatically compensates for the cross-over network. Alternatively, one can design inverse filter matrices for plants of each pair of driver units separately. It is also possible to obtain the plant matrix by measuring the transmission paths for each single transducer to the ears. In that case, the system is underdetermined and the solution of the inverse filter matrix distributes the signals to the different drivers such that *"least effort"* (i.e., the smallest output) is required [Takeuchi and Nelson, 2000a, 2000b]. Omitting the cross-over filters yields to a conventional multi-channel system, contrary to the "OSD" system which is a multi-way system.

In any case, the cross-over filters can be passive, active, or digital filters. Obviously, if they are digital filters, they can also be included in the same filters which implement the system inversion.

The aim of the present work is to investigate the technical feasibility of those various options, and, as far as possible, to evaluate their advantages and disadvantages. The performance in terms of accuracy of the inverse filtering, gain of dynamic range and crosstalk cancellation is examined by means of physical measurements on the investigated systems. Potential improvement of these parameters would eventually result in accurate virtual source imaging, good signal-to-noise ratio, and sound quality as a general impression. The subjective performance parameters are evaluated by means of extensive sound localisation experiments. The project has been undertaken by the author at the *Institute of Sound and Vibration Research (ISVR)*, University of Southampton, in the time between 1st of March and 31st of August 2000.

1.3 Organisation of this document

The present degree dissertation has 8 chapters. The first following chapters after this introduction will review two important topics relevant to this work. Chapter 2 discusses the human mechanism of sound localisation, and spatial hearing, respectively. In Chapter 3, a general discussion of 3D sound reproduction is addressed, particularly with regard to binaural techniques for virtual sound source imaging. Hereby, the basic idea related to the theory of crosstalk cancellation will be especially emphasised as well as particular features of the "Stereo Dipole" system. Digital signal processing theory concerning the practical design of digital inverse filters for crosstalk cancellation will be considered in Chapter 4. The problems of ill-conditioning and loss of dynamic range will be discussed in detail. In Chapter 5, the "OSD" system will be proposed as a possible solution of the mentioned problems. The basic ideas behind this method will be outlined based on the papers by Takeuchi and Nelson [2000a, 2000b]. Chapter 6 comprises a comprehensive discussion of the practical implementation of the systems, as well as a description of the experimental set-up and measurement procedures. Considerations about the subjective evaluation of the system are addressed in Chapter 7. In particular, the procedure of sound localisation experiments are explained. Finally, Chapter 8 concludes with a summary and discussion of the results of this

study. Areas of future work are suggested.

Chapter 2
Spatial Hearing

2.1 Introduction

As indicated in the first chapter, typical applications of 3D sound systems complement, modify, or replace sound attributes that occur in natural listening situations in order to obtain control on one's spatial perception. This control can not be achieved based on physical attributes only. Psychoacoustic considerations of the human sound localisation also play important roles in analysing, designing, and testing 3D sound systems. In order to manipulate a listener's spatial auditory perception, a thorough understanding of the psychoacoustical phenomena occurring in natural spatial hearing is essential. By modifying the physical parameters associated with those phenomena, the control goal may be achieved.

The important cues used by the human auditory system to localise sound sources in space, are identified by psychoacoustic experiments [Blauert, 1997]. It is widely believed that localisation of sources in the *horizontal plane* (*azimuth localisation*)[1] is due to the differences between the sound waves received at each ear (*interaural differences*). Localisation of sound sources not in the horizontal plane (*elevation localisation*) is strongly influenced by *spectral cues* due to the acoustic filtering of short wavelength sound waves. Human listeners are also capable of estimating the sound source *distance* in addition to azimuth and elevation angles. Interaural, spectral, and distance cues are discussed in Sections 2.3, 2.4, and 2.5, respectively.

When the above mentioned cues are ambiguous, humans usually move their heads (some animals move their ears), so that more (or less) interaural and spectral cues are

[1] See Figure 2.2.1 for the definition of these terms.

introduced, making the localisation task easier. These *dynamic* cues are addressed in Section 2.6.

Room *reverberation* degrades human localisation performance, since the direction of a reflected sound may be confused with the direction of the sound coming directly from the source. However, thanks to the *precedence effect*, human listeners are still able to localise sounds in reverberant environments. The precedence effect as well as physical and perceptual aspects of room reverberation are discussed in Sections 2.7 and 2.8, respectively.

All physical parameters associated with the localisation cues that occur in natural listening situations are embedded in the pair of acoustic transmissions from the source to each of the listener's eardrums. As mentioned in Chapter 1, these acoustic transmissions are usually referred to as the *Head-Related Transfer Function* (*HRTF*) pair, and can be measured and stored in the form of digital filters. The basic principle of modern 3D sound systems based on *binaural technology* [Begault, 1994; Duda, 1996; Gardner, 1997; Wightman and Kistler, 1989a] is to make use of this HRTF information in order to eventually control a listener's spatial perception. A thorough discussion of the physical properties of HRTFs follows in Section 2.9.

2.2 Head-related Coordinate Systems

References to position in connection with spatial hearing are usually made in terms of a head-related system of coordinates [Blauert, 1997]. This system is practically constant relative to the position of the listener's head and hence relative to the position of the ears. In the following discussion throughout this document, the systems shown in Figure 2.2.1 will be assumed. Both systems are chosen so that the origin is at the centre point between the listener's ears (the *interaural axis*). The +*x*-axis passes through the right ear, the +*y*-axis points straight ahead, and the +*z*-axis is vertical. This defines the three standard planes, the *xy* or *horizontal plane*, the *xz* or *frontal plane*, and the *yz* denotes the *median plane*.

Obviously, the horizontal plane defines up/down separation, the frontal plane defines front/back separation, and the median plane defines right/left separation.

Spherical coordinate systems are used here since the human head is approximately spherical. Hereby the standard coordinates are the *azimuth* angle φ, the *elevation* angle δ, and the *range r*. Unfortunately, these coordinates can be defined in different ways.

- The *vertical-polar coordinate system*, as shown in Figure 2.2.1[a], is the most popular and probably also the more natural one. Per definition, the azimuth angle is first measured from the median plane to a vertical plane containing the *z*-axis and the object (the sound source). The elevation angle is then the angle from the horizontal plane to the object on that plane. With this choice, surfaces of constant azimuth are planes through the z-axis, and surfaces of constant elevation are cones concentric about the *z*-axis.

- An important alternative is the *interaural-polar coordinate system*, as shown in Figure 2.2.1[b]. Here, the elevation angle is first measured as the angle from the horizontal plane to a plane containing the *x*-axis and the object. The azimuth angle is then measured as the angle from the median plane to the object on that plane. With this choice, surfaces of constant elevation are planes through the interaural axis, and surfaces of constant azimuth are cones concentric about the interaural axis.

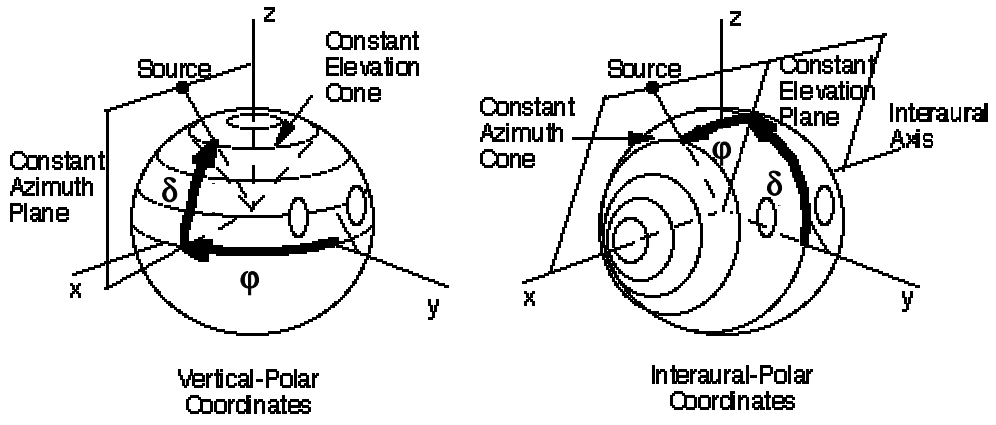

[a] [b]

Figure 2.2.1

Head-related systems of coordinates after Duda [1996].

The vertical-polar system is definitely more convenient for describing sources that are confined to the horizontal plane, since one merely has to specify the azimuth as an angle between −180° and +180°. With the interaural-polar system, the azimuth is always between −90° and +90° and the front/back distinction must be specified by the elevation, which is 0°

for sources in the front horizontal plane, and ±180° for sources in the back. Even though this may appear a bit clumsy, the interaural-polar system makes it significantly simpler to express interaural differences at all elevations.

When using an interaural-polar coordinate system and by holding the azimuth constant, a constant value for the *Interaural Time Difference* (ITD) is achieved. Thus, there is a simple one-to-one correspondence between the ITD and the *cone of constant azimuth*, which is usually called the "*cone of confusion*". This is not the case for the vertical-polar system. A detailed description of these terms is given in the following Section 2.3. Depending on whether azimuth or elevation was considered at a time, both coordinate systems were applied for subjective experiments and the analysis of the results, as discussed in Chapter 7 and Chapter 8, respectively.

2.3 Interaural Cues

In natural listening situations, the difference between sound waves received at the listener's left and right ears is an important cue used by the human auditory system to estimate the sound source position in space. These difference cues, referred to as *interaural* or *binaural* cues are best explained using the far field anechoic listening situation shown in Figure 2.3.1. A sound signal emitted from a source *S* located in the horizontal plane at azimuth angle φ and distance *r* from the centre of the listener's head travels to the listener's right (*ipsilateral*) and left (*contralateral*)[1] ears through path *SR* and *SL*, respectively. Since *SR* in this example is shorter than *SL*, a sound wave reaches the right ear before the left ear. This difference in arrival time is referred to as the *Interaural Time Difference* (ITD). Assuming a plane wave, the ITD as a function of the azimuth angle φ is given by

$$ITD = \frac{a}{c}(\varphi + \sin\varphi), \qquad -90° \le \varphi \le \varphi + 90°. \tag{2.3.1}$$

[1] The term *ipsilateral* refers to the ear which is closer to the sound source, whereas the term *contralateral* indicates the ear at the further distance to the sound source.

The ITD is zero when the source is at azimuth zero (that is in the median plane), and is a maximum at azimuth ±90°. This represents a difference of arrival time of about 0,7 ms for a typical-size human head [Blauert, 1997]. ITD represents a powerful and dominating cue at frequencies below about 1.5 kHz. At higher frequencies, the ITD represents an ambiguous cue since it corresponds to a shift of many cycles of the incident sound wave. For complex sound waves, the ITD of the envelope at high frequencies, which is referred to as the *Interaural Envelope Difference* (IED), is perceived.

On the other hand, the human head forms an obstacle for incident sound waves. This leads to a level difference between the two ears, known as the *Interaural Intensity Difference* (IID). Besides being dependent on azimuth angle, the IID is highly dependent on the frequency of the incident sound wave. At low frequencies, the wavelength is larger than the listener's head and the sound wave is diffracted around the head to reach the contralateral ear without noticeable attenuation. As the frequency increases, the head forms a bigger obstacle for the sound wave and the level at the contralateral ear decreases. This effect is known as the *head-shadow effect*. The IID is an effective cue in the frequency range above 1,5 kHz, and thus, forms a complementary cue to the ITD. Together, the ITD and IID eventually cover the whole audible frequency range.

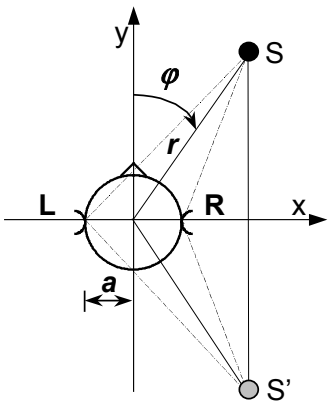

Figure 2.3.1

A sound source *S* and its image *S'* about the interaural axis introduce maximally similar interaural cues.

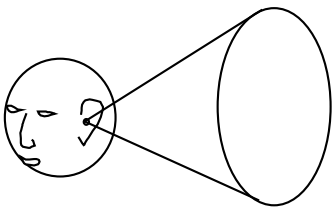

Figure 2.3.2

The cone of confusion.

A sound source at azimuth angle φ and its image about the interaural axis at azimuth 180°-φ, as sown in Figure 2.3.1, produce the same ITD and IID cues at the listener's ears. In fact, identical values of ITD and IID can be calculated for any sound source in space anywhere on a conical surface extending out from the

ear. In the literature, this surface is called the *cone of confusion* (Figure 2.3.2). In practice, ITDs and IIDs would never be completely identical unless a spherical head is assumed, with effects of asymmetry, features of the face, and the pinnae disregarded. However, when ITD and IID cues are maximally similar between two locations, such as on the cone of confusion, a potential for confusion between the positions exists in the absence of a spatial cue other than ITD and IID. This potential explains the often reported phenomenon of *front-back reversals* [Blauert, 1997; Begault, 1994], which can be considered as a special case, in the horizontal plane, of the general phenomenon of the cones of confusion.

The human ability to disambiguate sources from front to back or from above and below, in cases where ITD and IID would not supply this information, has brought about hypotheses regarding the role of *spectral cues* on localisation. These are discussed in the following section.

2.4 Spectral Cues

The primary cues used by the human auditory system are often said to be *monaural*. This is in contrast with the *interaural* or *binaural* cues used for azimuth localisation. Spectral cues are due to reflections of short wavelength sound waves off the listener's upper body (*torso*) and off the outer ears (*pinnae*) [Blauert, 1997]. Thus, torso and pinna act as an *acoustical filter* on the incoming sound. The main contribution to this filtering is due to the pinna with its irregular shape and resonant cavities. Sound waves reflected off the pinna interfere with the direct sound entering the ear canal constructively at some frequencies, and destructively at other frequencies as shown in Figure 2.4.1. This leads to *spectral peaks* at frequencies where *constructive interference* occurs, and *spectral dips* at frequencies where *destructive interference* takes place.

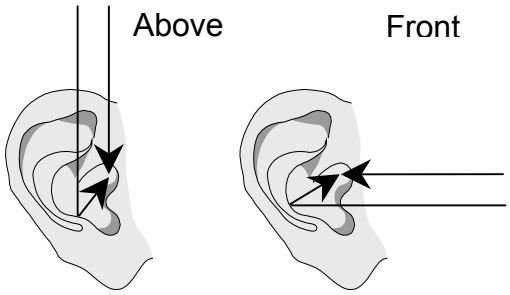

Figure 2.4.1

Schematic diagram of high frequency reflections off the pinna causing constructive and destructive interferences with the direct sound wave.

The frequencies at which those spectral peaks and dips appear, as well as the magnitude of these features, are highly dependent on the direction of the incoming sound wave. Spectral dips appear to be of more interest, since they are often more pronounced than the peaks. The first spectral dip, known as the *pinna notch* is believed to be the major cue for *elevation* localisation.

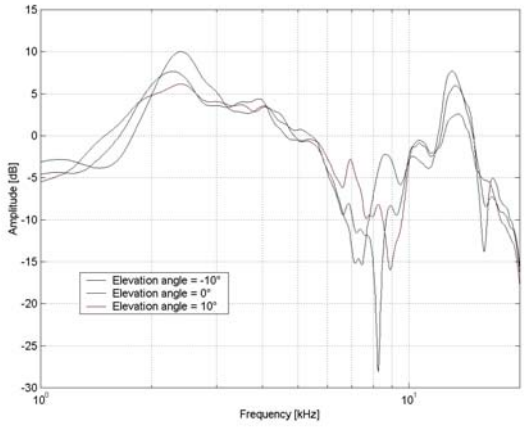

Figure 2.4.2

Measured pinna responses for sources in the median plane at elevation angles δ of −10°, 0°, and +10°.

The frequency at which the pinna notch appears changes from about 6 to 12 kHz as the elevation angle changes from −40° to 60° [Gardner, 1997] (see also Section 2.9). This is

shown in Figure 2.4.2 for the transfer functions measured for a *KEMAR*[1] dummy head with the sound source in the median plane at elevation angles −10°, 0°, and +10°[2].

Basically, from familiarity with their own pinna responses, human listeners are able to use spectral cues to estimate the sound source position. Since spectral cues are mainly due to high frequency reflections, slight changes in the pinna shape may lead to significant changes in its frequency response. Therefore, spectral cues vary significantly among people due to differences in pinna sizes and fine geometrical structure. In the literature, the above described spectral response due to the human pinnae and torso is usually referred to as a *Head Related Transfer Function* (HRTF). The use of HRTFs is typically featured as the key component of any modern 3D sound system, from either direct measurement or modelling. Therefore, the properties of HRTFs as well as their role in human sound localisation will be discussed in more detail in Section 2.9.

2.5 Distance Cues

Many phenomena have been noticed to influence the estimation of the distance of a sound source by the human auditory system. Loudness and the ratio of direct and reverberant energy are believed to be the most effective in influencing distance perception.

In the absence of other acoustic cues, the *intensity* of a sound source (and its interpretation as *loudness*) is the primary cue used by a listener to estimate distance. Loudness cues stem from the fact that the sound pressure in the far field decreases with increasing distance to the sound source. Therefore, nearby sound sources are perceived louder than distant sources emitting the same acoustic energy. The ratio of the sound intensity of two sources at distances r_1 and r_2 from a listener's ear is given by

$$\frac{I_1}{I_2} = \frac{r_2^2}{r_1^2}, \tag{2.5.1}$$

[1] KEMAR stands for Knowles Electronics Manikin for Auditory Research.

[2] Data from `ftp://sound.media.mit.edu/pub/Data/KEMAR`. See also [Gardner and Martin, 1994] for a description of the measurement procedure.

which is known as the *inverse square law* [Begault, 1994]. Thus, a distance doubling decreases the sound intensity at the listener's ear by 6 dB.

However, just playing a sound at a low volume level will not, in itself, make it seem to be far away. This is obvious since the energy received at the listener's ears depends not only upon the distance of the sound source but is also proportional to the energy emitted by the source. Thus, in order to use loudness as a cue to distance, listeners must also know something about the characteristics of a particular sound [Begault, 1994]. In the case of human speech, previous experience usually provides familiarity with the different quality of sound associated with whispering, normal talking, and shouting, no matter what sound level. This combination of loudness and knowledge of the source provides useful information for distance judgements. Thus, auditory distance is basically learned from a lifetime of visual-aural observations, correlating the physical displacement of sound sources with corresponding increases or decreases in intensity and loudness, respectively.

Another restriction on the loudness cue is that it is valid only under anechoic conditions, since in a reverberant environment the sound distribution is dependent on the reverberation characteristics of the enclosed space. For instance, in a reverberant room, the sound field beyond the *reverberation distance* may be considered diffuse, and theoretically independent on the distance from the source (see Section 2.8). Thus, in the case of a reverberant context, the change in the proportion of reflected to direct sound energy, known as the *R/D ratio*, acts as a stronger cue for distance than intensity scaling. Close to the sound source, the ratio is very large, while at long distances it is rather small. Reverberation and diffuse field characteristics as well as sound localisation in reverberant environment are discussed in more detail in Section 2.8.

A *binaural cue* to distance, known as the *motion parallax*, refers to the fact that if a listener translates his/her head, the change in azimuth will be dependent on distance [Duda, 1996]. For sources that are very close, a small shift causes a large change in azimuth, while for sources that are distant there is essentially no azimuth change. Moreover, as a sound source gets very close to the head, the IID will increase. This increase becomes noticeable for ranges under about one meter.

Several *spectral cues* which are also believed to contribute to distance estimation of a sound source are described by Blauert [1997] and Begault [1994]. The spectral content of a sound signal is modified as a function of distance by a number of parameters, such as

atmospheric conditions, molecular absorption of the air, the curvature of the wavefront, air humidity and temperature. At large distances in the environment outdoors, even the wind profiles, ground cover, and barriers such as buildings give contribution. However, from a psychoacoustic point of view, all these cues are relatively weak, compared to loudness, familiarity, and reverberation cues.

2.6 Dynamic Cues

In ambiguous listening situations where interaural and spectral cues produce insufficient information to localise the sound source, humans tend to turn their heads in order to minimise (or maximise) the interaural differences; i.e., use the head as a sort of ”pointer” to resolve ambiguity.

Ambiguous interaural cues are introduced at the listener’ ears due to the cone of confusion phenomenon. A sound source at a certain azimuth angle φ to the right of the listener in the horizontal plane introduces maximally similar interaural cues as a source at azimuth angle 180°-φ as mentioned in Section 2.3. A human listener would resolve the ambiguous interaural cues by turning his/her head to the right, since the ambiguous cues still suggest that the source is at the listener’s right. After turning right, if the interaural cues are minimised, the listener would decide that the source is in the front, otherwise if it is maximised, the decision would be that the source is at the back. In general, listeners apparently integrate some combination of the changes in ITD, IID, and movement of spectral notches and peaks that occur with head movement over time, and subsequently use this information to disambiguate, for instance, front imagery from rear imagery.

Although head movements improve the localisation performance in natural hearing, they give rise to great difficulties to synthetic 3D sound systems. Unlike natural spatial hearing, the integration of cues derived from head movement with both stereo loudspeakers and headphones will provide false information for localising a virtual source. With loudspeakers, a distortion of spatial imagery will occur when the head is turned to face the virtual sound source, since the processing to create the illusion depends on a known

orientation of the listener. With headphones, the head movement has no effect on localisation of the sound, a situation that does not correspond to actual circumstances.

Just as moving the head causes dynamic changes for a fixed source, a *moving source* will cause dynamic changes for a fixed head. One of the main cues for a moving source is the D*oppler shift*, which denotes the change in pitch associated with source movement (e.g., a jet plane passing overhead).

Cognitive cues are a large part of the sensation of motion. A monaural speaker, for example, can give the sensation of a speeding automobile on a racetrack, through the transmission of multiple, associative cues from experience.

2.7 The Precedence Effect

Natural sound localisation is affected by the above mentioned cues as well as by numerous other psychoacoustical phenomena. One of those phenomena, the *precedence effect*, that is directly related to localisation in reverberant environments, will be briefly mentioned in this section. The precedence effect, also known as the *law of the first wavefront* [Blauert, 1997], explains an important mechanism of the human auditory system that allows humans to localise sounds in reverberant environments.

When a combination of direct and reflected sounds is heard, the listener does perceive the sound to be coming from the direction of the direct sound, since it arrives first at his/her ears. This is even true when the reflected sound is more intense than the direct sound [Hartmann, 1997]. However, the precedence effect does not totally eliminate the effect of a reflection on sound localisation. Reflections add a sense of spaciousness and loudness to the sound. Experiments with two clicks of equal intensity have shown that if the second click arrives about 1 ms after the first, the two clicks are perceived as an integrated entity. The perceived location of this entity obeys the *summing localisation* regime [Hartmann, 1997]. Within this regime, there is a systematic weighting such that as the delay time increases, the weighting decreases. For delays between 1 and 4 ms, the precedence effect is in operation with its maximum at a delay about 2 ms, where the sound location is perceived to be at the

location of the first click. Finally, in the range between 5 to 10 ms, the sound is perceived as two separate clicks (*echo*) and the precedence effect starts to fail. However, it was noticed that the second click not only contributes to spaciousness but the perceived location is also biased towards the position of the second click. Furthermore, the second sound was found to decrease the accuracy of azimuth and elevation localisation compared to anechoic listening conditions [Begault, 1992 and 1994]. In normal listening situations, sound signals last longer than clicks, and reflections arrive at the listener's ears while the direct signal is still heard. In such situations, the precedence effect operates on the onsets and transients in the two signals.

Furthermore, it was found that the precedence effect for speech signals, better known as the *Haas effect*, has very different time constants than those mentioned above [Hartmann, 1997]. In that case, maximal suppression occurs for a delay between 10 to 20 ms, while speech intelligibility is affected by reflections later than 50 ms.

2.8 Localisation and Reverberation

As indicated in the previous Section 2.7, the fact that human listeners are able to estimate the direction of a sound source in a reverberant environment is basically due to the precedence effect. Of course, this does not mean that reflected sound is not relevant for the sense of human hearing. In fact, in natural listening situations most sound energy will always come from reflections at environmental surfaces. Even out of doors, a significant amount of energy is reflected by the ground and by surrounding structures and vegetation. Indeed, humans subconsciously use this information to estimate sound source distance and recognise *environmental context*. How used (even though not aware) the human hearing is to reverberation, becomes fairly obvious upon entering an anechoic chamber for the first time. Most people are astonished but also get an unpleasant feeling by how much softer and duller everything sounds. However, unless reverberation is severe, the reflections have relatively little effect on the human ability to localise sounds. The basic effects of reverberation and room acoustics will be pointed out in the following.

A very important parameter in room acoustics is the *reverberation time*. The

reverberation time T_{60} is defined as the time it takes for the sound pressure level to decay by 60 dB when a steady state sound source in a room is suddenly turned off. An approximate formula for the reverberation time is

$$T_{60} \approx \frac{V}{6\bar{\beta}S}, \tag{2.8.1}$$

where V is the *room volume* in m^3, $\bar{\beta}$ denotes the average *absorption coefficient* of the room boundaries, and S is the *surface area* of the room in m^2. Since the average absorption coefficient $\bar{\beta}$ is frequency dependent, the reverberation time is also frequency dependent, and is usually given as the average in an octave band.

The *reverberation distance* is an indication for the distance from the sound source beyond which the sound field may be considered diffuse. The direct sound pressure level L_d is dependent only on the source characteristics and the distance between source and receiver. Thus, it decreases by 6 dB per distance doubling. When the direct sound meets the boundaries of the enclosure, a fraction of the acoustic energy is reflected to build the reverberation field. When the reverberation field is a pure diffuse field, the reverberation sound pressure level L_r is independent on the distance from the sound source. The reverberation distance r_r is then defined as the distance from the sound source where the direct sound pressure and the reverberant sound pressure are equal, which may be approximated by

$$r_r = 0{,}25\sqrt{\frac{\bar{\beta}S}{\pi}} \approx 0{,}06\sqrt{\frac{V}{T_{60}}}\,. \tag{2.8.2}$$

Figure 2.8.1 shows the direct (L_d), reverberant (L_r), and total (L_t) sound pressure levels as a function of the distance r from the sound source. At distances close to the sound source (i.e., for $r/r_r < 1$), the direct sound L_d dominates. At the reverberation distance r_r, the direct level L_d and the reverberant level L_r are equal per definition. Thus, the total level L_t is 3 dB higher as a result of the addition of two uncorrelated signals with equal level. At distances beyond $3r_r$, the reverberation level L_r exceeds the direct level L_d more than 10 dB. In real rooms, however, the sound level tends to decrease slightly with increasing distance beyond the reverberation distance, and the sound field may be considered diffuse only by approximation.

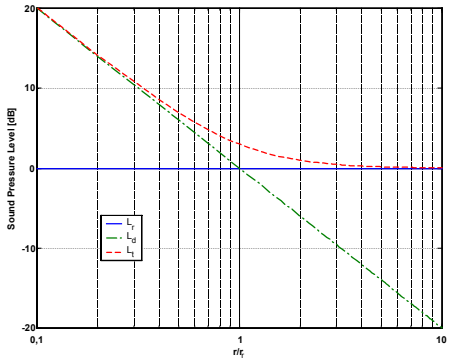

Figure 2.8.1

Direct, reverberant, and total sound pressure levels in an enclosure as functions of the distance from the sound source.

As mentioned in Section 2.5, the loudness cue for distance estimation is valid only in anechoic environments since it is based on the decrease in sound pressure with increasing distance from the source. Beyond the reverberation distance, which may be less than one meter in average rooms, the total sound pressure level is almost constant, and the loudness cue disappears. As the loudness cue becomes less effective with increasing reverberation, the ratio D/R becomes more effective in distance perception. This ratio can be shown to be

$$\frac{D}{R} = \frac{(P_{\mathrm{D}})_{rms}}{(P_{\mathrm{R}})_{rms}} = \frac{r_r}{r}, \tag{2.8.3}$$

which is dependent only on the reverberation distance r_r, a characteristic of the diffuse field in the enclosure, and the distance r from the sound source. Therefore, D/R is considered to be a much more effective distance cue than the loudness in a reverberant environment. Furthermore, reverberation is considered to be important for the perception of the environmental context. The reverberation time and level together with the experience with sounds in reverberant rooms enable a listener to estimate the size and absorptiveness of the surfaces in the environment.

Although, reverberation is important for distance and environmental context perception, it was found to degrade the localisation accuracy of azimuth and elevation [Begault, 1992 and 1994]. This is explained by the ability of humans to detect the direction of the early reflections in severe reverberation conditions. The precedence effect mentioned in Section 2.7 only partially suppresses the effects of reflected sounds. Moreover, the

reverberation makes it difficult for the auditory system to correctly estimate the ITD at low frequencies. This is because in typical rooms, the first reflections arrive before one period of a low frequency cycle is completed. Thus, in a reverberant room, low frequency information is essentially useless for localisation and azimuth localisation is severely degraded. In such cases, the important timing information comes from the *Interaural Envelope Difference* (IED), e.g. from the transients at the onset of a new sound.

2.9 Head-Related Transfer Functions

The most significant locationally dependent effect on the spectrum of a sound source can be traced to the outer ears (*pinnae*), as mentioned in Section 2.4. This spectral filtering of a sound source before it reaches the eardrum is usually termed the *Head-Related Transfer Function* (HRTF). Within the literature, other terms equivalent to the term HRTF are used, such as *Head Transfer Function* (HTF), *Pinnae Transform*, *Outer Ear Transfer Function* (OETF), or *Directional Transfer Function* (DTF) [Møller, 1992].

From a psychoacoustic standpoint, the main role of HRTFs is thought to be the disambiguation of front from back for sources on the cone of confusion, and, as an elevation cue, the distinction of up from down. In fact, it can be shown that HRTFs capture all physical cues to human sound localisation at once. This will be shown in the following by a discussion of the basic physical properties of HRTFs.

HRTFs are functions in four variables, that is to say angle of incidence (φ and δ), distance to the sound source (r), and frequency. If r is reasonably large (about one meter in an anechoic environment), the source is said to be in the *far field*, and the response falls inversely with the range as mentioned in Section 2.8. Most HRTF measurements are anechoic far field measurements, which reduces an HRTF to be a function of three variables, namely azimuth φ, elevation δ, and frequency.

HRTFs measured in an anechoic chamber do not include the effect of reverberation, which is important for range estimation and environmental context perception. In that case, unless binaural room simulation is used to introduce these important reflections, an improper

ratio D/R results. When reproduced through headphones for example, the sound often seems being either too close or inside the head[1]. It is possible, however, to measure the HRTFs in an actual reverberant setting, but this has the disadvantage of limiting the simulated virtual environment to a particular room and also leads to very long impulse responses.

Anechoic HRTFs of manikins and human subjects have been intensively studied in search for physical characteristics that are related to sound localisation. For the present work, a set of anechoic HRTFs measured on an acoustic manikin known as KEMAR by Gardner and Martin [1994], was used for the synthesis of virtual sound sources. Figure 2.9.1 [a] shows the impulse response (the HRIR) of KEMAR's right ear in the horizontal plane as a function of the azimuth angle. The interaural cues can be readily recognised in this graph as the sound has the highest amplitude and arrives first when it is coming from the right side ($\varphi = 90°$). Conversely, it has the lowest amplitude and arrives latest when it is coming from the left side ($\varphi = 270°$). The arrival time varies with azimuth in a more or less sinusoidal fashion as estimated by a spherical head model [Blauert, 1997; Duda, 1996]. In fact, the arrival time conforms quite well to the ITD equation (2.3.1). In particular, the difference between the shortest and the longest arrival times is about 0.7 ms, just as the theory in Section 2.3 predicts.

Pinna reflections can also be noticed in the initial sequence of rapid changes when the source is located at the right side of the head. The peak that arrives about 0.4 ms after the initial peak is due to reflections off the shoulder. Finally, the cone of confusion phenomenon can also be recognised as the response is almost symmetrical about the horizontal lines at azimuth $\varphi = 90°$ and $\varphi = 270°$, which constitute the interaural axis.

Figure 2.9.1 [b] shows the Fourier transform of the impulse response, i.e., the HRTF. Also from this graph it can be clearly seen that the response is highest when the source is at the right and weakest when the source is at the left. In addition, the pinna notch is easily visible around 10 kHz when the source is at the right side of the head. For the opposite side, the sound pressure is low due to head shadowing, and the notch appears not very clear. The broad peak in the range between 2 and 3 kHz can be attributed to the ear canal resonance

[1] This problem, which is very common particularly in headphone sound reproduction, is usually referred to as *Inside-Head Localisation* (IHL).

[Gardner, 1997]. Obviously, this peak is independent of the azimuth, which proves that the ear canal itself does not contribute any additional spatial information [Møller, 1992].

When the source moves around the head in the median plane, the interaural cues are negligible. This can be observed in Figure 2.9.2 [a] as the arrival time for elevation angles δ between –40° to +90° stays more or less the same. The main changes are in the relative arrival times and strengths of the pinna reflections. These become more noticeable in the frequency domain (Figure 2.9.2 [b]) as spectral peaks and notches whose frequency changes significantly with elevation. The frequency of the first notch (the pinna notch) ranges from 6 to 12 kHz as the elevation angle δ changes from –40° to 60°. For elevation angles above about 60°, the notch disappears and there is no more spectral dependency on elevation. Duda [1996], however, showed that it reappears as the source moves behind the head and back towards the floor. He also revealed another potential distinction between front and back in the time domain. That is the mild but clear lack of symmetry about a horizontal line at $\delta =$ 90°. The ear canal resonance is also visible in Figure 2.9.2 [b] as the first broad spectral peak which is also independent of the elevation angle.

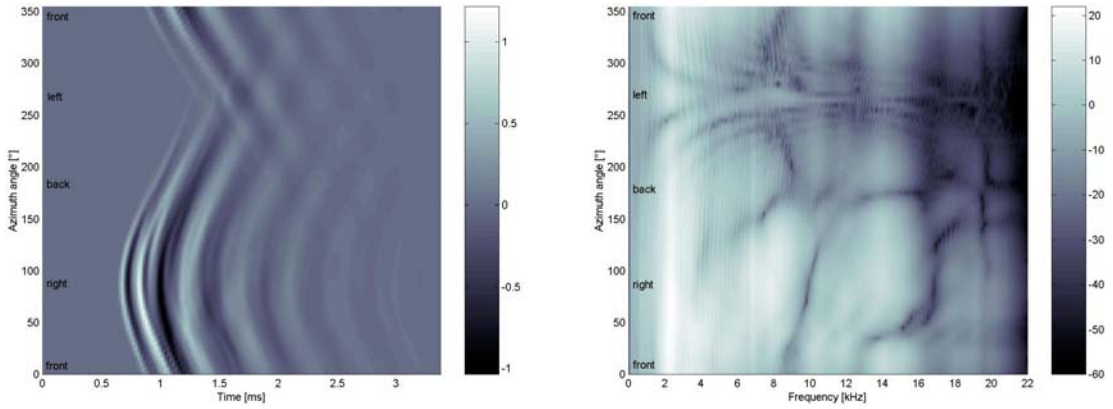

[a] [b]

Figure 2.9.1

Measured HRTFs of KEMAR's right ear for a source in the horizontal plane.[a] is the amplitude of the HRIR and [b] is the amplitude of the HRTF in dB.

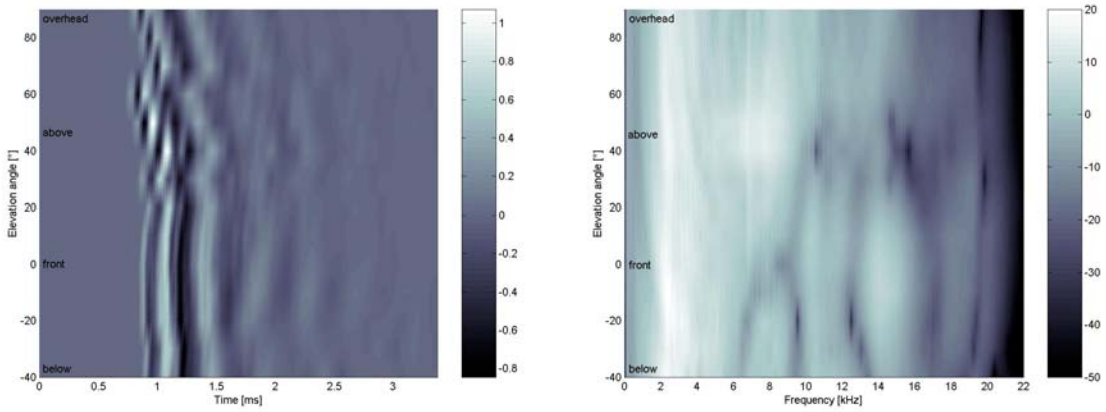

[a] [b]

Figure 2.9.2

Measured HRTFs of KEMAR's right ear for a source in the median plane.[a] is the amplitude of the HRIR and [b] is the amplitude of the HRTF in dB.

Chapter 3
3D Sound Reproduction

3.1 Introduction

Psychoacousticians distinguish between the location of a *sound source* and the location of an *auditory event*. The former is the position of a physical sound source in the listening space, while the latter is the position where the listener experiences the sound [Blauert, 1997]. From everyday experience, it is known that a monophonic audio signal played through a loudspeaker makes the sound source and the auditory event locations coincide. However, it is possible to process the audio signal so that the auditory event occurs at a different position in the listening space than the position of the physical loudspeaker which actually emits the sound. The listener perceives the sound to be coming from the auditory event position, which is therefore referred to as a *phantom* or *virtual sound source*.

A simple form of this audio processing is the *stereophonic* audio system [AES, 1986], where the amplitude or the phase of the sound is panned between two loudspeakers. Stereophonic systems are able to position the virtual *sound image* at any point on the line connecting the two loudspeakers. A direct extension to this technique is the *surround sound* technique, where more than two loudspeakers surrounding the listener are used. By panning the sound between every two adjacent loudspeakers, the auditory event can be positioned on lines connecting the loudspeakers [Pulkki, 1997].

As the number of reproduction loudspeakers increases, the auditory event can be accurately placed at any point in a three-dimensional (3D) space. This is exploited in the *wave field synthesis* or *holographic audio* technique [Berkhout *et al*., 1993; Boone *et al*.,

1995], which is based on the *Kirchhoff-Helmholtz integral* [Pierce, 1981]. The theory of the Kirchhoff-Helmholtz integral suggests that any sound field can be reconstructed perfectly in a given region by using a continuous layer of monopole and dipole sources. Although this is currently impossible in practice, it represents the theoretical limiting case of exact sound field reproduction.

In the present work, a more modest objective is considered, that is to say the problem of reproducing a sound field locally at the eardrums of a listener. This approach requires far fewer transducers than a system that attempts to reconstruct a complex sound field over a relatively large area. As indicated in Chapter 1, the idea is to deliver binaural signals to the ears of a listener. This is achieved by audio systems based on Head-Related Transfer Functions (HRTFs). HRTF-based systems are also able to create multiple virtual sound images simultaneously at different positions in the same listening space using two loudspeakers only. This chapter introduces the basic principles behind virtual sound imaging systems of this type.

3.2 Binaural Synthesis of Virtual Sound Sources

As discussed in Chapter 2, an HRTF measured from the source to the listener's eardrum captures all the physical cues to source localisation. This is also true if the HRTF was measured at any point in the ear canals-possibly even a few millimetres outside and even with a blocked ear canal, since all those measurements include the full spatial information given to the ear [Møller, 1992]. Once the HRTFs corresponding to any desired position are known, one can synthesise accurate binaural signals from any monaural source, and thus place this source virtually at this desired location.

Consider the natural listening situation where a monophonic sound signal $u(t)$[1] is emitted from a source located at an arbitrary point (r, φ, δ) relatively to the centre of the

[1] Note that this signal does not contain any spatial information.

listener's head. In principle, the sound pressure occurring in this situation at the listener's ears can be modelled by the *convolution* (filtering) between $u(t)$ and the pair of *Head-Related Impulse Responses* (HRIRs)[1] between sound source and the listener's left and right eardrums. Conversely, filtering of the signal $u(t)$ through the HRIR pair measured for a sound source at the point (r, φ, δ) results in a pair of binaural signals which eventually create an auditory event right at that measured point. This process-usually referred to as *binaural synthesis*-can be expressed in the frequency domain by

$$\mathbf{d}(\omega, r, \varphi, \delta) = \mathbf{a}(\omega, r, \varphi, \delta) \cdot u(\omega), \tag{3.2.1}$$

$$\mathbf{d}(\omega,r,\varphi,\delta) = \begin{bmatrix} d_L(\omega,r,\varphi,\delta) \\ d_R(\omega,r,\varphi,\delta) \end{bmatrix}, \qquad \mathbf{a}(\omega,r,\varphi,\delta) = \begin{bmatrix} A_L(\omega,r,\varphi,\delta) \\ A_R(\omega,r,\varphi,\delta) \end{bmatrix},$$

where $u(\omega)$ is the monophonic input signal, $\mathbf{d}(\omega,r,\varphi,\delta)$ is a column vector of the desired binaural signals, and $\mathbf{a}(\omega,r,\varphi,\delta)$ is a column vector of the appropriate synthesis HRTFs. Provided that the used HRTF pair matches those of the listener, delivering of the binaural signals at the listener's eardrums creates an auditory event (a virtual source) at (r, φ, δ).

In general, T auditory events may be created simultaneously in the same virtual space by extending the scalar input of Equation (3.2.1) to be a column vector containing T monophonic input sound signals. Omitting the dependencies on spatial coordinates, this can be expressed as

$$\begin{bmatrix} d_L(\omega) \\ d_R(\omega) \end{bmatrix} = \begin{bmatrix} A_{L_1}(\omega) & A_{L_2}(\omega) & \dots & \dots & A_{L_T}(\omega) \\ A_{R_1}(\omega) & A_{R_2}(\omega) & \dots & \dots & A_{R_T}(\omega) \end{bmatrix} \cdot \begin{bmatrix} u_1(\omega) \\ u_2(\omega) \\ \vdots \\ \vdots \\ u_T(\omega) \end{bmatrix}, \tag{3.2.2}$$

Consequently, the binaural signal is the sum of multiple input sounds rendered at different locations.

While Equation (3.2.2) gives the binaural signals at one frequency only, it should be

[1] The HRIRs refer to the inverse Fourier Transforms of the HRTFs.

kept in mind that there are as many equations of this form as there are frequencies. Assuming the system is operating at a single frequency only, complex notation can be used to describe the signals. Thus, it is assumed that all the signals are complex scalars. This allows the use of well known matrix algebra for the proceeding discussion. Making those assumptions in the following, the explicit dependency on the frequency ω may also be dropped to enhance the readability of the equations. Thus, Equation (3.2.2) can be expressed in compact matrix notation as

$$\mathbf{d} = \mathbf{A} \cdot \mathbf{u} \,. \tag{3.2.3}$$

Figure 3.2.1 shows the block diagram of a multiple source binaural synthesiser. This principle can be further generalised to the creation of T virtual sound images at the R ears of $R/2$ listeners by expanding the column vector **d** and the HRTF matrix **A** to be of the dimensions $[R \times 1]$ and $[R \times T]$, respectively. For simplicity, however, the further discussion will be restricted to a single source and a single listener only.

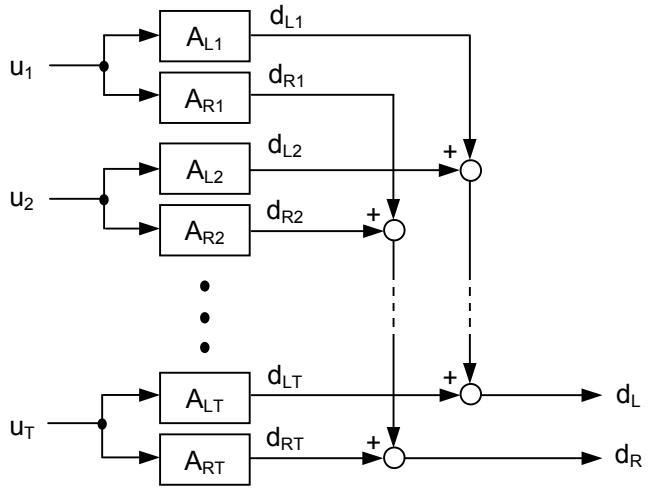

Figure 3.2.1
Principle of binaural synthesis of multiple virtual sound sources.

Binaural signals may also be obtained simply from head-related recordings using an artificial head microphone, rather than from binaural synthesis. In that case, the spatial cues are encoded within the recorded signals and hence the synthesis HRTFs have already been applied. However, using such pre-recorded binaural signals restricts the achievable virtual

images to those already included with the recording. Subsequent processing in order to manipulate the individual synthesis HRTFs is only possible with prior performing a complicated unmixing procedure.

3.3 Headphone Displays

In 3D sound systems, the question arises of how to deliver the electrical binaural signals to the listener's eardrums as acoustic waves. In any case, the transmission paths from the transducers to the listener's ears (the listener's HRTFs) have to be compensated in order to correctly deliver the binaural signals. Headphones deliver d_L at the left ear only and d_R at the right ear only, respectively, without any crosstalk from the opposite signal. Thus, the use of headphones certainly simplifies the problem of transmission path inversion between the transducers and the listener's ears.

However, headphones have their own drawbacks: they may not be comfortable to wear for a long time period. They also attenuate external sounds and isolate the user from the surrounding environment. Sounds heard over headphones often seem to be too close or inside the listener's head as previously mentioned in Section 2.9. Since the physical sources (the headphones) are actually very close to the listener's ears, compensation is needed to eliminate the acoustic cues to their locations. This compensation is very sensitive to the headphone position. Finally, headphones can have notches and peaks in their frequency responses that resemble the pinna responses. If uncompensated headphones are used, elevation effects can be severely compromised [Duda, 1996].

3.4 Theory of Crosstalk Cancellation

By using loudspeakers for binaural sound reproduction[1], one can circumvent most of the problems one encounters with headphone displays. However, as opposed to headphone reproduction, the use of loudspeakers introduces the major problem of crosstalk. Thus, the transmission path equalisation is considerably more difficult to achieve, since it also has to take into account for the cancellation of crosstalk. Figure 3.4.1 shows the problem in hand for the standard two channel listening situation in a free field. On its way to the listener's ears, the sound it filtered through a [2 × 2] mixing matrix **C** of the four acoustic transfer functions between the two loudspeakers and the two ears. This matrix is usually referred to as the "*plant"*, which-in terms of control theory-denotes the physical system to be controlled. Using matrix notation, the reproduced ear signals **w** are related to the speaker signals **v** through the equation

$$\mathbf{w} = \mathbf{C} \cdot \mathbf{v} \,, \tag{3.4.1}$$

$$\mathbf{w} = \begin{bmatrix} w_L \\ w_R \end{bmatrix}, \qquad \mathbf{C} = \begin{bmatrix} C_{LL} & C_{RL} \\ C_{LR} & C_{RR} \end{bmatrix}, \qquad \mathbf{v} = \begin{bmatrix} v_L \\ v_R \end{bmatrix}.$$

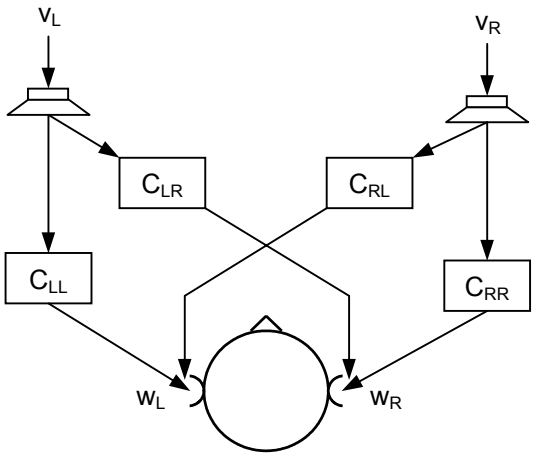

Figure 3.4.1

Acoustic transfer functions between two loudspeakers and the ears of a listener.

[1] Cooper and Bauck [1989] use the term *transaural audio* for binaural sound reproduction over loudspeakers.

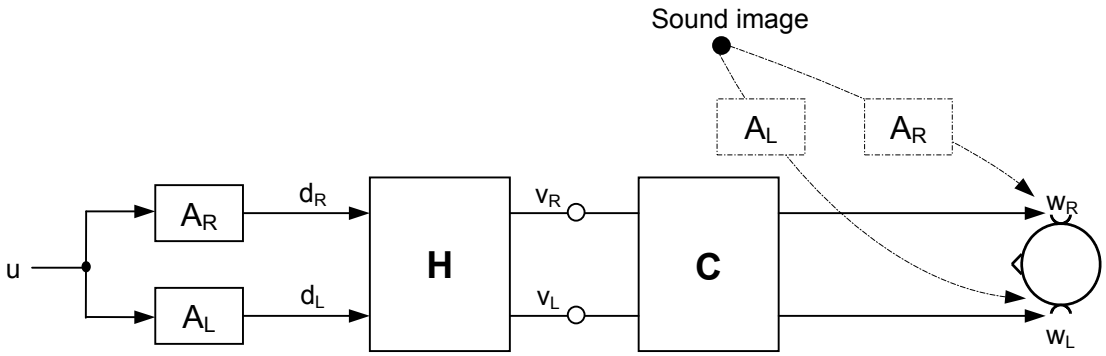

Figure 3.4.2

Schematic playback system including binaural synthesiser, crosstalk canceller, and acoustic transfer to the listener.

The complete playback system is given in Figure 3.4.2, including the HRTF filters **A** for the synthesis of the *desired* binaural signals $\mathbf{d} = [d_L \quad d_R]^T$. In order to eventually create a virtual source image corresponding to **d**, the reproduced signals **w** must equal **d**. Thus, it is necessary to introduce a network of filters **H** (the *crosstalk canceller*), which performs the inversion of the plant matrix **C** in order to correctly deliver the binaural signals **d**. Consequently, the inverse filter matrix **H** is given by

$$\mathbf{H} = \begin{bmatrix} H_{11} & H_{12} \\ H_{21} & H_{22} \end{bmatrix} = \mathbf{C}^{-1} = \frac{1}{C_{LL}C_{RR} - C_{LR}C_{RL}} \begin{bmatrix} C_{RR} & -C_{RL} \\ -C_{LR} & C_{LL} \end{bmatrix}. \tag{3.4.2}$$

Hence, the combined solution for the reproduced ear signals is

$$\mathbf{w} = \mathbf{C} \cdot \mathbf{H} \cdot \mathbf{A} \cdot u\,. \tag{3.4.3}$$

Considering, that

$$\mathbf{d} = \mathbf{A} \cdot u\,, \tag{3.4.4}$$

according to Equation (3.2.3), and assuming a correct system inversion such that

$$\mathbf{C} \cdot \mathbf{H} = \mathbf{C} \cdot \mathbf{C}^{-1} = \mathbf{I}\,, \tag{3.4.5}$$

where **I** denotes the $[2 \times 2]$ unity matrix, Equation (3.4.3) turns into the desired result

$$\mathbf{w} = \mathbf{d}\,. \tag{3.4.6}$$

In general, the ear signals **w** are considered to be measured by an ideal transducer somewhere in the ear canal such that all direction-dependent features of the head response are captured. Each of the functions C_{XY} in the plant matrix **C** denote the transfer functions from speaker X to ear Y and include the frequency response of loudspeaker and measurement microphone as well as air propagation and the HRTF. Therefore, the elements of **C** are complex functions in frequency and space coordinates. They are often said to be *non-minimum phase* and contain deep notches due to the pinna reflections, particularly in reverberant conditions. Moreover, since loudspeakers act like acoustic band-pass filters, their responses lead to much less energy at the upper and lower ends of the audio frequency band. For that reasons, the inversion of **C** required by the crosstalk cancellation matrix **H** in Equation (3.4.2) is difficult to calculate. Considerations of achieving the system inversion by means of numerical filtering will be discussed in Chapter 4.

3.5 Physical Interpretation of Crosstalk Cancellation

Usually, the plant transfer functions C_{XY} are measured with a dummy head microphone. Another measurement of the playback system only may be made with a single microphone and no head present. The microphone (ideally the same as used for the dummy head measurements) may be placed at the position where the centre of the dummy head was placed before. Equalising the plant transfer functions with the inverse of this system response results in a plant matrix

$$\mathbf{C} = \begin{bmatrix} H_{LL} & H_{RL} \\ H_{LR} & H_{RR} \end{bmatrix}. \tag{3.5.1}$$

Thus, **C** now contains only the HRTFs normalised with respect to the free-field response at the centre of the head, but with no head present. [Møller, 1992]. The inverse head transfer matrix, regarding Equation (3.4.2) is now given as

$$\mathbf{H} = \mathbf{C}^{-1} = \frac{1}{D}\begin{bmatrix} H_{RR} & -H_{RL} \\ -H_{LR} & H_{LL} \end{bmatrix} \qquad D = H_{LL}H_{RR} - H_{LR}H_{RL}, \tag{3.5.2}$$

where D is the determinant of the matrix **C**. The inverse determinant $1/D$ is common to all terms and determines the stability of the inverse filter as will be shown in Chapter 4. However, because it is a common factor, it only affects the overall equalisation and does not affect crosstalk cancellation. When D is zero at any frequency, the matrix **C** is *singular* and the inverse matrix **H** is undefined. Figure 3.5.1 shows the principle of a single source binaural synthesiser cascaded with a crosstalk canceller. This block diagram is based on the system suggested initially by Atal *et al*. [1966].

Dividing numerator and denominator by $H_{LL}H_{RR}$, Equation (3.5.2) can be rewritten as

$$\mathbf{H} = \begin{bmatrix} 1/H_{LL} & 0 \\ 0 & 1/H_{RR} \end{bmatrix} \cdot \begin{bmatrix} 1 & -ITF_R \\ -ITF_L & 1 \end{bmatrix} \cdot \frac{1}{1 - ITF_L \cdot ITF_R}, \tag{3.5.3}$$

$$ITF_L := \frac{H_{LR}}{H_{LL}}, \qquad ITF_R := \frac{H_{RL}}{H_{RR}}$$

Here, the *ITF* functions denote the so-called *Interaural Transfer Functions*, which describe the difference in transmission to the ipsilateral and to the contralateral ear, respectively [Møller, 1992].

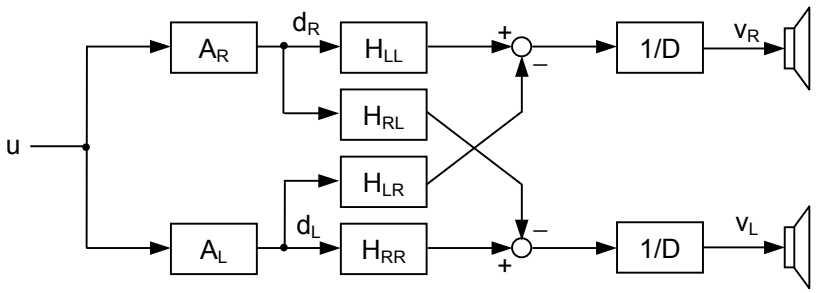

Figure 3.5.1

Single source binaural synthesiser cascaded with a crosstalk canceller in block diagram form.

Observing Equation (3.5.3) reveals much about the physical process of crosstalk cancellation. That is to say, crosstalk cancellation is effected by the *ITF*-terms in the off-diagonal positions of the righthand matrix. These terms predict the crosstalk and send out an out-of-phase cancellation signal into the opposite channel. For instance, the right input signal is convolved with ITF_R, which predicts the crosstalk that will reach the left ear, and the result is subtracted from the left output signal. The common term $1/(1-ITF_L \cdot ITF_R)$ compensates for higher-order crosstalks, in other words, the fact that each crosstalk cancellation signal itself transits to the opposite ear and must be cancelled by another cancellation signal. This intrinsically recursive process, as recognised by Atal *et al*. [1966] will be further discussed in the following section.

3.6 Stereo Dipole

As discussed above, the recursive nature of the crosstalk cancellation process gives rise to an audible and hence undesirable frequency f_0, usually referred to as the "*ringing frequency*". Obviously, this ringing frequency is also related to the time delay between the two loudspeakers due to the finite distance between them. Thus, the value of f_0 increases for decreasing subtended angles 2θ [1]. For a traditional stereo set-up with typically $2\theta = 60°$, the value of f_0 is about 1,9 kHz, whereas with $2\theta = 10°$ the ringing frequency f_0 becomes 10,8 kHz [Kirkeby *et al*., 1997]. Furthermore, it can be shown that the limiting case is equivalent to a superposition of a point monopole and a point dipole source, both being placed at the same point. A crosstalk cancellation system based on this source combination is considered to be optimal since the reproduced sound field does not contain any "ringing" [Nelson *et al*., 1997]. A system, referred to as the "Stereo Dipole" system, with a source span of $2\theta = 10°$ is a good approximation of this theoretical set-up.

A free field simulation of the crosstalk cancellation principle is illustrated in Figure

[1] The subtended angles, referred to as the *loudspeaker span*, are denoted here by 2θ (according to Figure 5.2.1).

3.6.1, where a sequence of "snapshots" of the instantaneous pressure field produced by the two sources is shown. The desired signal is a Hanning pulse[1] at the right ear and zero pressure at the left ear. Values greater than 1 are plotted as white, values smaller than –1 are plotted as black, and values between –1 and 1 are shaded appropriately. The positions of the sources and the microphones are indicated by circles. The plots contain 9 snapshots which are listed in a reading sequence, i.e., the top left is the earliest in time and the bottom right is the latest.

With a span 2θ=60°, it is easy to identify a sequence of positive pulses from the right source, and a sequence of negative pulses from the left source (Figure 3.6.1 [a]). Only the first pulse emitted from the right source is actually "seen" by the right microphone, whereas consecutive pulses cancel each other out at both microphones. However, many "copies" of the original Hanning pulse are present at other locations in the sound field, even very close to the two microphones. Therefore, this set-up is not very robust with respect to head movement. In fact, the listener will hear the ringing frequency if he/she is outside the controlled region while a virtual sound is being created.

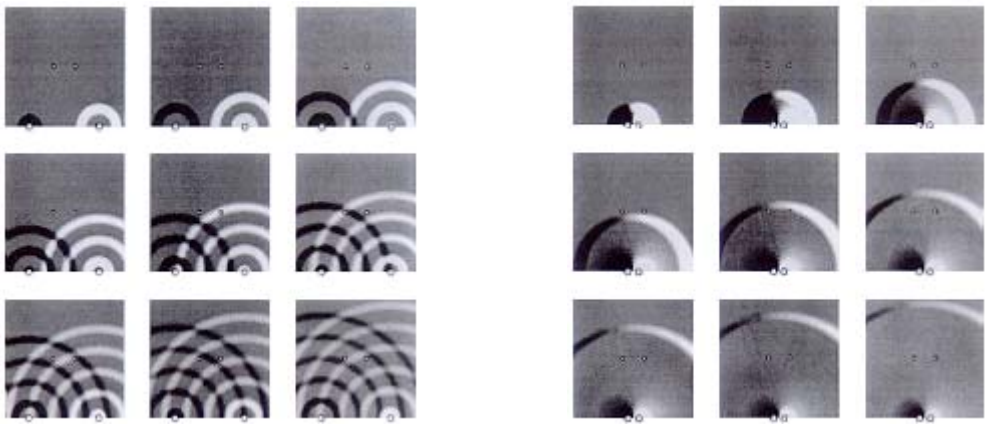

[a] [b]

Figure 3.6.1

The sound field reproduced by two monopole sources in order to achieve perfect crosstalk cancellation (i.e., a desired pulse at the right ear and zero pressure at the left ear) under free-field conditions. The two source spans are [a] 60° and [b] 10°.

When the loudspeaker span is reduced to 2θ=10°, as shown in Figure 3.6.1 [b], the ringing frequency is much higher and hence its effect is considerably reduced. Thus, the

[1] A Hanning pulse represents one periode of a "raised" cosine.

reproduced sound field is much simpler, and consequently, the area over which the sound field can be controlled is larger. This suggests which was verified later by Takeuchi et al. [1997], viz. that reducing the loudspeaker span 2θ improves the system's robustness with respect to head misalignment. In addition, since the ringing frequency and its harmonics are more efficiently suppressed, the reproduced sound results in a more natural quality.

However, as the ringing frequency is increased, it is obvious that the adjacent pulses overlap increasingly. Thus, it is also intuitively obvious that by increasing f_0, the low-frequency content of the signals is also increased. Consequently, in order to achieve perfect crosstalk cancellation with a pair of closely spaced loudspeakers, a very large low-frequency output is necessary. This happens because the crosstalk cancellation problem is said to be *ill-conditioned* at low frequencies (see Section 4.7). In the case of virtual source imaging, i.e., when one attempts to produce a sound at both ears rather than at one ear only, the low-frequency content is reduced because the positive and negative parts of the pulse trains cancel each other out. Therefore, it is an easier task to create a virtual sound image than to achieve perfect crosstalk cancellation [Kirkeby *et al*., 1997]. However, creating virtual sources well outside 2θ still requires a considerable amount of low frequency, especially with a small loudspeaker span.

Fortunately, though, as long as the loudspeaker span is not too small only a moderate boost of low frequencies is required. In practice, the "Stereo Dipole" system with a loudspeaker span of 10° is a good compromise.

Chapter 4
Inverse Filter Design

4.1 Introduction

The control filters in loudspeaker displays must implement both binaural synthesis and crosstalk cancellation functions as discussed in the previous chapter. The task of the crosstalk cancellation subsystem is to invert a matrix **C** of electro-acoustic transfer functions.

In practice, the exact inverse is difficult to calculate and in some cases, may not be possible to achieve at certain frequencies. Only when **C** is a *minimum phase* system, it is possible to achieve a stable time response for the inverse filter **H**. Basically, a minimum phase signal has a minimum delay property, which effectively guarantees that the signal has its energy concentrated at its start [Oppenheim and Schafer, 1975]. However, the electro-acoustic transfer functions contained in **C** are not likely to be minimum phase, since they contain echoes due to pinna reflections and the room response. If the impulse response of the inverse of such a signal has to be stable, it generally has to start before time zero, hence, it is said to be *non-causal*. In fact, the exact inverse of a non-minimum phase system has an impulse response which begins infinitely far back in time. Another problem encountered with the system inversion is that if $C(\omega)$ is very small within a narrow range of frequencies, the inversion $H(\omega) = 1/C(\omega)$ becomes very large. Such problems are said to be *ill-conditioned*. Finally, since the performance of a digital filter is inevitably limited by the number of filter coefficients, it is not realistic to expect an exact inversion.

However, by aiming at an approximation rather than at the exact inversion, it is possible to design a digital *finite impulse response* (FIR) filter, such that the system is

inverted (*deconvolved*) almost perfectly. Obviously, a good approximation is characterised by being close, in some sense, to the exact solution. In order to be able to find the best approximation, it is necessary to have a measure for the difference between the two: a *"cost function"*[1]. The most common choice is to use a cost function which is a time average of the squared deviations (the error) between the desired output and the actual output from the system.

Various methods for multi-channel inverse filter design have been suggested, both in the time and frequency domain. Most of them apply the principle of minimisation or optimisation in this "statistical" *least squares* sense. Initially, the principle of multi-channel inverse filtering has been widely used in active noise control systems [Nelson and Elliott, 1992]. In terms of signal processing, the suppression of an unwanted sound and the reproduction of a desired sound turn out to be very similar problems. Therefore, it is fairly straightforward to apply these inverse filtering techniques also to sound reproduction systems.

A very versatile adaptive time domain algorithm is the steepest descent *Least-Mean-Square* (LMS) algorithm [Widrow and Stearns, 1985]. The method of *fast deconvolution using regularisation*, on the other hand, is based on determining the inverse (FIR) filters in the frequency domain, and was applied on multi-channel systems by Kirkeby *et al*. [1996a]. This method as well as a general study of the mentioned problems in digital inverse filter design will be discussed in the following sections of this chapter.

4.2 Exact Inversion of Single Channel Systems

For the study of inverse filter design, the first requirement is an understanding of the basic problems in the simplest case: the single channel case. The acoustic path between a source and a receiver can be thought as a filter of a particular length. Representing this filter as a discrete-time system, it may be analysed by using the z-transform [Oppenheim and Schafer, 1975]

[1] Sometimes also called "*error function*" or "*performance index*"

$$C(z) = \sum_{n=0}^{N-1} c(n) z^{-n} = c(0) + c(1) z^{-1} + ... + c(N-1) z^{-(N-1)} .$$

(4.2.1)

As introduced above, the task is to create an inverse filter $H(z)$, which "undoes" the undesired modification to a signal due to $C(z)$ in order to restore the original. This equalisation problem for the case of a single channel is sketched in Figure 4.2.1, and can be expressed in the z-domain as

$$w(z) = C(z) H(z) d(z) ,$$

(4.2.2)

which ideally leads to $w(z) = d(z)$, for the case of an exact inversion $H(z) = C(z)^{-1}$. A causal filter sequence as in equation (4.2.1) can also be expressed in factored form as

$$C(z) = \alpha \prod_{i=0}^{N-1} \left(1 - a_i z^{-1}\right),$$

(4.2.3)

where each of the coefficients a_i contributes a solution of C(z) = 0, and α is a linear scale factor.

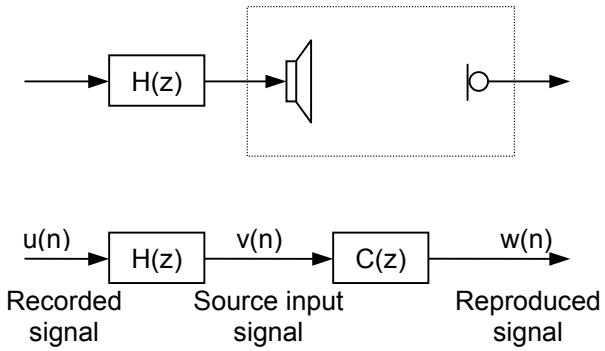

Figure 4.2.1

Diagram of a single channel equalisation system.

As a simple example, consider the inversion of

$$C(z) = 1 + a z^{-1}$$

(4.2.4)

to give an illustration of the problems involved in the single channel inversion. The inverse filter may be first calculated directly as

$$H(z) = \frac{1}{C(z)} = \frac{1}{1 + az^{-1}} .$$

(4.2.5)

Observing equation (4.2.5) reveals that the zero of $C(z)$ is now mapped into a pole of the inverse filter function $H(z)$. In general, an exact inversion of $C(z)$ always maps the poles of $C(z)$ to the zeros of $H(z)$, and the zeros of $C(z)$ to the poles of $H(z)$, respectively.

For the underlying example, two different cases have to be investigated in order to determine the inverse filter in the z-domain and in terms of the corresponding pole-zero map.

- For the case that |a| < 1, using the binomial expansion

$$(1+x)^{-1} = \sum_{k=0}^{\infty} (-1)^k x^k = 1 - x + x^2 - x^3 + ... ,$$

(4.2.6)

the inverse filter H can be turned into the all-zero model

$$H(z) = \left(1 + az^{-1}\right)^{-1} = \sum_{n=0}^{\infty} (-a)^n z^{-n} = 1 - az^{-1} + a^2 z^{-2} - a^3 z^{-3} + ...$$

(4.2.7)

This geometric series shows that, due to |a| < 1, the sequence is causal and convergent.
Thus, the designed inverse filter is causal and stable. The pole of $H(z)$ is inside the unit circle as can be observed in the pole-zero map of Figure 4.2.2. In general, a filter system with all its zeros inside the unit circle, as $C(z)$ is in this case, is called a *minimum-phase* system.

- For the case that |a| > 1, the filter system C in Equation (4.2.4) has its zero outside the unit circle, and therefore, it is called a *non-minimum phase* system. Actually, systems with all their zeros outside the unit circle are generally called *maximum phase*. On the contrary, systems with some zeros inside the unit circle and the remaining zeros outside the unit circle are usually referred to as *non-minimum phase* or *mixed-phase* systems [Proakis and Manolakis, 1996]. For the present system, the inverse filter H can be turned into an all-zero model by exploiting the geometric series as

$$H(z) = \begin{cases} \sum_{n=0}^{\infty} (-a)^n z^{-n} & \text{causal, unstable} \\ \dfrac{a^{-1}z}{1+a^{-1}z} = -\sum_{n=1}^{\infty} (-a)^{-n} z^n & \text{anti - causal, stable} \end{cases} \tag{4.2.8}$$

The upper expansion of Equation (4.2.8) leads to an unstable filter since its causal sequence diverges. Hence, a small error in the value of a would cause a considerable error in the inverse filter H. However, when H is required to be stable (lower expansion), the resulting sequence converges in reverse time. Thus, the inverse filter is said to be stable and anti-causal. Therefore, for the practical realisation, it is crucial to implement a "*modelling delay*" in order to include the non-causal component of the exact inverse in its response [Widrow and Stearns, 1985]. Otherwise, only the minimum phase portion of the transfer function will be inverted. Such a modelling delay also serves another purpose, that is to compensate for the initial delay, which is the time it takes for the sound to travel from the source to the receiver.

The above discussion leads to an important point that should be emphasised as a conclusion. That is, a stable pole-zero system that is minimum phase has a stable inverse which is also minimum phase. Hence the minimum-phase property of $C(z)$ ensures the stability of the inverse system $H(z)$ and the stability of $C(z)$ implies the minimum-phase property of $H(z)$, whereas non-minimum phase and maximum phase systems result in unstable inverse systems.

The decay rate of the inverse filter can be characterised by the time constant τ, which, in both cases[1], is given by

$$\tau = \frac{1}{r}, \tag{4.2.9}$$

where $r << 1$ is the distance from the pole to the unit circle [Bellanger, 1989]. This means that systems with zeros close to the unit circle result in inverse filters of longer duration.

Another problem with direct system inversion is that if the inverse is calculated using

[1] Either in positive time for the minimum phase filter or in reverse time for the non-minimum phase filter.

finite length sequences, the inverse in the z-domain follows as

$$H(z) = \frac{1}{C(z)}\,.$$

(4.2.10)

However, in the discrete time domain, the impulse response $h(n)$ of the inverse filter is in general not exactly the inverse of the system's impulse response $c(n)$

$$h(n) = \mathbf{Z}^{-1}\{H(z)\} \neq c^{-1}(n)\,.$$

(4.2.11)

This results because even if $c(n)$ is of finite length, the inverse impulse response $h(n)$ will generally not be of finite length. This can be observed on the simple example in Figure 4.2.2.

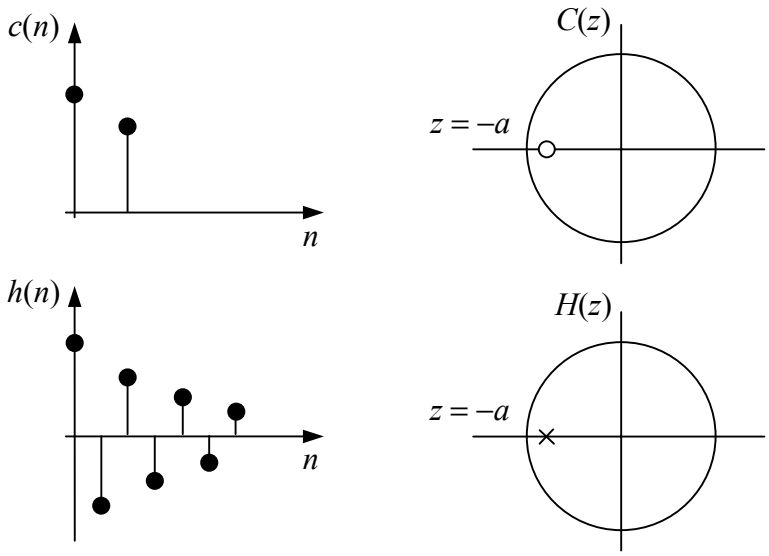

[a]

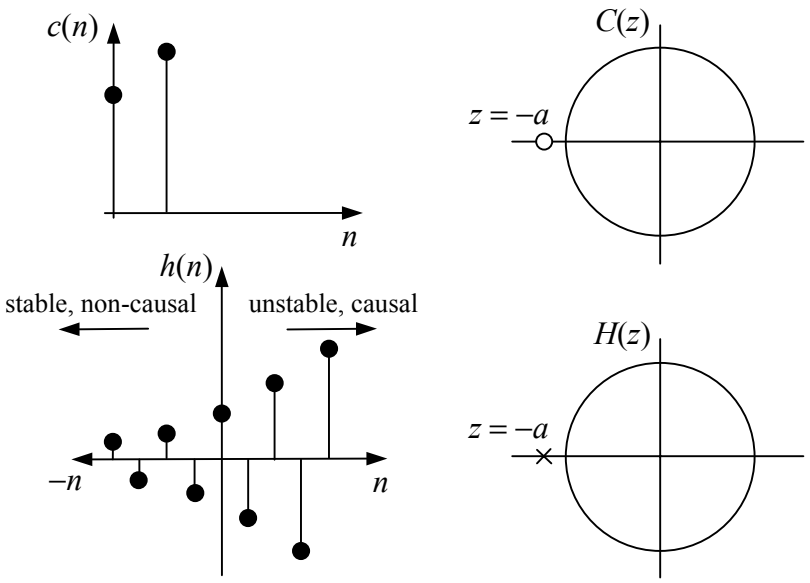

[b]

Figure 4.2.2

Simple examples of minimum phase [a] and non-minimum phase filters [b]. Upper rows show the impulse responses of the original systems $c(n)$ with the corresponding pole-zero maps. Lower rows show the impulse responses of the exact inverse filters $h(n)$ with the corresponding pole-zero maps.

4.3 Optimal Single Channel Inversion

The transfer function of the electroacoustic path can be expressed in the z-domain as

$$C(z) = \frac{z^{-k} B(z)}{A(z)},$$

(4.3.1)

where $B(z)$ and $A(z)$ respectively define the poles and zeros. As mentioned above, $C(z)$ inevitably contains an initial delay of k samples, which is represented by the term z^{-k}. Therefore, it is impossible to correctly reproduce the recorded signal with a realisable $H(z)$, i.e., $w(n) \neq u(n)$.

However, the reproduced signal can be made a very good approximation to a delayed version of the recorded signal, i.e., $w(n) \approx u(n-\Delta)$. Hence, the desired signal $d(n)$ has to be defined by a *modelling delay* of Δ samples, as indicated in Figure 4.3.1. As mentioned in the previous section, this modelling delay not only needs to account for the initial delay, but also for the non-causal part of the exact inverse. A rule of thumb for the choice of Δ is to take the initial delay k and add half the filter length. The exact value is not critical since there is

usually a fairly wide range of modelling delays that will work almost equally well [Widrow and Stearns, 1985].

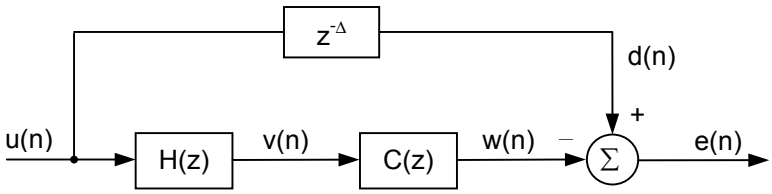

Figure 4.3.1
Block diagram of the single channel inversion problem.

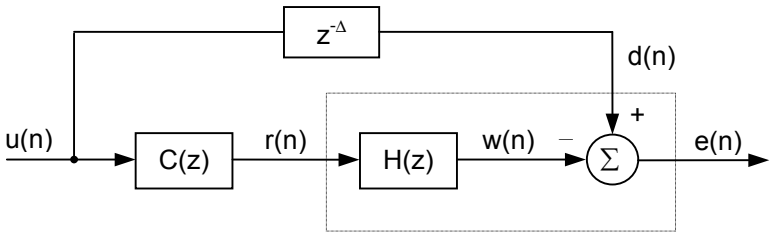

Figure 4.3.2
Single channel inversion as a Wiener filtering problem.

Since the systems are assumed to be linear and time-invariant, the block diagram in Figure 4.3.1 may be rearranged as shown in Figure 4.3.2. The determination of the inverse filter $H(z)$ that minimises the *cost function* of the error

$$J = E[e^2(n)],$$

(4.3.2)

is now exactly in the form of a so-called *Wiener filtering problem* [Proakis and Manolakis, 1996], after the famous mathematician Norbert Wiener [1949]. The operator E in Equation (4.3.2) denotes the *mathematical expectation*, which refers to an average over ensembles of the random error sequence

$$e(n) = d(n) - w(n).$$

(4.3.3)

Recall the electroacoustic transfer function given by Equation (4.3.1). As any other non-minimum phase system, $C(z)$ can be decomposed into a "minimum phase" part $C_{min}(z)$ and an "all pass" part $C_{ap}(z)$ as

$$C(z) = \frac{z^{-k} B^{+}(z)\, B^{-}(z)}{A(z)},$$

(4.3.4)

where $B^{+}(z)$ has all its roots inside the unit circle |z| = 1 and $B^{-}(z)$ has all its roots outside the unit circle [Proakis and Manolakis, 1996]. Consequently, $B^{-}(z^{-1})$ has all its roots inside the unit circle. Defining the minimum phase system

$$C_{min}(z) = \frac{B^{+}(z) z^{-N} B^{-}(z^{-1})}{A(z)}$$

(4.3.5)

and the all-pass system

$$C_{ap}(z) = \frac{B^{-}(z)}{z^{-N} B^{-}(z^{-1})},$$

(4.3.6)

Equation (4.3.4) can be expressed as

$$C(z) = z^{-k} C_{min}(z) C_{ap}(z),$$

(4.3.7)

where it is assumed that the polynomial $B^{-}(z)$ has degree N. Hence, $z^{-N} B^{-}(z^{-1})$ reflects the non-minimum phase zeros outside the unit circle to their corresponding positions inside the unit circle. This in turn means that the system inversion is always stable, but for non-minimum phase inputs, it is inaccurate, leaving a residual all-pass component.

For example, if $C(z) = 1 + az^{-1}$, with |a| > 1, the equivalent filter to be inverted follows as $C_{eq,min}(z) = 1 + z^{-1}/a$ by reflecting the zero into the inside of the unit circle. Calculating the inverse filter (see Figure 4.3.3) leads to $H(z) = 1/(1 + z^{-1}/a)$ and hence the combination of the two filters results in $H(z) \cdot C(z) = (1 + az^{-1})/(1 + z^{-1}/a) \neq 1$. This illustrates that for finite filters the result will, in principle, always be an approximation.

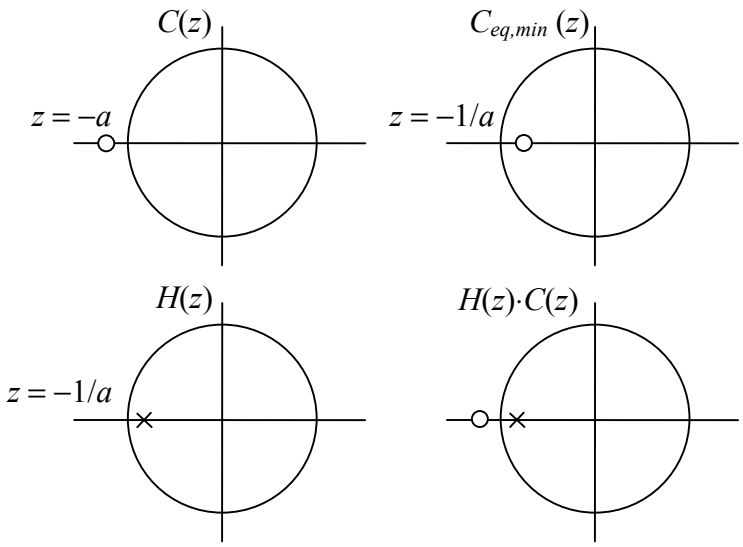

Figure 4.3.3

Least mean squares inversion of the system $C(z) = 1 + az^{-1}$.

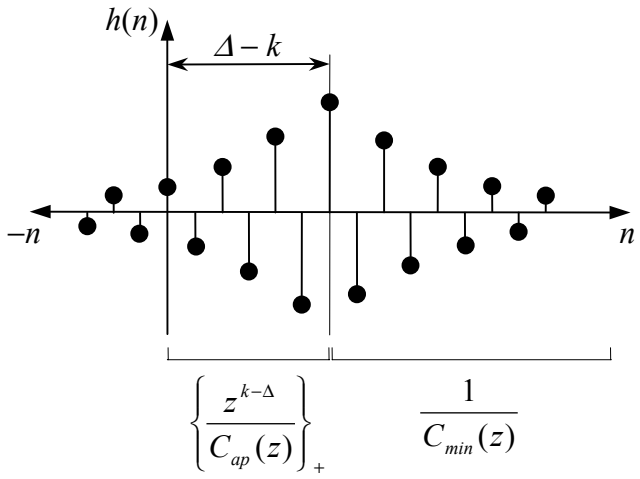

Figure 4.3.4

Sequence of an optimised single channel inverse filter.

Assuming a stationary ergodic random process, the cross-correlation between the input signal $r(n)$ and the desired output signal $d(n)$ of the Wiener problem can be written as

$$R_{rd}(m) = E[r(n)d(n+m)] = \lim_{N\to\infty} \frac{1}{N} \sum_{n=0}^{N-1} r(n)d(n+m)\,, \tag{4.3.8}$$

where E denotes the mathematical expectation. The corresponding cross spectrum is derived from the z-transform

$$S_{rd}(z) = \sum_{m=-\infty}^{\infty} R_{rd}(m) z^{-m} \ .$$

(4.3.9)

The auto spectrum can be defined in the same way and may also be written as the product of its minimum phase part $S(z)$ and its non-minimum phase part $S(z^{-1})$, viz.

$$S_{rr}(z) = \sum_{m=-\infty}^{\infty} R_{rr}(m) z^{-m} = S(z) \cdot S(z^{-1}) \, .$$

(4.3.10)

The optimal solution for the filter that minimises the cost function $J = E[e^2(n)]$ is given by

$$H(z) = \frac{1}{S(z)} \left\{ \frac{S_{rd}(z)}{S(z^{-1})} \right\}_{+} ,$$

(4.3.11)

where $\{ \}_{+}$ denotes the causal part of what is inside the brackets [Widrow and Stearns, 1985] and

$$S_{rd}(z) = S_{dr}(z^{-1}) = \frac{z^{k-\Delta} B(z^{-1})}{A(z^{-1})} \, .$$

(4.3.12)

If the recorded input signal $u(n)$ is assumed to be white noise, then

$$S_{rr}(z) = C_{min}(z) \cdot C_{min}(z^{-1}) \, ,$$

(4.3.13)

and thus the *spectral factors* can be written as

$$S(z) = C_{min}(z), \quad \mathrm{S}(z^{-1}) = C_{min}(z^{-1}) \, .$$

(4.3.14)

The substitution of these values yields the classical Wiener solution

$$H(z) = \frac{1}{C_{min}(z)} \left\{ \frac{z^{k-\Delta}}{C_{ap}(z)} \right\}_{+} \, .$$

(4.3.15)

This is equivalent to separately calculating the inverse filter of the minimum phase part and the non-minimum phase part respectively, and allowing a modelling delay for the response. From Figure 4.3.4, it is obvious that the modelling delay Δ must be much greater than the plant delay k, if the system to be inverted is non-minimum phase. Moreover, the closer the system's zeros are to the unit circle, the greater $(\Delta - k)$ must be. The best approximations to an exact inverse are produced if the impulse response of the inverse filter decays rapidly (in

forward or reverse time) compared to the available filter length.

4.4 Regularisation

The technique of zero'th order regularisation [Press *et al*., 1992] is traditionally used when one encounters *ill-conditioned* inversion problems, as will be discussed later in Section 4.7. Basically, regularisation implies an optimisation process of the "*effort*" which is put into the system by means of the source input signal $v(n)$. This is done in addition to the optimisation of the inverse filtering error "*performance*". Correspondingly, the inverse filter $H(z)$ has now to be designed in order to minimise the modified cost function

$$J = E[e^2(n)] + \beta E[v^2(n)], \tag{4.4.1}$$

The *regularisation parameter* β is a positive real constant that determines how much weight to assign to the effort term $E[v^2(n)]$. By varying β from zero to infinity, the solution changes gradually from minimising the performance $E[e^2(n)]$ only to minimising the effort cost $E[v^2(n)]$ only. Thus, regularisation represents a trade-off process between effort cost and performance error in a way that a large value of β will minimise the effort at the expense of the performance and vice versa for a small value of β.

The optimal solution for the Wiener filter which minimises J in that case is then given by

$$H(z) = \frac{1}{S(z)} \left\{ \frac{z^{k-\Delta} C_{min}(z^{-1})}{S(z^{-1}) C_{ap}(z)} \right\}_+, \tag{4.4.2}$$

where, for white noise at the input $u(n)$,

$$S(z)S(z^{-1}) = S_{rr}(z) + \beta = C_{min}(z)C_{min}(z^{-1}) + \beta . \tag{4.4.3}$$

Since a large value of β means that the optimal solution will favour a low power output from the inverse filters (low effort) at the expense of a low performance, the physical

effect of regularisation is that β is used to control the power output of the inverse filters. This suggests that β can be used to control the "duration" of the inverse filters. In reality, what happens is that the poles of the inverse filter $H(z)$ are "pushed" away from the unit circle as β is increased. Thus, by giving β an appropriate value, it is possible to control the shortest distance from the set of poles of $H(z)$ to the unit circle, which is, according to Equation (4.2.9), equivalent to controlling the duration of the time response of the inverse filters (see Figure 4.4.1).

Unfortunately, a relatively simple relationship between β and τ only exists for a single pole filter. For the more realistic case of a multi-pole filter, this relationship is considerably more complicated as the poles of the inverse filter that are close to the unit circle are pushed away by a greater distance than the poles that are further away from it [Kirkeby *et al.*, 1996a].

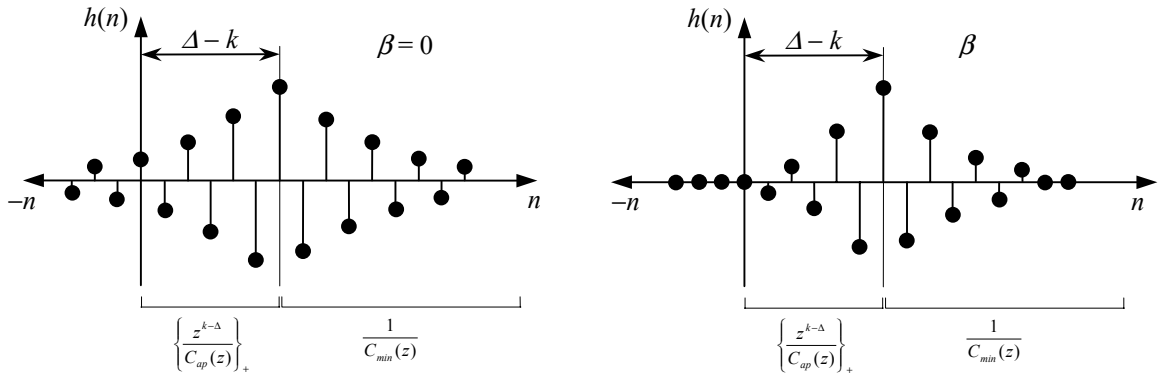

Figure 4.4.1
Effect of regularisation on the time response of the inverse filter.

As shown in Figure 4.4.1, with carefully chosen values of Δ and β, the causal part of the solution will almost all be included in the impulse response for n ≥ 0. Thus, the meaningful part of the sequence is causal. Therefore, the brackets $\{\ \}_+$ in Equation (4.4.2) may be omitted and, taking Equation (4.4.3) into account and $C_{ap}(z)C_{ap}(z^{-1}) = 1$, one can simplify the expression for the optimal inverse filter to

$$H(z) = \frac{z^{-\Delta} C(z^{-1})}{C(z)C(z^{-1}) + \beta}. \tag{4.4.4}$$

The practical implementation of this inversion method is straightforward and will be

explained later in Section 4.6.

4.5 Multi-Channel System Inversion

The generalised inversion problem for a multi-channel sound reproduction system is shown in the block diagram in Figure 4.5.1. The variables are defined in the same way as in the single channel case but now all the signals are represented by vectors and all the filters are represented by matrices of a certain dimension. Define **u**(z) as a vector of T input signals, **v**(z) as a vector of S source input or loudspeaker signals, **w**(z) as vector of R reproduced signals, **d**(z) as a vector of R desired signals, and **e**(z) as a vector of R error signals. All vectors are column vectors, so that

$$\mathbf{u}(z)=\begin{bmatrix} U_1(z) \\ \vdots \\ U_T(z) \end{bmatrix}, \quad \mathbf{v}(z)=\begin{bmatrix} V_1(z) \\ \vdots \\ V_S(z) \end{bmatrix}, \quad \mathbf{w}(z)=\begin{bmatrix} W_1(z) \\ \vdots \\ W_R(z) \end{bmatrix}, \quad \mathbf{d}(z)=\begin{bmatrix} D_1(z) \\ \vdots \\ D_R(z) \end{bmatrix}, \quad \mathbf{e}(z)=\begin{bmatrix} E_1(z) \\ \vdots \\ E_R(z) \end{bmatrix}. \tag{4.5.1}$$

Correspondingly, the multi-channel filters have the following structures: A(z) is an [$R \times T$] target matrix, C(z) is an [$R \times S$] plant (electroacoustic) matrix, and H(z) is [$S \times T$] matrix of inverse filters.

$$\mathbf{A}(z)=\begin{bmatrix} A_{11}(z) & \cdots & A_{1T}(z) \\ \vdots & \ddots & \vdots \\ A_{R1}(z) & \cdots & A_{RT}(z) \end{bmatrix} \qquad \mathbf{C}(z)=\begin{bmatrix} C_{11}(z) & \cdots & C_{1S}(z) \\ \vdots & \ddots & \vdots \\ C_{R1}(z) & \cdots & C_{RS}(z) \end{bmatrix} \tag{4.5.2}$$

$$\mathbf{H}(z)=\begin{bmatrix} H_{11}(z) & \cdots & H_{1T}(z) \\ \vdots & \ddots & \vdots \\ H_{S1}(z) & \cdots & H_{ST}(z) \end{bmatrix}$$

From the block diagram shown in Figure 4.5.1, it is straightforward to derive the following relationships:

$$\mathbf{v}(z) = \mathbf{H}(z)\mathbf{u}(z), \quad \text{a)}$$

$$\mathbf{d}(z) = \mathbf{A}(z)\mathbf{u}(z), \quad \text{b)}$$

$$\mathbf{w}(z) = \mathbf{C}(z)\mathbf{v}(z), \quad \text{c)}$$

$$\mathbf{e}(z) = \mathbf{d}(z) - \mathbf{w}(z). \quad \text{d)}$$

(4.5.3)

For a multi-channel system, the aim is now to determine a matrix of inverse filters $\mathbf{H}(z)$ that minimises the quadratic cost function

$$J = E[\mathbf{e}^T(n)\mathbf{e}(n)] + \beta E[\mathbf{v}^T(n)\mathbf{v}(n)],$$

(4.5.4)

where the superscript T denotes the transpose of its argument. As a generalisation of the single channel case [Kirkeby *et al.*, 1996a], the optimal solution for the inverse filter matrix is given by

$$\mathbf{H}_0(z) = [\mathbf{C}^T(z^{-1})\mathbf{C}(z) + \beta\mathbf{I}]^{-1}\mathbf{C}^T(z^{-1})\mathbf{A}(z).$$

(4.5.5)

In the present work, the system was restricted to a conventional two channel sound reproduction system and one listener, i.e., the number of sources $S = 2$ and the number of reproduced signals, or receivers, $R = 2$. For the purpose of crosstalk cancellation with such a system, the inverse filters have to ensure that independent desired signals $d(z)$ are reproduced at the 2 ears of a listener. In this case, the target matrix $\mathbf{A}(z)=z^{-\Delta}\mathbf{I}$, where $\mathbf{I}$ denotes a unity matrix of order $R = T$ (see Section 3.4). With no modelling delay ($\Delta = 0$), the desired signals $d(z)$ are identical to the observed signal $u(z)$, and the optimal inverse filter matrix is given by

$$\mathbf{H}_I(z) = [\mathbf{C}^T(z^{-1})\mathbf{C}(z) + \beta\mathbf{I}]^{-1}\mathbf{C}^T(z^{-1}),$$

(4.5.6)

the so-called *generalised crosstalk cancellation matrix*. Once $\mathbf{H}_I(z)$ is known, it is a trivial matter to calculate $\mathbf{H}_0(z)$ for any desired target matrix $\mathbf{A}(z)$, since, according to Equation (4.5.5) and Equation (4.5.6),

$$\mathbf{H}_0(z) = \mathbf{H}_I(z)\mathbf{A}(z).$$

(4.5.7)

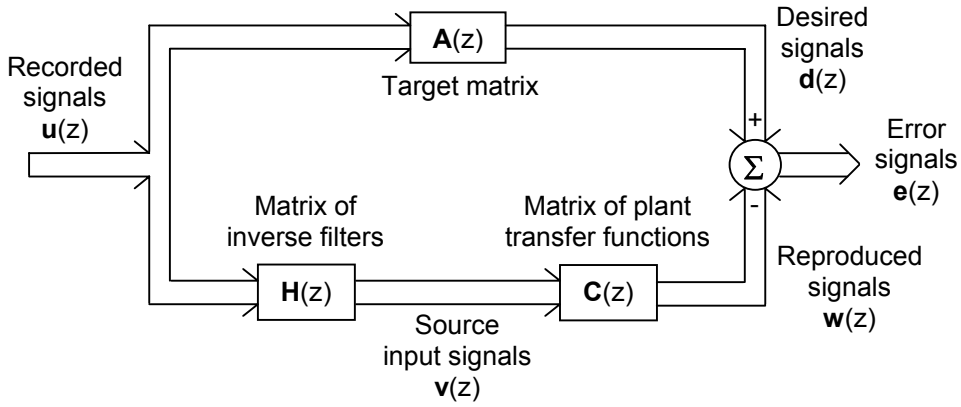

Figure 4.5.1

A block diagram of the multi-channel inversion problem.

4.6 Fast Deconvolution using Regularisation

The expression for the inverse filter's optimal z-transforms in Equation (4.5.5) is derived under the constraint that they are stable. In practice, however, the filters also have to be causal and of finite duration. Kirkeby *et al*. [1996a] presented a computationally efficient method of how to calculate a matrix of realisable causal FIR inverse filters, each containing N_h coefficients. In general, N_h must be equal to a power of two, because this method makes use of the *Fast Fourier Transforms* (FFTs).

Since the practical computation is undertaken in discrete time and discrete frequency domain, the impulse response will in effect be a result of a *circular convolution*, in the time domain, sometimes referred to as *wrap-around effect* [Oppenheim and Schafer, 1975]. In order to reduce the significance of the circular convolution effect, it is important to reduce the effective duration of the inverse filter to approximately $N_h/2$ by means of regularisation. Furthermore, it is important that the energy of the inverse filter sequence is concentrated in its central part between $n > N_h/4$ and $n < 3N_h/4$.

If an FFT is used to sample the frequency response of the optimal inverse filter $\mathbf{H}_0$ at N_h

points around the unit circle, then the value of $\mathbf{H}_0(k)$ at those frequencies is given by

$$\mathbf{H}_0(k) = [\mathbf{C}^H(k)\mathbf{C}(k) + \beta\mathbf{I}]^{-1}\mathbf{C}^H(k)\mathbf{A}(k), \tag{4.6.1}$$

where k denotes the k'th frequency line, that is the frequency corresponding to the complex number $\exp(j2\pi k/N_h)$. The superscript H stands for the Hermitian operator which transposes and conjugates its argument [Nelson and Elliott, 1992, Appendix A]. Consequently, the generalised crosstalk cancellation matrix, according to Equation (4.5.6), is given by

$$\mathbf{H}_I(k) = [\mathbf{C}^H(k)\mathbf{C}(k) + \beta\mathbf{I}]^{-1}\mathbf{C}^H(k). \tag{4.6.2}$$

Thus, for the practical implementation of the algorithm in order to calculate the impulse responses of the inverse filters $\mathbf{h}_I(n)$, the following steps are necessary:

1. Calculate C(k) by taking $[R \times S]$ N_h-point FFTs of the plant impulse responses $c_{rs}(n)$.
2. For each of the N_h values of k, calculate the $[S \times R]$ matrix $\mathbf{H}_I(k)$ from Equation (4.6.2).
3. Calculate $\mathbf{h}_I(n)$ by taking $[S \times R]$ N_h-point inverse FFTs of the elements of $\mathbf{H}_I(k)$ followed by a cyclic shift of $N_h/2$ points in order to implement the modelling delay.

It should be mentioned that this method, referred to as "*fast deconvolution*", is typically several hundred times faster than a conventional time domain steepest descent algorithm. However, this frequency domain method requires relatively long inverse filters. Thus, it should be used only when hardware- or memory restrictions are not too severe. It is necessary to set the regularisation parameter β to an appropriate value, but the ecaxt value of β is usually not critical, and can be determined by a few trial-and-error experiments.

4.7 Ill-conditioning and the effect of regularisation

As described in the previous sections, the whole physical process of inverse filtering is solved numerically by means of equation systems which are usually cast into matrix form. From matrix algebra, it is well known that the inverse of a matrix **C** can be calculated only when **C** is not *singular*, i.e., its determinant is not zero. Any [$R \times S$] matrix **C** can be factorised into a product of three matrices **U**, **Σ**, and $\mathbf{V}^{\mathrm{H}}$, such as

$$\mathbf{C} = \mathbf{U}\,\mathbf{\Sigma}\,\mathbf{V}^{\mathrm{H}} = \mathbf{U}\begin{bmatrix} \sigma_1 & & \\ & \ddots & \\ & & \sigma_S \end{bmatrix}\mathbf{V}^{\mathrm{H}}, \tag{4.7.1}$$

where **U** and **V** are *orthonormal*. **Σ** is a diagonal matrix containing the *singular values* σ_S of **C** where $\sigma_1 \geq \sigma_2 \geq \ldots \geq \sigma_S$. Therefore, Equation (4.7.1) is called the *singular value decomposition* of **C** [Bronstein and Semendjajew, 1996], which illustrates some important properties of linear equation systems. The singular values are defined as the square roots of the eigenvalues of $\mathbf{C}^{\mathrm{H}}\mathbf{C}$, and since $\mathbf{C}^{\mathrm{H}}\mathbf{C}$ is Hermitian, they are always real and positive [Kreyszig, 1983].

If **Σ** contains a singular value of zero, the matrix **C** does not have *full rank*, i.e., there is a linear dependence between its columns. In that case, the matrix **C** is said to be singular and, consequently, its inversion does not exist. If **C** is not singular, its exact inverse is given by

$$\mathbf{C}^{-1} = \left[\mathbf{U}\,\mathbf{\Sigma}\,\mathbf{V}^{\mathrm{H}}\right]^{-1} = \mathbf{V}\,\mathbf{\Sigma}^{-1}\,\mathbf{U}^{\mathrm{H}} = \mathbf{V}\begin{bmatrix} 1/\sigma_1 & & \\ & \ddots & \\ & & 1/\sigma_S \end{bmatrix}\mathbf{U}^{\mathrm{H}}. \tag{4.7.2}$$

In theory, a singular value is either zero or not zero, but when singular values are calculated by a numerical algorithm, a true singular value of zero will usually come out as a very small number [Press *et al.*, 1992]. Similarly, if the equations are close to being linearly dependent, but without being exactly linearly dependent, they will also result in a very small singular value. A very small singular value σ_S makes the corresponding element $1/\sigma_S$ in $\mathbf{\Sigma}^{-1}$ very large. This phenomenon is called *ill-conditioning*, and it is usually undesirable because it makes the solution very sensitive to small changes in the data.

A quantifier of the ill-conditioning problem is the so-called *condition number*,

sometimes referred to as the spectral condition number [Wilkinson, 1965], which is defined as the ratio between the maximum and the minimum singular value of **C**,

$$\kappa(\mathbf{C}) = \frac{\sigma_{\max}}{\sigma_{\min}} . \tag{4.7.3}$$

A well-conditioned matrix has a condition number close to one, while an ill-conditioned matrix has a large condition number.

Considering the crosstalk cancellation problem for a typical two channel sound reproduction system, as it was applied in the present work, $\mathbf{C}(\omega)$ is a [2 × 2] matrix of electro-acoustic transfer functions between the two loudspeakers and the two microphones or ears. For the arrangement given in Figure 3.4.1 and according to Equation 3.4.1, ill-conditioning will occur for the following situations:

1. $C_{LL}(\omega) = C_{RL}(\omega) = 0$ or $C_{RR}(\omega) = C_{LR}(\omega) = 0$. This occurs when all transfer functions from all loudspeakers to any of the microphones are zeros at the same frequency, leading to a zero row in the matrix $\mathbf{C}(\omega)$. In practice, this may happen when the frequency responses of all loudspeakers have a notch at the same frequency, or the concerned microphone is insensitive at a certain frequency.

2. $C_{LL}(\omega) = C_{LR}(\omega) = 0$ or $C_{RR}(\omega) = C_{RL}(\omega) = 0$. This occurs when all transfer functions from any of the loudspeakers to all microphones are zeros at the same frequency, leading to a zero column in the matrix $\mathbf{C}(\omega)$. Similar practical causes as those mentioned above may also be valid in this case.

3. $C_{LL}(\omega)\cdot C_{RR}(\omega) = C_{LR}(\omega)\cdot C_{RL}(\omega)$. This situation occurs in special symmetrical acoustic arrangements. For example, at low frequencies, the difference between the direct and the crosstalk path length is very small compared to the wavelength. Therefore, all four transfer functions show maximum similarity between each other, which leads to ill-conditioning. This explains the particular difficulties of crosstalk cancellation systems at low frequencies as mentioned in Section 3.4.

For the case of the crosstalk cancellation problem, ill-conditioning is undesirable

since it tends to make the inverse filter's output signals **v** very large. These signals in turn represent the input signals to audio amplifiers which drive the reproduction loudspeakers of the system. Thus, without any precautions, the inverse filters would excessively amplify the ill-conditioned frequencies, which likely leads to saturation of the audio amplifiers and/or damage of the loudspeakers.

If regularisation is applied to the system inversion, the optimal solution for the inverse filters will be forced to a lower power output, as discussed in Section 4.4. Thus, by setting β to an appropriate value it can be ensured that the system does not boost any ill-conditioned frequencies to much. In other words, by means of the regularisation parameter β, it can be exactly specified how "non-singular" the plant matrix C should be.

Chapter 5
Optimal Source Distribution

5.1 Introduction

As discussed in the previous chapter, the problem of ill-conditioning leads to a lack of robustness of the system inversion involved with crosstalk cancellation. Moreover, the system inversion requires amplification of the signal at certain frequencies and attenuation of the signal at other frequencies. This amplification directly results in a *loss of dynamic range* of the system. The technique of regularisation allows to reduce both dynamic range loss and the sensitivity to small errors around ill-conditioned frequencies.

In general, as already indicated in Section 4.7, the conditioning of a system depends on frequency and on the positions of the reproduction loudspeakers relative to the microphones (ears). Investigations of the problem with respect to frequency and the system's geometry were undertaken by Takeuchi and Nelson [2000a; 2000b]. Thereby, based on an analysis of a free field model of the system, it was shown that if one were able to vary the loudspeaker span as a function of frequency, the problems of loss of dynamic range and robustness, could be ideally solved. This idea has resulted in the proposal of a new system, referred to as the *"Optimal Source Distribution"* or "*OSD"* system, by Takeuchi and Nelson [2000a; 2000b]. In the present work, such a system was put into practice and its performance investigated. Therefore, based on the publications of Takeuchi and Nelson [2000a; 2000b], the essential points in the theory and the idea behind the „OSD" system as well as practical design considerations will be described in this chapter.

5.2 Free field model of the system

In Figure 5.2.1, the geometry of the 2-source 2-receiver system under investigation is illustrated. The fundamental problems with regard to the system inversion can be outlined here, where the control of two monopole receivers with two monopole sources is considered. For the simple case under free field conditions, the effect of path length difference dominates the problem, such as the plant transfer function matrix can be modelled as

$$\mathbf{C} = \frac{\rho_0}{4\pi}\begin{bmatrix} \mathrm{e}^{-\mathrm{j}kl_1}/l_1 & \mathrm{e}^{-\mathrm{j}kl_2}/l_2 \\ \mathrm{e}^{-\mathrm{j}kl_2}/l_2 & \mathrm{e}^{-\mathrm{j}kl_1}/l_1 \end{bmatrix}, \tag{5.2.1}$$

An $\mathrm{e}^{\mathrm{j}\omega t}$ time dependence is assumed with $k = \omega/c_0$, and where ρ_0 and c_0 denote the medium density and the speed of sound, respectively. By defining $g = l_1/l_2$ as the ratio of the path lengths, and $\Delta l = l_2 - l_1$ as the path lengths difference, Equation (5.2.1) may be expressed as

$$\mathbf{C} = \frac{\rho_0\,\mathrm{e}^{-\mathrm{j}kl_1}}{4\pi l_1}\begin{bmatrix} 1 & g\,\mathrm{e}^{-\mathrm{j}k\Delta l} \\ g\,\mathrm{e}^{-\mathrm{j}k\Delta l} & 1 \end{bmatrix}. \tag{5.2.2}$$

Now consider the case

$$\mathbf{d} = \frac{\rho_0 \mathrm{e}^{-\mathrm{j}kl_1}}{4\pi l_1}\begin{bmatrix} D_1(\mathrm{j}\omega) \\ D_2(\mathrm{j}\omega) \end{bmatrix}, \tag{5.2.3}$$

i.e., the desired signals **d** are the acoustic pressure signals which would have been produced by the closer sound source in each case and whose values are either $D_1(\mathrm{j}\omega)$ or $D_2(\mathrm{j}\omega)$ without disturbance due to the other source (crosstalk). This enables a description of the effect of system inversion as well as ensuring a causal solution. The inverse filter matrix **H** can be obtained from the exact inverse of **C** and, considering Equation (5.2.3), it can be written as

$$\mathbf{H} = \begin{bmatrix} 1 & g\,\mathrm{e}^{-\mathrm{j}k\Delta l} \\ g\,\mathrm{e}^{-\mathrm{j}k\Delta l} & 1 \end{bmatrix}^{-1} = \frac{1}{1-g^2\mathrm{e}^{-2\mathrm{j}k\Delta l}}\begin{bmatrix} 1 & -g\,\mathrm{e}^{-\mathrm{j}k\Delta l} \\ -g\,\mathrm{e}^{-\mathrm{j}k\Delta l} & 1 \end{bmatrix}. \tag{5.2.4}$$

When $l >> \Delta r$, the approximation $\Delta l \approx \Delta r \sin\theta$ may be applied, where 2θ is the "*source span*" of the system. Thus, the inverse filter matrix **H** is expressed as

$$\mathbf{H} = \frac{1}{1-g^2\mathrm{e}^{-2\mathrm{j}k\Delta \mathrm{r}\sin\theta}}\begin{bmatrix} 1 & -g\mathrm{e}^{-\mathrm{j}k\Delta \mathrm{r}\sin\theta} \\ -g\mathrm{e}^{-\mathrm{j}k\Delta \mathrm{r}\sin\theta} & 1 \end{bmatrix}, \qquad 0 < \theta \le (\pi/2). \tag{5.2.5}$$

The magnitude of the elements of **H** ($|H_{mn}(j\omega)|$) show the amplification of the desired signals required by each inverse filter in **H**. The maximum amplification of the source strengths can be found from the *2-norm* of **H** ($\|\mathbf{H}\|$), which is the largest of the singular values of **H**.

$$\|\mathbf{H}\| = \max(\sigma_o, \sigma_i)$$

(5.2.6)

$$\sigma_o = \frac{1}{\sqrt{\left(1 - g\mathrm{e}^{-\mathrm{j}k\Delta r\sin\theta}\right)\left(1 - g\mathrm{e}^{\mathrm{j}k\Delta r\sin\theta}\right)}},\ \sigma_i = \frac{1}{\sqrt{\left(1 + g\mathrm{e}^{-\mathrm{j}k\Delta r\sin\theta}\right)\left(1 + g\mathrm{e}^{\mathrm{j}k\Delta r\sin\theta}\right)}}.$$

The singular values σ_o and σ_i correspond to orthogonal components of the inverse filters. Thereby, the amplification factor of the *out-of-phase component* of the desired signals is denoted by σ_o, whereas σ_i corresponds to the amplification factor of the *in-phase component* of the desired signals. Figure 5.2.2 illustrates σ_o, σ_i, and $\|\mathbf{H}\|$ with respect to frequency and source span, represented by the product $k\Delta r\sin\theta$. It can be seen that $\|\mathbf{H}\|$ changes periodically and has peaks where k and θ satisfy the relationship

$$k\Delta r\sin\theta = \frac{n\pi}{2}$$

(5.2.7)

with even values of the integer number n. The singular value σ_o has peaks at n = 0, 4, 8, ... where the system has difficulties to reproduce the out-of-phase component of the desired signals and σ_i has peaks at n = 2, 6, 10, ... where the system has difficulties to reproduce the in-phase component.

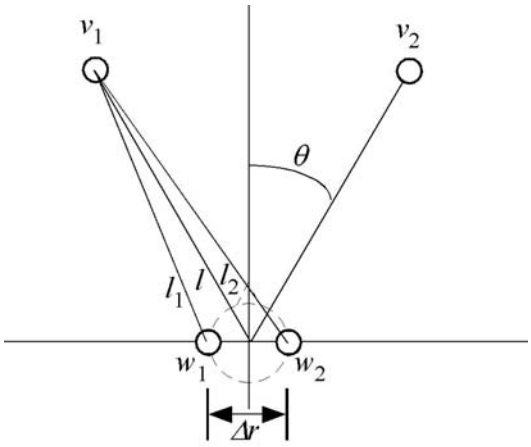

Figure 5.2.1

Geometry of a 2-source 2-receiver system.

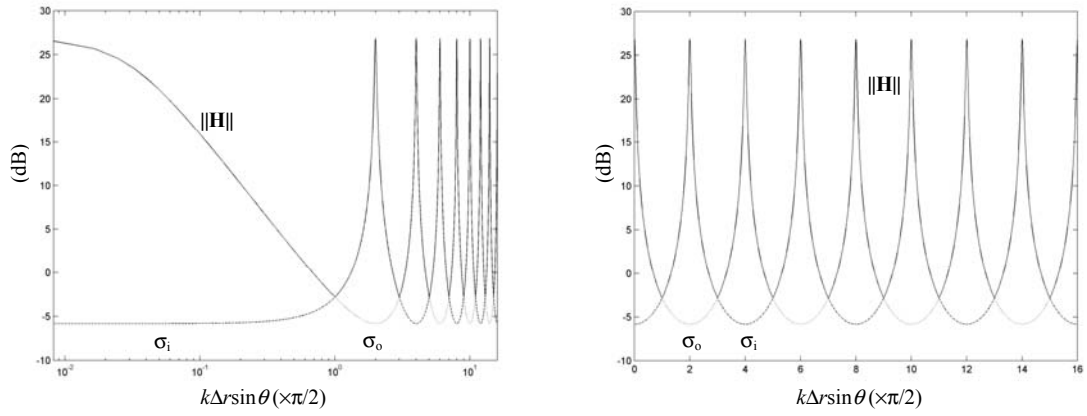

[a] [b]

Figure 5.2.2

Norm ||**H**|| and singular values σ_o, σ_i of the inverse filter matrix **H** as a function of $k\Delta r\sin\theta$. [a] Logarithmic scale. [b] Linear scale.

5.3 Dynamic Range Loss

In practice, since the maximum source output is given by $||\mathbf{H}||_{\max}$, it must be within the range of the system in order to avoid clipping of the signals. As illustrated in Figure 5.3.1, the required amplification directly results in a loss of dynamic range. The level of the output source signal **v** and the resulting level of the acoustic pressure **w** are plotted both with and without system inversion, assuming that the maximum output level and the dynamic range of the system are the same. While the frequencies where the peaks occur do not affect the amount of dynamic range loss, the magnitude of the peaks do. The amount of dynamic range loss is defined by the difference between the signal level at the receiver with one monopole source and the signal level reproduced by two sources having the same maximum source strength when the system is inverted. Since ||**H**|| here is normalised by the case without system inversion by Equation (5.2.3), the dynamic range loss Γ is given by

$$\Gamma = \left\|\mathbf{H}\right\|_{\max} = \frac{1}{1-g}. \tag{5.3.1}$$

In Figure 5.3.2, it is shown how the dynamic range loss varies as a function of the source span. Since $g \approx 1 - \Delta r \sin\theta / l$, the dynamic range loss Γ can be approximated as

$$\Gamma \approx \frac{l}{\Delta r \sin\theta}. \tag{5.3.2}$$

Thus, it can be concluded that the dynamic range loss decreases with increasing source span θ.

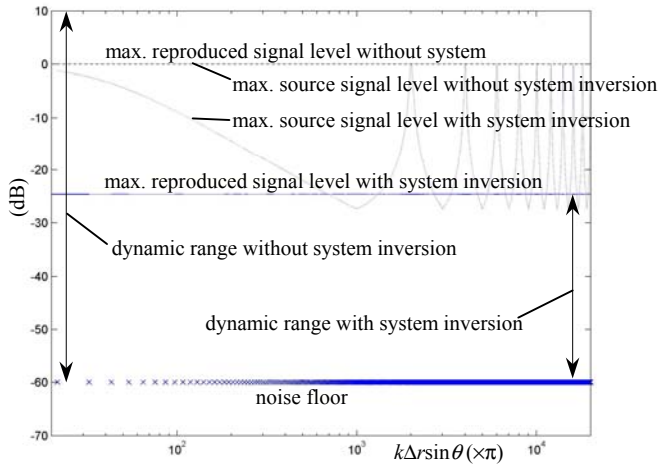

Figure 5.3.1

Dynamic range loss due to system inversion.
Source signal levels are normalised by the maximum source signal level without system inversion. Reproduced signal levels are normalised by the reproduced signal level without system inversion. A noise floor is assumed at –60 dB to provide an aid for the illustration of the dynamic range.

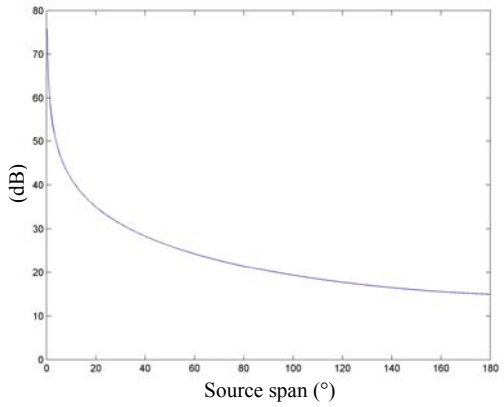

Figure 5.3.2

Dynamic range loss as a function of source span.

5.4 Robustness of the System Inversion

As mentioned in Section 4.7, the conditioning of a system is usually quantified by means of the condition number $\kappa(\mathbf{C})$. For the system under investigation, the condition number is given by

$$\kappa(\mathbf{C}) = \left\|\mathbf{C}\right\|\left\|\mathbf{C}^{-1}\right\| = \left\|\mathbf{C}\right\|\left\|\mathbf{H}\right\| = \left\|\mathbf{H}^{-1}\right\|\left\|\mathbf{H}\right\| = \max\left(\sqrt{\frac{\left(1+ge^{-jk\Delta r\sin\theta}\right)\left(1+ge^{jk\Delta r\sin\theta}\right)}{\left(1-ge^{-jk\Delta r\sin\theta}\right)\left(1-ge^{jk\Delta r\sin\theta}\right)}}, \sqrt{\frac{\left(1-ge^{-jk\Delta r\sin\theta}\right)\left(1-ge^{jk\Delta r\sin\theta}\right)}{\left(1+ge^{-jk\Delta r\sin\theta}\right)\left(1+ge^{jk\Delta r\sin\theta}\right)}} \right) \tag{5.4.1}$$

Observing Figure 5.4.1 reveals that the frequencies which give peaks of $\kappa(\mathbf{C})$, are the same as those which give peaks of the norm $\|\mathbf{H}\|$. At these frequencies, the system inversion is very sensitive to small errors in the assumed plant $\mathbf{C}$. Furthermore, since $\mathbf{v} = \mathbf{C}^{-1}\mathbf{w}$ (according to Equation 4.5.3c) and $\kappa(\mathbf{C}^{-1}) = \kappa(\mathbf{C})$, the reproduced signals $\mathbf{w}$ are less robust to small changes in the inverse filter $\mathbf{H}$, where $\kappa(\mathbf{C})$ is large. Therefore, even if $\mathbf{C}$ does not contain any errors, the reproduction of the signals at the receiver is too sensitive to the small errors in the inverse filter matrix $\mathbf{H}$ to be useful. On the contrary, $\kappa(\mathbf{C})$ is small around the frequencies where n is an odd integer number in Equation (5.2.7). Around these frequencies, a practical and close to ideal inverse filter matrix $\mathbf{H}$ is easily obtained.

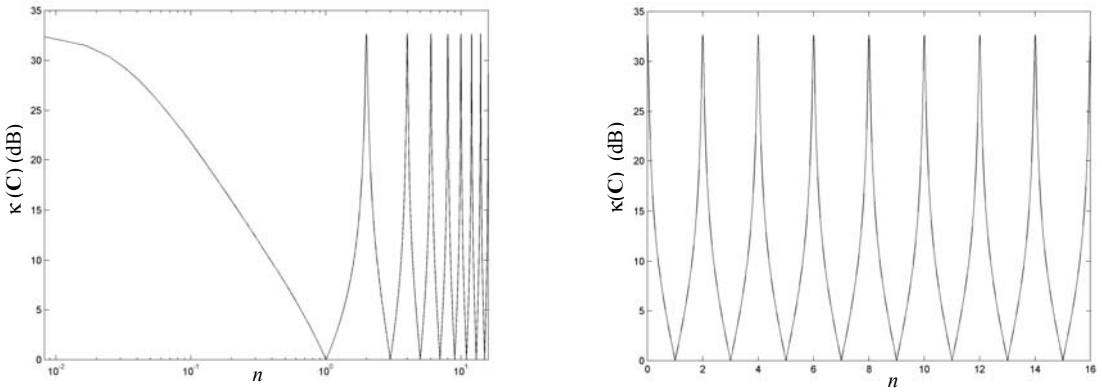

[a] [b]

Figure 5.4.1

Condition number $\kappa(\mathbf{C})$ as a function of n. [a] Logarithmic scale. [b] Linear scale.

5.5 Effect of Regularisation

As already explained in the previous chapter, it is possible to reduce the excess amplification of ill-conditioned frequencies by means of regularisation. Thus, the regularisation parameter β penalises large values of **H** and hence limits the dynamic range loss of the system. Since ||**H**|| is normalised by the case without system inversion by Equation (5.2.3), the regularisation parameter limits the dynamic range loss to less than about

$$\Gamma \approx -10\log_{10}\beta - 6 \text{ (dB)}. \tag{5.5.1}$$

However, the regularisation parameter inevitably introduces a small error in the inversion process. This gives rise to a problem for the filter design for frequencies where $\kappa(\mathbf{C})$ is large. As shown in Figure 5.5.1, while the dynamic range loss is reduced due to regularisation, the system performs less control (crosstalk cancellation) around these frequencies. The contribution of the correct desired signals (denoted by R_{11} and R_{22}) is reduced only slightly but the contribution of the wrong desired signals (R_{12} and R_{21}, the crosstalk component) is increased significantly. This problem is significant at lower frequencies (n<1 in Equation (5.2.7)) in the sense that the region without crosstalk suppression is large, and at higher frequencies (n>1) in the sense that there are many frequencies at which the plant is ill-conditioned. With an equivalent dynamic range loss, making the source span larger leads to a better control performance at lower frequencies but a poorer performance at higher frequencies. On the contrary, making the source span smaller leads to better control performance at higher frequencies but poorer performance at lower frequencies.

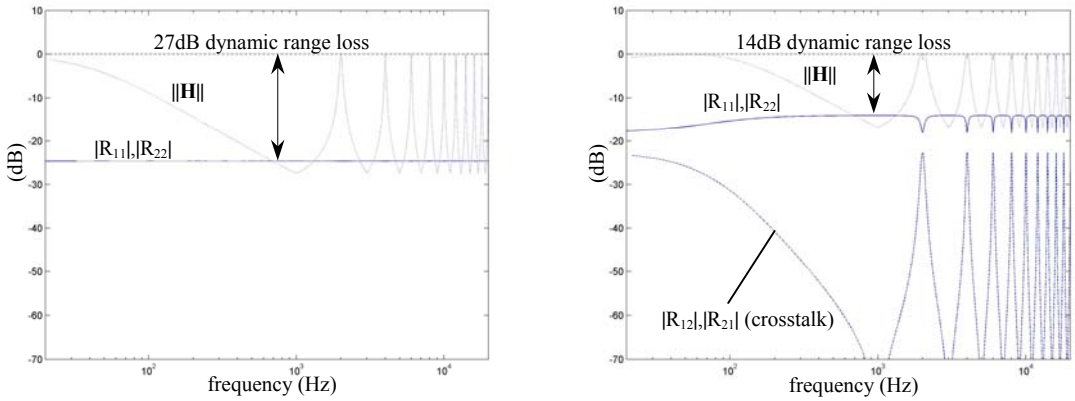

[a] [b]

Figure 5.5.1

Dynamic range improvement and loss of control performance due to regularisation.
a) Without regularisation. [b] With regularisation.

5.6 Principle of the "OSD" system

As discussed above, there is always a trade-off between allowed dynamic range loss, robustness and control performance. However, a system which aims to overcome these fundamental problems, referred to as the *Optimal Source Distribution* (OSD) system, is proposed in the following.

In the analysis above, it was shown that systems with the source span where n is an odd integer number in Equation (5.2.7) give the best control performance as well as the best robustness. This implies that the optimal source span 2θ must vary continuously as a function of frequency in order to satisfy

$$2\theta = 2\arcsin\left(\frac{n\pi}{2k\Delta r}\right), \tag{5.6.1}$$

for n being an odd integer number. Thereby, Equation (5.6.1) corresponds to the rewritten form of Equation (5.2.7) in terms of the source span 2θ. According to this, as shown in Figure 5.6.1, the source span becomes smaller as the frequency becomes higher. With this assumption, Equation (5.2.5) can be expressed as

$$\mathbf{H} = \frac{1}{1+g^2}\begin{bmatrix} 1 & -\mathrm{j}g \\ -\mathrm{j}g & 1 \end{bmatrix}. \tag{5.6.2}$$

Note that $\|\mathbf{H}\| = 1/\sqrt{2}$ and $\kappa(\mathbf{C}) = 1$ for all frequencies. Therefore, there is no dynamic range loss compared to the case without system inversion. In fact, the dynamic range is gained by 3dB since the two orthogonal components of the desired signals are $\pi/2$ out of phase. The error in calculating the inverse filter is small and the system has very good control over the reproduced signals. The system is also very robust to changes in the plant matrix.

According to Equation (5.6.1), the range of source span is given by the frequency range of interest. In Figure 5.6.1 it can be seen that a smaller value of n gives a smaller source span for the same frequency. Therefore, the smallest source span $2\theta_h$ for the same high frequency limit is given by $n = 1$. This value is about 8° to give optimal control of the sound field at two positions separated by the distance between two ears (about 0.13m for a KEMAR dummy head) up to a frequency of 20kHz.

Equation (5.2.7) can also be rewritten in terms of frequency as

$$f = \frac{nc_0}{4\Delta r \sin\theta}. \tag{5.6.3}$$

The smallest value of n gives the lowest frequency limit for a given source span. Because $\sin\theta \le 1$,

$$f \ge \frac{nc_0}{4\Delta r}, \tag{5.6.4}$$

i.e., the physically maximum source span of $2\theta = 180°$ gives the low frequency limit f_l. Obviously, the lowest low frequency limit is given by $n = 1$. For a system designed to control the sound field at the two ear positions, this value is about $f_l = 300 \sim 400$ Hz.

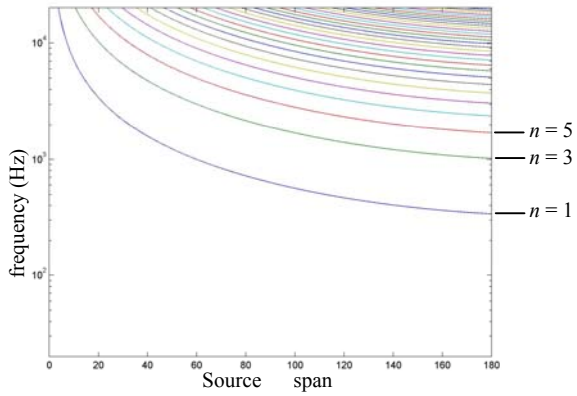

Figure 5.6.1

The principle of the "OSD" system. The relationship between source span and frequency for different odd integer numbers *n*.

5.7 Practical Discrete System

The „OSD"-principle requires a pair of monopole transducers whose span varies continuously as a function of frequency. In practice, however, this type of transducers are currently not available. However, a practical system can be realised by discretising the source span as illustrated in Figure 5.7.1. This dicretisation and the allocation of a certain frequency range to a certain transducer span is equivalent to allowing *n* to have some width, say $\pm\nu\,(0 < \nu < 1)$. This in turn results in a small amount of dynamic range loss and slightly reduced robustness, but the frequency region, for a given span, where the plant matrix **C** is reasonably well conditioned, is relatively wide around the optimal frequency, as can be seen in Figure 5.7.2 [a]. Therefore, a certain transducer span can nevertheless be allocated to cover a certain frequency range where control performance and robustness of the system are still reasonably good. Such a practical system can also be interpreted as making use of better conditioned frequencies only and excluding ill-conditioned frequencies by limiting the frequency range to be used by a certain transducer span. By making use of different transducer spans for different frequency ranges, a system may be constructed which can eventually cover almost the whole audible frequency range.

It should be noted that this is still a simple "2-channel" system where only two independent control signals are necessary to create any form of virtual auditory images. The difference from the conventional 2-channel system is that the two control signals are divided into multiple frequency bands and fed into the different pairs of driver units with different spans.

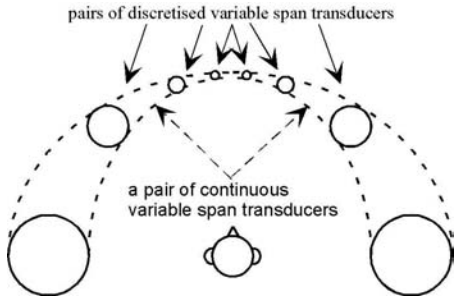

Figure 5.7.1

Dicretisation of the variable source span.

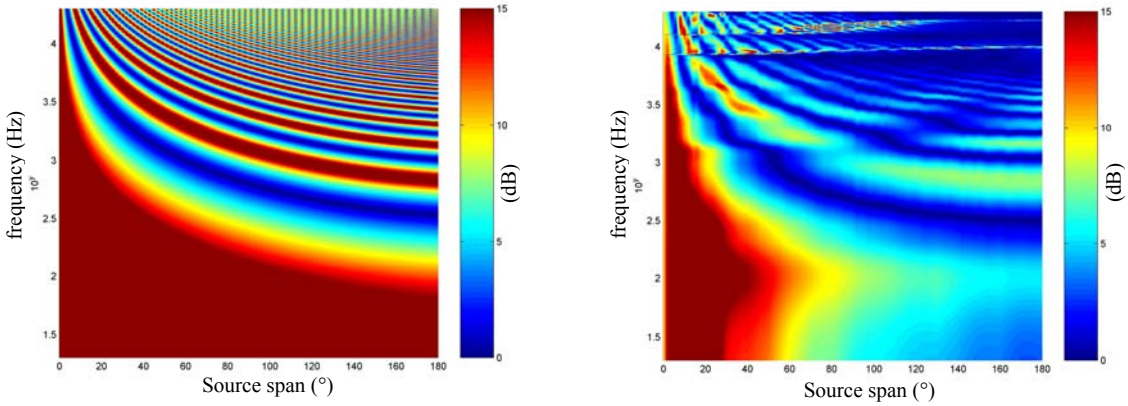

[a] [b]

Figure 5.7.2

Condition number $\kappa(\mathbf{C})$ as a function of source span and frequency. [a] of a free field plant matrix $\mathbf{C}$. [b] of a HRTF plant matrix $\mathbf{C}$.

5.8 Design Considerations

The relationships between the different parameters, such as regularisation, loss of dynamic range, robustness, frequency, and source span, suggest various ways of how to choose an appropriate compromise by means of discretisation of the transducer span and division of the frequency range.

First of all, it is important to design the system to ensure a condition number that is as small as possible over a frequency range that is as wide as possible. Therefore, the spans for each pair of transducers in each frequency range can be decided to ensure that the smallest possible values of ν are used over the whole frequency range of interest above f_l. The condition number $\kappa(\mathbf{C})$ of the free field plant matrix is plotted in Figure 5.7.2 [a] as a function of frequency and source span for the audible frequency range (20Hz ~ 20kHz). A similar trend can clearly be recognised for the condition number of a more realistic HRTF[1] plant matrix, which is plotted in Figure 5.7.2 [b].

As can be seen from Figure 5.6.1, in the higher frequency range where the source span is very small, the frequency range to be covered is very sensitive to small differences in the transducer span. On the contrary, it is very insensitive to the source span at lower frequencies. Consequently, the range of practical spans for the low frequency units is very large, which can practically be anywhere from 60° to 180° introducing only a very slight increase of f_l.

Another possible design strategy is to decide the transducer spans and frequency ranges to be covered by each pair of driver units (i.e. range of n) in terms of a tolerable dynamic range loss. The dynamic range loss of the entire system is now given by the maximum value among the values given by each discretised transducer span.

If less dynamic range loss is allowed, a larger regularisation parameter is needed to suppress the amplitude of the inverse filter. This in turn results in considerably more crosstalk, especially in the ill-conditioned low frequency region. Therefore, it may also be an idea to design the system by selecting the required low frequency crosstalk cancellation performance.

---

[1] HRTFs were measured on a KEMAR dummy head [Gardner and Martin, 1994]. Data from `ftp://sound.media.mit.edu/pub/Data/KEMAR`.

5.9 Examples of "OSD" systems

A thorough discussion of the considerations involved with the practical design of "OSD" systems is given in Takeushi and Nelson [2000a; 2000b]. According to these considerations, some examples of "OSD" systems were designed and investigated. In the following, the most important examples, which were of use for the later practical realisation of such systems, will be outlined.

- 3-way systems

Figure 5.9.1 illustrates the frequency/span region with $0{,}3 < n < 1{,}7$ (i.e., $\nu = 0{,}7$). In general, all examples aim to ensure a condition number that is as small as possible over a frequency range that is as wide as possible. Therefore, the transducer spans for the high frequency units and the low frequency units were chosen at the two extreme positions which gives $\nu = 0{,}7$. Consequently, the high frequency units span 6,2° and cover the frequencies up to 20kHz while a pair of low frequency units spanning 180° is chosen to cover the frequencies as low as possible. The span for the mid frequency units is 32°.

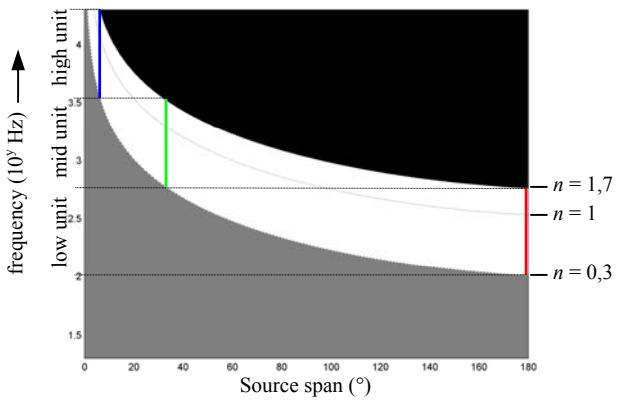

Figure 5.9.1

The frequency/span region for systems with $n \approx 1$ and $\nu = 0{,}7$ with an example of descretisation for a 3-way system.

The cross-over frequencies of about 600Hz and 4kHz are determined by $n = 0{,}3$ and $n = 1{,}7$ for each pair of units. As shown in Figure 5.9.2, the condition number (denoted by the xxxx-

line) always remains limited due to the "take-over" by the other pair of units. According to Takeuchi and Nelson [2000a], a minimum dynamic range loss of about 7dB with a limit for the lowest frequency $f_l \approx 110$Hz can be achieved with this arrangement. With regularisation of 7dB for frequencies below f_l, the low frequency units can also cover frequencies down to about 100Hz with reasonable crosstalk cancellation of more than 20dB. By allowing a dynamic range loss of 13dB, the low frequency units can even cover frequencies down to 20 Hz with more than 20dB crosstalk suppression.

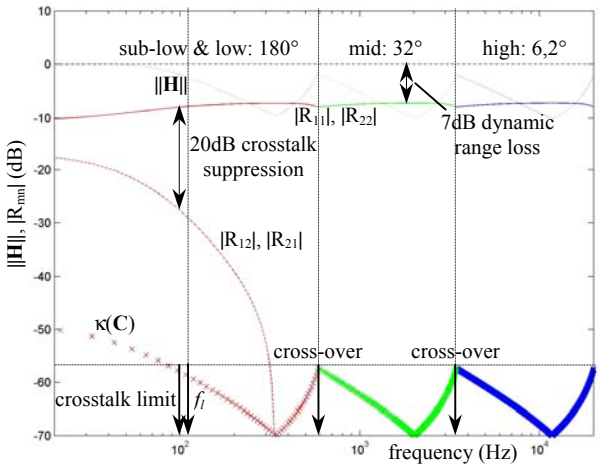

Figure 5.9.2
An example of a 3-way system with regularisation for 7dB dynamic range loss.

- 2-way systems

As the discretisation becomes coarser, more frequency regions become severely ill-conditioned. Figure 5.9.3 shows an example of a 2-way system which is obtained by omitting the woofer units from the 3-way system ($\nu \approx 0.7$) described above. The dynamic range in this example is regularised to 18dB. The mid-low frequency units cover the frequency range below $f_l \approx 600$Hz with a crosstalk cancellation performance of more than 20dB. The frequencies below 200Hz are also covered with a crosstalk cancellation performance less than 20dB. The cross-over frequency is now at around 4kHz and the conditioning above $f_l \approx$

600Hz is as good as for the 3-way system.

With increasing transducer spans, the low frequency crosstalk performance is improved at the expense of the robustness at higher frequencies. Thus, the condition number of a 2-way system with larger source spans is much higher compared to the example given in Figure 5.9.3.

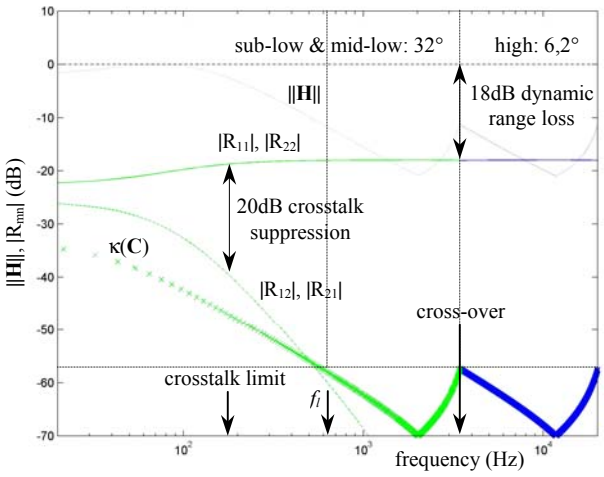

Figure 5.9.3

An example of a 2-way system with $n \approx 1$ and $\nu = 0{,}7$ with regularisation for 18dB dynamic range loss.

- 1-way systems

The coarsest discretisation is given by an example of a 1-way virtual acoustic imaging system In that case, the benefit available with this principle is very limited. The dynamic range loss is very high compared to the previous examples and very large condition numbers are noticeable in a wide range of low frequencies and at the high frequency end. When regularisation is used to limit the dynamic range loss, the lowest frequency with reasonable crosstalk cancellation performance is too high to be of any use for virtual acoustic imaging.

Such a system is not practical anyway since a practical single transducer which can cover the whole audible frequency range is not available. However, it is possible to come to a compromise design by sacrificing the system's performance in the high and low frequency ranges where a practical full-range unit can not be used anyway.

- "Multi-region" systems

It is also possible to compromise further by utilising two or more regions of n. This approach is beneficial when one attempts to cover a wider frequency range with a smaller number of transducer pairs. The "Stereo Dipole" system [Kirkeby *et al.*, 1996b], which uses a source span of 10°, is such a system. The simplest case with a single pair of transducers is when the regions of $0 < n < 2$ and $2 < n < 4$ are utilised. In that case, the cross-talk cancellation performance in the low frequency range is improved compared to a 1-way system described above. However, the system makes also use of the region where $n = 2$ (even). Thus, the system has little control and is not robust at the frequencies corresponding to this (unusable) region of n.

5.10 Inverse filtering when using cross-over filters

In order to distribute the frequencies of the signal to the appropriate pair of driver units, cross-over filters (low pass, high pass or band pass filters) have to be applied to the "OSD" system. Since an ideal filter which gives a rectangular window in the frequency domain can not be realised in practice, there are frequency regions around the cross-over frequency where multiple pairs of driver units are contributing to the synthesis of the reproduced signals **w**. Therefore, it is important to ensure that this transition region is also within the well-conditioned region of the principle.

For the practical design, the plant matrix **C** of the system needs to be known in order to enable an appropriate inverse filtering for the crosstalk cancellation. The most obvious way of obtaining **C** is when the cross-over network is included in the measurements, as it is illustrated for a 2-way system in Figure 5.10.1. In this case, the plant **C** consists of a single [2 × 2] matrix of electro-acoustic transfer functions and the obtained inverse filter matrix **H** automatically compensates for the response of the cross-over network and the interaction

between different pairs of driver units around the cross-over frequency.

Alternatively, one can design m inverse filter matrices $\mathbf{H}_1$, $\mathbf{H}_2$, ... $\mathbf{H}_m$ for plants $\mathbf{C}_1$, $\mathbf{C}_2$, ... $\mathbf{C}_m$ of m pairs of driver units (Figure 5.10.2). In this case, around cross-over frequencies, a virtual acoustic environment is synthesised with two adjacent inverse filter matrices. Provided the cross-over filters behave well, the correct desired signals are reproduced as a simple sum of the two involved desired signals. Since the system inversion is now independent of the cross-over filters, the cross-over filters can be applied both after and prior to the inverse filters.

It is also possible to obtain a $[2 \times 2m]$ plant matrix $\mathbf{C}$, between each driver unit and the two ears separately, where m is the number of driver pairs (Figure 5.10.3).
The system is now *underdetermined* and a $[2m \times 2]$ pseudo inverse filter matrix $\mathbf{H}$ is given by

$$\mathbf{H} = \mathbf{C}^{\mathrm{H}}\left[\mathbf{C}\mathbf{C}^{\mathrm{H}} + \beta\mathbf{I}\right]^{-1}. \tag{5.10.1}$$

This solution ensures that the least effort (smallest output) of the transducers is used in providing the desired signals at the listener's ears. The net result is similar to the case with a single $[2 \times 2]$ plant matrix inversion described above.

When the cross-over filters are omitted, the problem becomes a conventional multi-channel system, contrary to the "OSD" system which is a multi-way system. In this case, the plant matrix is again of dimension $[2 \times 2m]$ where $2m$ is the number of channels. The $[2m \times 2]$ pseudo inverse filter matrix $\mathbf{H}$ given by Equation (5.10.1) automatically distributes the signal to different drivers so that least effort is required. This property is beneficial since ill-conditioned frequencies and HRTF-minima are automatically avoided. On the other hand, with the absence of the cross-over filters, multi-channel systems do not have some of the merit of the "OSD" system. Even though the inversion of multi-channel systems ensures that most of the lower frequency signals are distributed to the pair of units with larger span (woofers), some of the higher frequency signals are also distributed to the woofers. This is because due to its periodic nature there are a number of frequencies for which the larger span gives a smaller condition number. This in turn requires the woofers to produce a very wide frequency range of signals, which is not practical. Another merit of the "OSD" system is also lost in a multi-channel system. That is to say that only two independent output signals, hence only two amplifier channels, are required for a "OSD" system whereas the same number of channels as the number of driver units are always required for a multi-channel system.

In any case, the cross-over filters can be passive, active or digital filters. If they are digital filters, they can also be included in the same filters which implement the system inversion in the exactly the same way as the filters for binaural synthesis. In case the inverse filters are designed without including the cross-over filters in the plant response, it would be possible to design optimised digital cross-over filters. This could be done such that the transition regions around the cross-over frequencies are best matched (in the sense of the principle) to the plant response. Since the present work was a first approach to study the feasibility of an "OSD" system, it was confined to the use of analogue off-the-shelf cross-over filters. Furthermore, only the method equivalent to Figure 5.10.1 was applied.

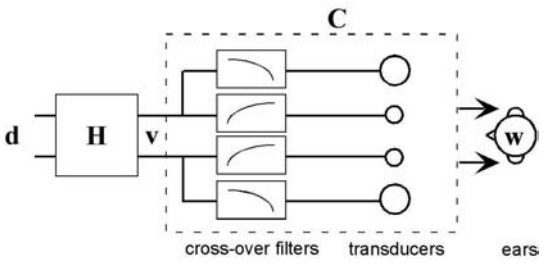

Figure 5.10.1

Block diagram when a [2 × 2] plant matrix **C** is used for the design of the inverse filters **H**.

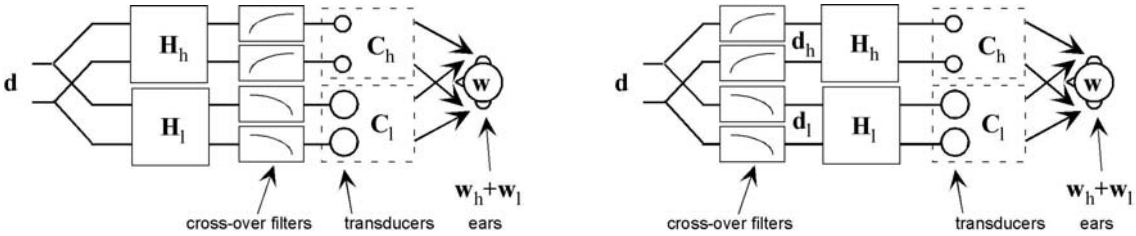

[a] [b]

Figure 5.10.2

Block diagram when m (number of driver pairs) [2 × 2] plant matrices $\mathbf{C}_m$ are used separately to design m inverse filter matrices $\mathbf{H}_m$. [a] Cross-over filters after inverse filters. [b] Cross-over filters prior to inverse filters.

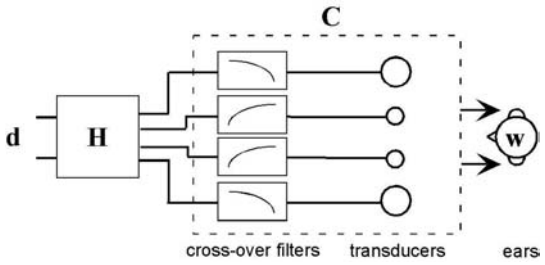

Figure 5.10.3

Block diagram when a [2 × 2*m*] plant matrix **C** is used to design a [2*m* × 2] inverse filter matrix **H**.

Chapter 6
System Design

6.1 Introduction

In the previous chapter, the theoretical ideas behind a so-called *„OSD“ system* were shown. This chapter describes now the procedure of putting such systems into practice and the evaluation of their performance. It was decided to study the general feasibility of a 3-way system and a 2-way system. For comparison purposes, a conventional “*Stereo Dipole*” system was also realised. As it was discussed in Section 5.9, a 2-way system can be made by simply omitting the low frequency unit of a 3-way system and just using 2-way cross-over filters (instead of 3-way) for the retained mid- and high-frequency loudspeakers. Thus, the realisation of both the 3-way system and the 2-way system was possible with a minimum expenditure of necessary loudspeakers for the experimental set-up. Impulse response measurements were undertaken to obtain information about the system's plant response. The inverse filters were calculated based on these measurements, in order to equalise for crosstalk. The performance of the realised systems was investigated later by means of extensive subjective experiments, as will be addressed in Chapter 7.

The following considerations regarding the practical system design consists of a thorough description of the experimental set-up and the used equipment, the method and procedure of free-field and HRTF measurements as well as a discussion of the measured results.

6.2 General Set-up Description

As it is presented in the photograph in Figure 6.2.1, the entire system was set up based on a rotating steel frame ring with a radius of r = 1,6 m. Mounting the loudspeakers onto this ring ensures a source layout which is very accurate, both in terms of constant distance and constant angles (source spans). A sketch of the set-up's geometry is shown in Figure 6.2.2.

The loudspeaker driver units used for the system were chosen considering the specifications given in Chapter 5.9. Thus, the woofer units should have the flattest possible frequency response up to an upper frequency limit of f_u > 600Hz and the mid-frequency unit should feature f_u > 3500Hz while still performing reasonably well at low frequencies down to about 200Hz. Another critical consideration for the choice of driver units was the necessary volume of their enclosures, since the geometrical dimensions of the speakers were fairly restricted due to the source layout (see Figure 6.2.2). Eventually, after considering various other options, the following driver units were chosen:

- for the „OSD" systems:
  - ✓ Dome tweeter, Visaton[1] DT 94
  - ✓ Low-Midrange driver, Visaton W 100 S
  - ✓ Woofer, Visaton W 200 S
- for the „Stereo Dipole" system:
  - ✓ Fullrange driver, Visaton FRS 8.

Cross-over filters are necessary in order to distribute the frequencies to the appropriate pair of loudspeakers. As discussed in Section 5.10, it is most straightforward to use a pair of passive analogue cross-overs, as they are available "off the shelf". Since the object of this project was rather a first approach, it was decided to confine oneself to the use of following commercial cross-over filters in the first place:

- ✓ Cross-over "Alto IIIc", 3-way
- ✓ Cross-over "Alto I/II", 2-way

Since *Visaton-Speakers*, the manufacturer of the loudspeakers, offers those cross-overs in combination with the chosen driver units, they were expected to be of best use for the present purpose. In fact, their given cut-off frequencies of 450Hz/3500Hz and 3500Hz, respectively,

[1] Manufactured by VISATON-Speakers, D-42781 Haan, Germany.

matched almost exactly to the requirements according to Section 5.9. Consequently, this was another reason for the choice of this particular equipment.

The cross-over units were built each into a separate plastic box, equipped with connection terminals, in order to be able to mount them on the steel ring independently from each other. The driver units were also enclosed each by a separate box made of 18mm plywood panels. All loudspeaker enclosures were constructed as closed cabinets and in particular consideration of the geometrical limitations due to the required source layout. The geometrical depth of the cabinets had to be chosen such that when mounted at the ring, the distance between each driver unit and the centre of the ring was exactly 1,4m. Never the less, it was possible to provide the driver units with the necessary cabinet volume for optimal acoustic performance.

As depicted in Figure 6.2.2, the high frequency units were mounted such that they give a source span of $2\theta = 6°$. The mid-frequency units subtend an angle $2\theta = 32°$ while the pair of low-frequency speakers are mounted to span $2\theta = 180°$. For measurements on the „Stereo Dipole“ system, the tweeters had to be removed in order to make room for the fullrange loudspeakers, which were mounted under a source span $2\theta = 10°$. Depending on the considered system, three cases have to be distinguished where one loudspeaker at the time is represented by:

- a 3-way combination consisting of tweeter, midrange unit, woofer, and 3-way cross-over,
- a 2-way combination consisting of tweeter, low/midrange unit, and 2-way cross-over,
- a fullrange speaker for the case of a „Stereo Dipole“ system.

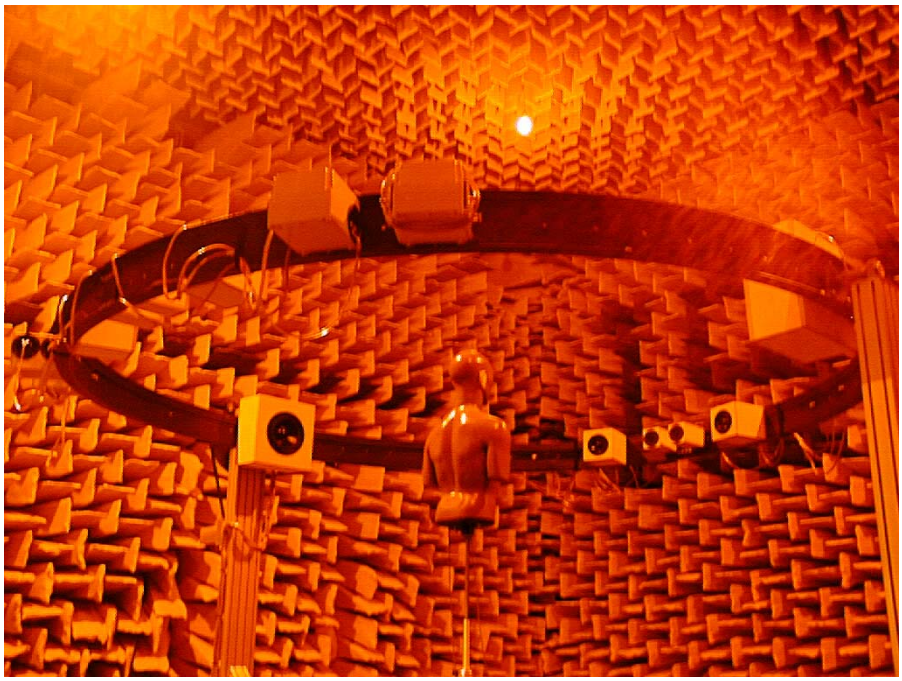

Figure 6.2.1

Photograph of the experimental rig in the measurement stage.

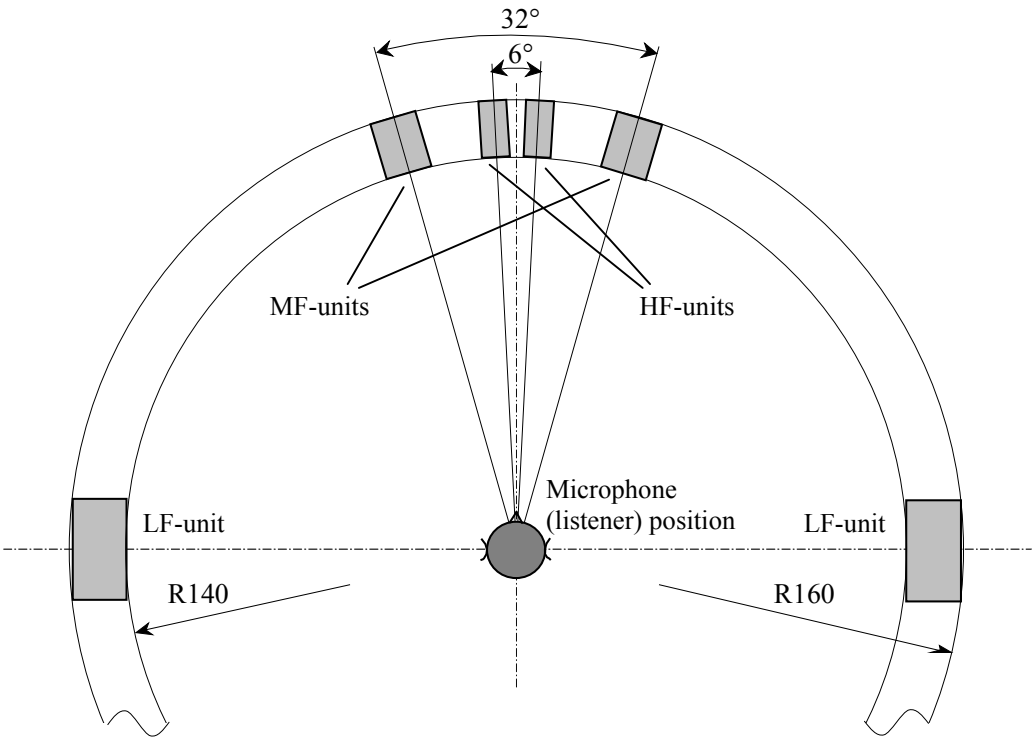

Figure 6.2.2

Geometry of the „OSD“ set-up’s loudspeaker layout (top view).

6.3 Measurements of the Plant Matrix

As discussed earlier, the task of binaural virtual acoustic imaging with loudspeakers requires an appropriate inverse filtering for the crosstalk cancellation. Thus, the system's plant matrix of the electro-acoustic paths **C** has to be measured. In consideration of section 5.10, there are various options of obtaining the plant, which differ mainly depending on where the cross-over network is inserted to the system. Therefore, measurements were made for the two different „OSD“ systems (3-way and 2-way) and the „Stereo Dipole“ system as well as for every single loudspeaker of the arrangements separately. This was made in order to provide data about the appropriate plants for all of those different options. Some of them may be subject of investigations in future experiments. For the present experiment, only the data for "OSD" systems including the cross-over filter network were used to calculate the crosstalk cancellation filters **H**. As shown in Figure 5.10.1, the plant **C** consists of a [2 × 2] matrix of electro-acoustic transfer functions in this case. The response of the cross-over filters is already included in the plant measurement. Consequently, the obtained inverse filter matrix **H** automatically compensates for the cross-over network as well as for the interaction between different pairs of driver units around the cut-off frequencies of the cross-over filters.

Measurements were made of four impulse responses that represent the Head-Related Transfer Functions (HRTFs) in the time domain between the two loudspeakers and the two ears of a KEMAR dummy head. The dummy head was positioned at the centre of the steel ring such that the distance of the KEMAR’s centre to each speaker was 1,4m.

In order to obtain two different sets of HRTF measurements at once, two different pinna styles were installed on the KEMAR. The left was the smaller model DB-061 and the right was the larger model DB-065. Assuming the KEMAR had perfect medial symmetry, including the pinnae, the resulting sets of HRTF measurements would be symmetric within the limits of measurement accuracy. In other words, two complete sets of measurements can be obtained by mirroring the two half sets on the median plane. This was also done with respect to the HRTF measurements of the KEMAR accomplished by Gardner and Martin [1994], since their set of HRTFs was applied later for the binaural synthesis of virtual acoustic images. Thus, the option of trying both ear type’s HRTFs was left open and it had not to be decided in the measurement stage of the project which set to use later on.

Generally, the measurements always include not only the HRTFs but also the

response of the measurement system itself, consisting of the loudspeakers, the microphones, D/A and A/D converters, anti-alias filters, audio and microphone amplifiers, and inevitably some room characteristics. Interference due to reflections can be avoided by ensuring that they occur well after the head response time, which is several milliseconds. This is certainly the case for room reflections but some reflections off certain obstacles of the experimental set-up might falsify the measurements slightly. Therefore, additional measurements were made of all loudspeakers and the two “OSD” systems. This system's free-field response may be deconvolved from the HRTF data if necessary. The measurement method (to be discussed in the following section) was exactly the same as for the HRTF measurements, except that the KEMAR dummy head was replaced by a single microphone, in particular the one which was mounted in KEMAR’s right ear.

6.4 Measurement Method

The impulse responses were obtained using a *maximum length sequence* (*MLS*) measurement technique. This method which is based on a time-domain cross-correlation between input and output signal and is implemented in the *MLSSA*[1] computer package [Rife, 1994]. MLSSA is based on a DSP card installed in a personal computer and the software is running either in DOS or Windows environments. The main advantage of MLSSA over other measurement methods such as FFT frequency analyser, is the high noise and distortion immunity due to pre-averaging techniques and the capability to measure long impulse responses quickly [Rife and Vanderkooy, 1989; Vanderkooy, 1994]. Interfering background noise in the measurement is reduced by means of *pre-averaging* of the measurement system's output. This is possible since background noise is usually equally distributed over the measurement time. The averaging is made prior to the cross-correlation process, which is indicated by the term "pre-averaging". By this means, the signal-to-noise ratio is increased by 3dB per measurement doubling. Errors due to non-linearities (e.g., caused by the loudspeakers) result, unlike background noise, in rather impulsive and non-uniformly spread irregularities in the

[1] MLSSA (Maximum Length Sequence System Analyser) is a trademark of DRA laboratories.

measured impulse response. Repeating the measurement with a new (cyclically shifted) maximum length sequence leads to a shift of the same irregularities. Therefore, averaging of repeated measurements reduces these noise peaks by 6dB with each doubling of measurements. This type of averaging is referred to as *post-averaging*, since the averaging is executed after cross-correlation of input and output signal. The following parameter settings were chosen in the MLSSA software:

- Sampling rate: 88,89 kHz
- Pre-averages: 16 records
- Post-averages: 16 records
- Bandwidth: 20,0 kHz
- Antialiasing filter: Butterworth
- MLS order (period): 16 (65535 points)
- Stimulus mode: Burst MLS

The entire apparatus for the case of measurements on a 3-way system is depicted in Figure 6.4.1. Besides the MLSSA system, the following equipment was used for the measurements:

- Artificial head and torso KEMAR DB-4004
- Artificial pinnae: model DB-061 (left ear), model DB-065 (right ear)
- Ear canal simulator Zwislocki DB-100
- Ear canal adaptor Brüel & Kjaer UA-0122
- 2 microphones Brüel & Kjaer Type 4165
- 2 microphone pre-amplifiers Brüel & Kjaer Type 2619
- Microphone amplifier Brüel & Kjaer “Nexus”
- Power amplfier H & H Electronics V200 Mos-Fet
- Switching box (designed and built in ISVR’s Electronics Workshop)

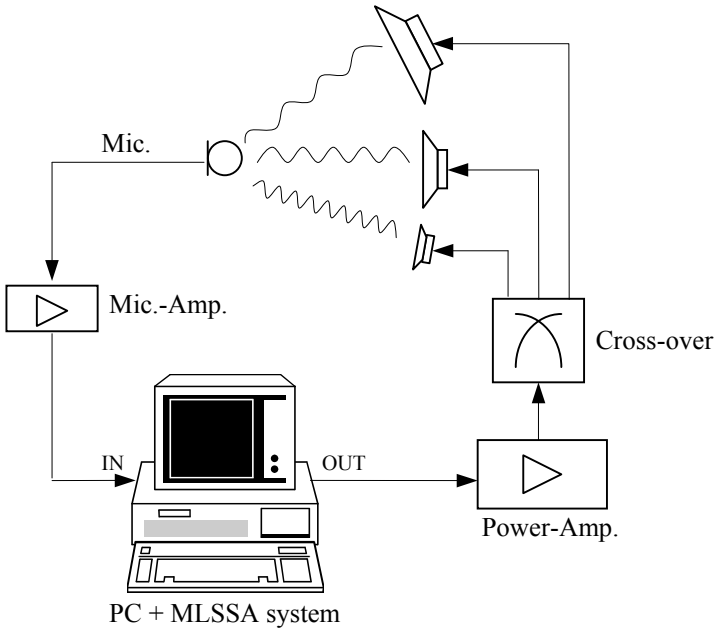

Figure 6.4.1

Apparatus for impulse response measurements with MLSSA on a 3-way "OSD" system.

6.5 Measurement Procedures

All measurements were conducted in a large anechoic chamber with a usable volume of 295m^3 (7,33m × 7,33m × 5,50m) located in the Rayleigh Building at the Institute of Sound and Vibration Research of the University of Southampton. The cut-on frequency for free-field conditions in the anechoic chamber is estimated to be about 70Hz. The chamber has a floating floor consisting of squared pieces of metallic grid.

The measurement system was set up as shown in Figure 6.2.1, and according to the arrangements given in Figure 6.2.2, and Figure 6.4.1, respectively. All noisy parts of the system, like the operating PC for the MLSSA software, power amplifier, etc. were kept outside the anechoic chamber and placed in the adjacent control. Thus, the whole measurement procedure could be operated there without causing additional noise in the chamber. The gain setting of the power amplifier was always chosen such that the sound pressure level (SPL) at the microphone position (the listener's position) was 60 dB @ 2kHz.

This was controlled with a sound level meter since the same SPL was intended to use for the later subjective experiments. Only for the direct measurements on the high frequency units, the gain was reduced significantly in order to avoid damage due to the low-frequency content in the MLS signal.

The position of the free-field microphone was calibrated by means of "trial-and-error" impulse response measurements. Thereby, the time delays between two opposite loudspeakers were compared and the microphone was moved around until both impulse responses had the same delay (± 1 sample). This comparison was done between both corresponding loudspeakers left and right and corresponding loudspeakers in front and behind the microphone position. Therefore, the same set of loudspeakers (apart from the woofers) was installed on both sides of the steel ring, in front and in the rear of the listener (microphone). This can be recognised on the left of Figure 6.2.1. The correct height of the microphone was controlled with a tape measure and two pieces of string which were spanned each between two opposite facing holes in the steel ring.

For the HRTF measurements, the KEMAR dummy head was mounted in the middle of the loudspeaker arrangement. The correct alignment of the KEMAR was achieved in a similar manner. Because the KEMAR was equipped with two different pinna types, they were removed and hence only the microphones in the two ear canals were used for the alignment process to ensure symmetry. The point of origin in terms of "left-right" position was reached when the time delays between left microphone and left woofer and between right microphone and right woofer, respectively, were equal (± 1 sample). In the same way, the impulse responses between the midrange units and the respective opposite ear were compared to ensure the KEMAR wasn't rotated towards either side. The height and the "front-back" position of the two ears (microphones) were again aligned with spanned strings.

6.6 Processing and Data Reduction

Each measurement yielded a 65535 points impulse response at a f_S = 88,89 kHz sampling frequency. Most of these data are irrelevant since the length of the stored responses is larger than necessary to cover the duration of the response of interest. The 1,4m air travel between the loudspeakers and the microphones corresponds to about 360 samples. After this initial delay follows the system response, which persists typically only a few milliseconds in the case of a head response (HRTF). Data after the system response are due to reflections off objects in the anechoic chamber such as the steel ring and other reflecting obstacles of the experimental rig.

In order to reduce the size of the data set without eliminating anything of potential interest, the first 360 samples of each impulse response were discarded. The following samples were truncated where the response became smallest just before the onset of the first major reflection. This was after around 900 samples (~10 msec) but the exact number varies for each conditions and units. The truncation of the impulse response data is known to introduce ripples in the frequency domain, an effect referred to as the *Gibbs phenomenon* [Oppenheim and Schafer, 1975]. Therefore, the retained data were multiplied with a half *Hanning* window in order to smooth the response and alleviate the effect of ripples.

Before the impulse response was further processed for the implementation of crosstalk-cancellation filters, the data were downsampled by the factor 2, i.e., every second sample was left out. It should be noted that there was a slight discrepancy between the sampling rate resulting from the downsampling, which is f_S = 44,445 kHz and the usual sampling frequency f_S = 44,1 kHz. However, it was assumed that this error would not affect the later subjective experiments significantly. In fact, considering the HRTF measurements, this sampling rate difference corresponds to a negligible enlargement of the geometrical head dimensions. In other words, the effect is the same as when the KEMAR was larger of the factor 1,0078 when measuring with f_S = 44,1 kHz. Seeing that the morphological dimensions of KEMAR appear fairly small compared to a typical size European head, this might even be a desirable effect than a drawback due to the awkward parameter options with MLSSA.

6.7 Measurement Results

The single loudspeaker's frequency responses are depicted in Figure 6.7.1 and it can be seen that they are reasonably flat within the frequency range they were intended to be operated. The characteristics of the loudspeaker pairs were well-matched. Significant differences between two loudspeakers would degrade the HRTF synthesis considerably. When their responses are identical, their effect becomes independent of virtual source directions and can be regarded as degrading the sound source signal itself rather than the synthesised HRTFs. Thus, the loudspeaker response affect monaural cues to spatial hearing (this is also the case for real sound sources), but they do not affect the binaural cues. Therefore, it is very important for binaural synthesis, to use a well-matched pair of loudspeakers.

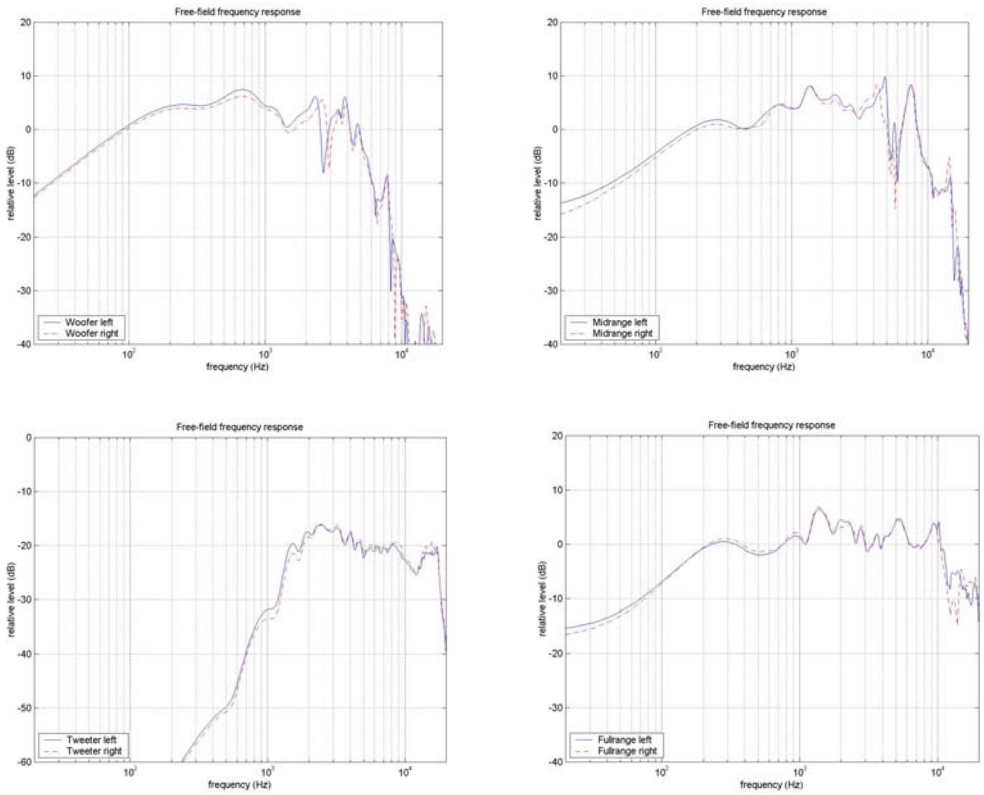

Figure 6.7.1

Free-field frequency responses of the single loudspeakers.

For the "OSD" systems, it is also important to used a pair of well-matched cross-over filters, since they affect the system response as well. Therefore, all loudspeakers and cross-over filters were available multiple times and various combinations were tested in order to find the best possible match. The free-field frequency responses of the 2-way and the 3-way system are shown in Figure 6.7.2.

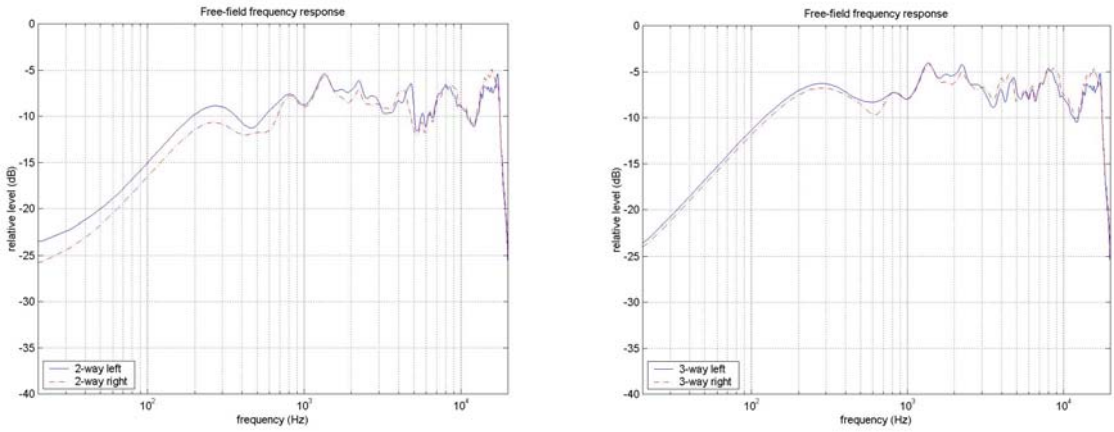

Figure 6.7.2
Free-field frequency responses of the "OSD" systems.

In general, the high frequency sound reaches the microphone earlier than lower frequencies. This results because the tweeter has its *acoustical centre* [Colloms, 1997] further in the front compared to the midrange unit, i.e., the tweeter is actually closer to the microphone. This insufficient "*time-alignment*" between midrange and high frequency units led to a significant dip in the response around the cross-over frequency. Therefore, the mounting device for the tweeters was designed such that they could moved forward and backward in radial direction. In order to flatten the response, additional measurements were accomplished with the tweeters moved further away. Eventually, it was decided to keep the high frequency units about 7 mm behind the midrange speakers. In the lower frequencies, time-alignment between woofer and midrange unit is negligible because of the large wavelength.

Although a complete set of measurements for both two pinna models was obtained, it

was decided to use the data from the larger model DB-065 (rigth ear) exclusively for the following experiments. This choice was made mainly considering the size of the pinna compared to typical European size ears. Therefore, all HRTF responses are only shown for the right ear in the following of this document. The HRTFs of the single sources are shown in Figure 6.7.3. Thereby, according to the theoretical discussions in the previous chapters, the blue graph C_{11} denotes the response of the direct acoustic path while the crosstalk path C_{12} is characterised by the red line. A comparison of the "OSD" free-field responses Figure 6.7.2 and the appropriate HRTFs in Figure 6.7.4 reveals two characteristic notches in the response due to the KEMAR head and pinna around 3,2 kHz and 8 kHz. Assuming perfect symmetry of the system, these represent the acoustic plant matrix such that

$$\mathbf{C} = \begin{pmatrix} C_{11} & C_{12} \\ C_{12} & C_{11} \end{pmatrix}. \tag{6.7.1}$$

This information about the system will be the basis for the design of crosstalk cancellation inverse filters.

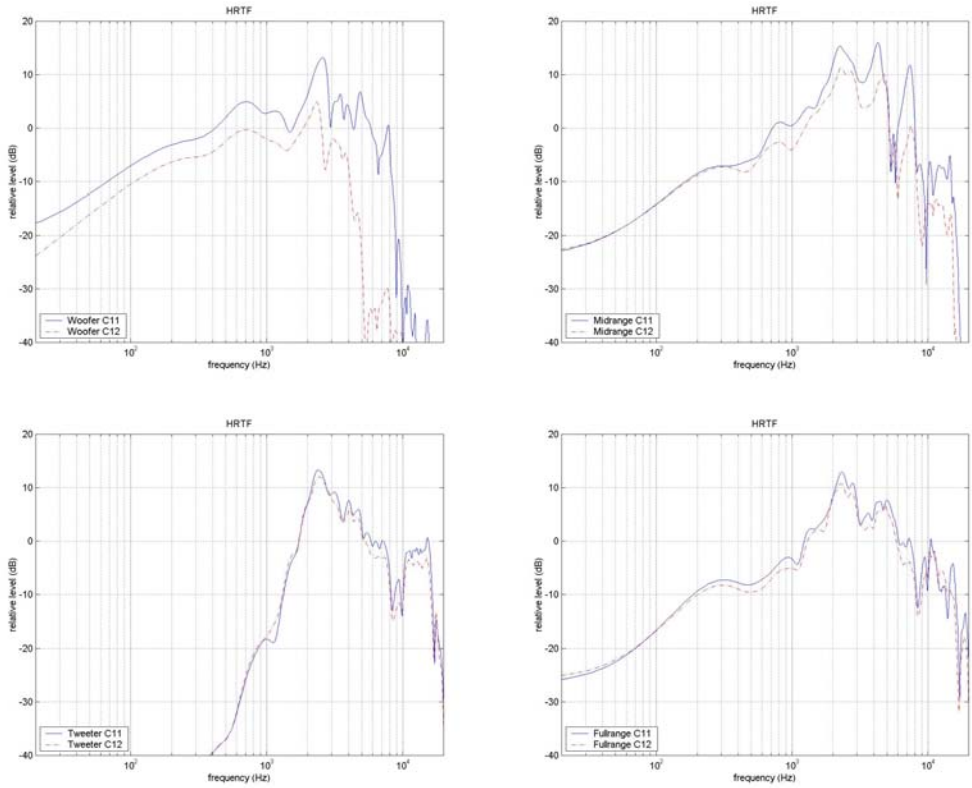

Figure 6.7.3

Head related frequency responses (HRTFs) of the single loudspeakers.

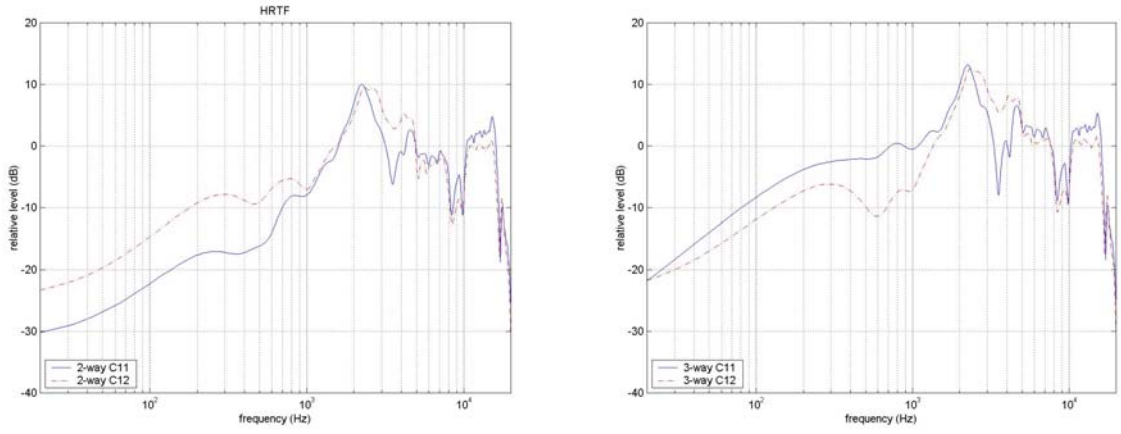

Figure 6.7.4

Head related frequency responses (HRTFs) of the "OSD" systems.

Chapter 7
Subjective Experiments

7.1 Introduction

This chapter describes a set of experiments which investigated up to what extent an „OSD“ system can successfully reproduce virtual acoustic images around a single listener. In order to establish this, the main objective of these experiments was to evaluate the performance of subjective sound localisation in an anechoic environment. Furthermore, it was intended to conduct a direct comparison between an „OSD“ system and a conventional "Stereo Dipole" system. This comparison was made both in terms of a rather informal personal preference study as well as in terms of sound localisation experiments.

Twelve young adults (1 female, 11 male) served as paid volunteers. All had normal hearing with no history of hearing problems of any kind. A description of the nature of these tests, their duration, and the guide of safety and ethics accompanying them were explained to the volunteers before they signed a consent form agreeing to participate in the experiments. None of the subjects had any previous experience with 3D audio systems or sound localisation experiments, and all were naive regarding the purpose of the tests.

In the following sections, the set-up and procedure of the subjective experiments is addressed as well as a presentation of the statistical analysis of the data.

7.2 Experimental set-up

Basically, the set-up which was used in the measurement stage, was modified to make it suitable for the subjective experiments. This modification consisted of an adjustable chair in the middle of the system which was surrounded by a metallic grid of spherical shape. This sphere, as shown in the photograph of Figure 7.2.1, served for two purposes. One was to be covered by black acoustical transparent fabric in order to hide the system loudspeaker system from the subject. The blue metal rods of the spherical grid were all in 15 degree distance, both in azimuth and elevation direction. Thus, the second purpose of the sphere was that it could be used as a coordinate system in order to help the subjects specifying directional judgements. As depicted in Figure 7.2.2, the grid lines were marked with red number labels indicating azimuth and blue numbers indicating elevation angles.

Figure 7.2.1

Seat for test subjects, surrounded by a metallic spherical grid, before it was mounted to the rest of the

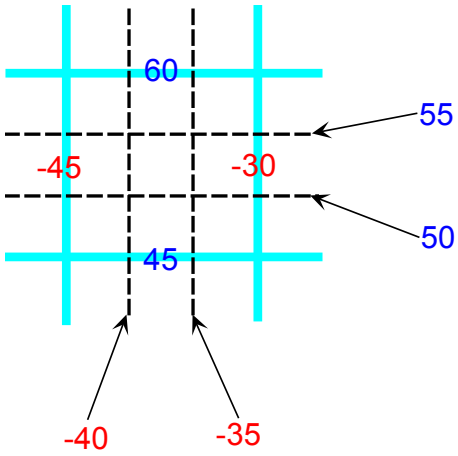

Figure 7.2.2

Use of the spherical grid lines as a coordinate system.

The whole "cage" including the seat was attached on the horizontal bar in the middle of the main rig, as shown in Figure 7.2.3. As it is known from previous theoretical discussions in this document, the success of virtual acoustic imaging with such systems is fairly sensitive to the position of the listener. Therefore, the spherical grid was positioned most possible at the centre point of the system. As a consequence, the grid lines of the sphere and their joints could be used as an aid in order to adjust the subjects. Thus, the head position was adjusted

visually by means of aligning the subject's ear canals with appropriate reference points on the rig. In order to avoid parallax errors, one of these reference points had to be in front of the subject and one behind. The height of the subject's *interaural axis* (see Section 2.2) was aligned on a horizontal string spanned at 0° elevation and the grid line of the sphere at 0° elevation. The "front-back" positioning was achieved by aligning the subject's ears on the two vertical grid lines at +90° and –90°. The "left-right" centre was always ensured due to the proper position of the chair. Furthermore, the chair was equipped with a small head rest in order to maintain the adjusted head position. It is believed that the subject's head was always within ±1 cm of the desired position. Lateral head movements or rotations, which are deemed to be most important to control, were exceptionally constrained due to the head rest.

Figure 7.2.3

Experimental set-up with a test subject sitting on the chair.

Since experiments were accomplished both with "OSD" systems and with the "Stereo Dipole", both loudspeaker arrangements had to be set up at the same time, as opposed to for the measurements. This was solved by mounting the two fullrange units for the "Stereo Dipole" on two angle brackets which were attached to the ring. Consequently, when the "Stereo Dipole" was tested, the ring had to be rotated in order to bring the fullrange speakers to a horizontal position with respect to the listener.

7.3 Pilot Study - General Impression

The first step of the experiments was to investigate the system's general performance and

whether the system is able to create virtual acoustic images at all. For these purposes, crosstalk cancellation filters were implemented based on the previously measured system plants. All filters were calcualted off-line in *MATLAB*®[1]. The algorithm for the system inversion was implemented in the frequency domain, based on the method of fast deconvolution using regularisation [Kirkeby *et al*., 1996a], as it was discussed previously in Chapter 4. For all investigated system configurations, the inversion process was regularised to ensure about 20dB dynamic range loss, according to the considerations in Chapter 5. Further processing which was included later for the binaural synthesis of virtual sources, would lead to additional dynamic range loss (or sometimes gain). The caculated inverse filters were implemented in the *HURON*[2] digital audio convolution workstation, using 8638-point FIR filters. The HURON workstation utilises low-latency convolution algorithms to enable the convolution of signals and impulse responses in real-time.

For initial trials, binaural recordings of sounds in the nature[3] on Compact Disc were used as source signals. Most of these recordings were reported to be made with the "Aachen Head", an artficial head microphone from Head Acoustics, Germany. The CD-signal was fed into the input of the Huron where the signal was processed with the appropriate inverse filters, depending on the system under investigation. A rather informal study was undertaken by comparing the general impression of the three evaluated systems.

The most remarkable difference was the far wider lateral range of the sound stage with the use of an "OSD" system as opposed to the "Stereo Dipole" configuration. In fact, all participating listeners reacted amazed and where overwhelmed by the clarity of the sound images and how differentiated one could perceive particular details in the recordings. This was also true for a 2-way system but clearly the 3-way "OSD" system left the best impression.

One reason for this unisonous preference probably were the additional woofer speakers. Due to the better low-frequency reproduction, the system itself just sounded more impressing. Hence, there was no evidence yet that the performance in terms of convincing virtual acoustic imaging and sound localisation accuracy was superior compared to the other systems. Therefore, more sophisticated and extensive listening tests were undertaken in order

[1] The MathWorks, Inc.

[2] Lake® DSP Pty Ltd., Ultimo, Australia.

[3] Published by the Japan Audio Society.

to validate the subjective perormance. It was decided to run two sets of localisation tests, one with the 3-way "OSD" system and one with the "Stereo Dipole" system. On the one hand, the decision not to test the 2-way system was made because of the shortage of time, on the other hand because the 3-way system promised more significant results since it represents the extreme variant of an "OSD" system.

7.4 Choice of Target Locations

The stimuli were created by processing a monophonic sound source with a binaural synthesis filter using a KEMAR HRTF data base measured and provided by Gardner and Martin [1994] of the MIT media lab. Pink noise was used as the source signal because of its roll-off towards higher frequencies. This should help to minimise the negative consequences of potential discrepancies between the subject's HRTFs and the measured KEMAR HRTFs in the high frequencies.

Out of the 710 measured locations in the MIT data base, 50 were chosen to be presented. Each of these 50 locations, referred to as the "*target locations*", was tested exactly once per subject. The choice of 50 was made with the aim of sampling the possible range of azimuths and elevations equally. The MIT data base is divided into groups of constant elevations between –40° and 90° (overhead). As opposed to this grouping, importance was attached to choose the locations such that they can be divided into groups of *constant azimuth* angles, i.e., locations which are situated on common *cones of confusion*. Figure 7.4.1 shows the positions of the chosen targets where the green circles indicate cones of confusions with their corresponding azimuth angles from –80° to +80°. All chosen targets are situated on one of these cones; if not exactly then at least approximately. Note that azimuth angles are given here according to the *interaural polar coordinate system*, as explained in Section 2.2.

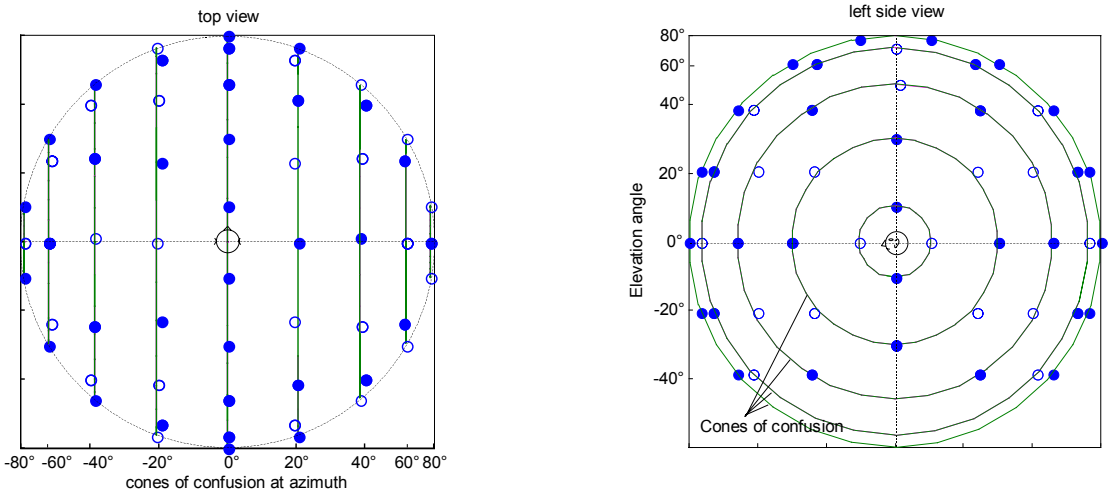

Figure 7.4.1

Positions of all chosen "target sources" for the localisation experiments.

	Low		Middle		High		Very high	
	azimuth	elevation	azimuth	elevation	azimuth	elevation	azimuth	elevation
Front	-26	-40	**-40**	**0**	**-20**	**20**	**-40**	**60**
	0	**-40**	-20	0	**0**	**20**	**0**	**60**
	26	**-40**	**0**	**0**	**45**	**20**	40	60
	-45	-20	**20**	**0**	20	20	**0**	**80**
	-20	**-20**	40	0	-45	20		
	0	**-20**			**0**	**40**		
	20	-20			**26**	**40**		
	45	**-20**			-26	40		
Side	**-122**	**-40**	**-90**	**-10**	-115	20	-88	50
	-58	**-40**	90	-10	-65	20	**88**	**50**
	-90	**-30**	**-120**	**0**	**65**	**20**	-90	70
	65	**-20**	-100	0	**115**	**20**	**90**	**70**
	115	**-20**	-80	0	**-90**	**30**		
			-60	**0**	90	30		
			60	0	**-122**	**40**		
			80	**0**	**-58**	**40**		
			100	**0**	58	40		
			120	0	122	40		
			-90	**10**				
			90	10				
Back	-154	-40	-160	0	**-160**	**20**	**-140**	**60**
	154	**-40**	**-140**	**0**	-135	20	140	60
	180	**-40**	140	0	**135**	**20**	**180**	**60**
	-160	**-20**	**160**	**0**	160	20	**180**	**80**
	-135	-20	**180**	**0**	**180**	**20**		
	135	**-20**			-154	40		
	160	-20			**154**	**40**		
	180	**-20**			**180**	**40**		

Table 7.4.1

Target locations assigned to appropriate regions of auditory space.

Blue dots in the charts represent the target locations which were used for the localisation tests. Their mirrored counterparts with respect to the median plane are denoted by open circles. The latter where not actually presented to the listeners but for the statistical analysis, all responses were mirrored about the median plane. Thus, considering that 14 targets were located at the median plane (i.e., they are not mirrored), a total number of 86 targets was investigated, while only 50 were actually presented. Considering that left-right confusions occur very seldom, neither in natural hearing nor with virtual acoustics, this efficient method of gathering more data was believed to be passable. Table 7.4.1 gives the coordinates of all investigated targets, where bold numbers denote the 50 presented targets. Unlike in Figure 7.4.1, azimuth angles are given according to standard coordinates!

7.5 Preparations of Test Stimuli

For the task of virtual source imaging, the loudspeaker signals were created now by processing the pink noise input with two cascaded sections of digital filters. The first was the crosstalk cancelling filter network, as already implemented successfully for the pilot study mentioned in Section 7.3. The second section was the binaural synthesis filter to encode the directional cues of the desired virtual sound source. All these synthesis filters corresponding to the chosen target locations were also implemented in the HURON workstation prior to the experiments. In addition, another set of synthesis filters was implemented for source locations according to Figure 7.5.1. Since these sounds were presented to the subjects for training purposes, it was decided to keep the locations on cones of constant elevation. Thus, as opposed to the actual test targets, the training targets were chosen according to standard spherical coordinates. This coordinate system was considered as appearing more natural to the subjects. For the same reason, the subjects were asked to give their localisation judgements according to a standard coordinate system, as will be explained in the following section.

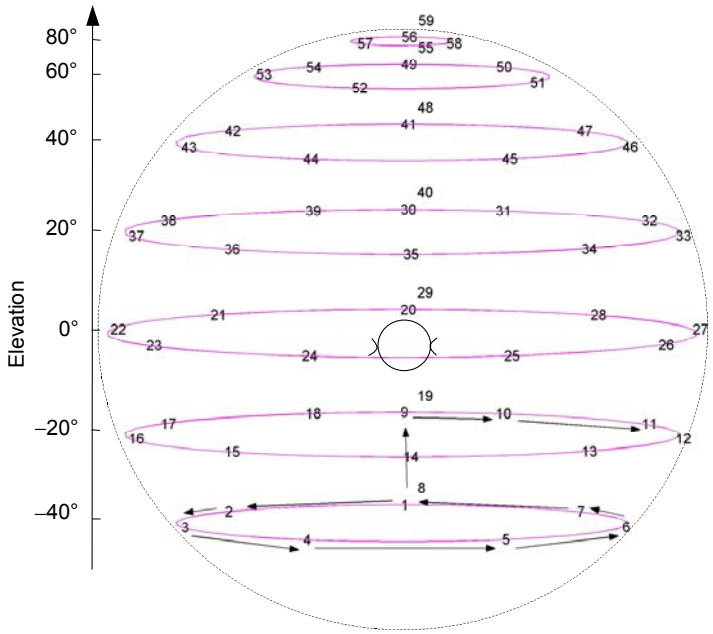

Figure 7.5.1

Virtual source positions for the training sequence. The chart shows the back view where the ovals indicate cones of constant elevation.

Each time the presented source location was changed, the appropriate synthesis filters had to be updated. This updating was necessary for sequences of 50 target sounds (plus 59 times for the training sequence), and for the two tested systems. Therefore, a code was programmed in MATLAB which automatically switches the filters in the desired order. This is possible because the HURON is able to interface with the MATLAB software.

Prior to the experiments, all sequences of filtered signals were recorded on Digital Audio Tapes (DAT) in order to be independent of the HURON workstation during the test sessions. For both tested systems (i.e., "3-way OSD" and "Stereo Dipole"), a set of the following stimuli was prepared:

- ***Demonstration:*** Binaural recordings of nature sounds (inverse filtered as described in Section 7.3). These demonstrations of virtual acoustic environment were presented as the rather enjoyable part of the experiments. It was also expected to keep the subjects motivated in between the test sessions by playing impressing demonstration sounds.

- ***Training sequence:*** Pink noise filtered for virtual images in sequential order according to Figure 7.5.1 was presented to familiarize the subjects with their task and with the type of the test signal.

- ***Test sequence:*** Virtual images with the same pink noise input signal but locations were chosen according to Figure 7.4.1 and their presented order was randomised. The random order was different for the two test sessions.

7.6 Localisation Experiment Procedure

At the beginning of a test run, the subject's position was adjusted as described in Section 7.2. Figure 7.2.3 shows that, at this stage, the steel ring was kept in vertical position. This was done for safety reasons mainly, avoiding risks when a subject went in or out the "cage", and considering that the experimenter had to handle on the rig in order to bring the test person into correct position.

Prior to the test, subjects were provided with instructions explaining the test environment and their task, respectively. A main concern was to familiarize the subjects with the coordinate system, which was essential for them to specify the perceived directions. Therefore, subjects were trained and asked to indicate the directions of some supposed examples at which the experimenter pointed. Subjects were asked to specify directions by calling out numerical estimates of the azimuth angle followed by the elevation angle (including the sign), using the standard spherical coordinate system as given by the grid lines of the "cage". Thereby, the experimenter recommended to divide the gridlines into three equal distances in order to get an idea of the 5 degree steps (see Figure 7.2.2). However, it was considered to be important not to restrict the responses alternatives to the 15° steps of the grid lines and not even to the recommended 5° steps. Therefore, it was emphasised that the subjects should make their estimations as accurate as they were able to.

After the subjects felt comfortable with the task and their position was adjusted, the black fabric around the spherical grid was closed. As shown in Figure 7.6.1, a desk lamp was installed inside the sphere. After the lights in the anechoic chamber were switched off, the subjects had no sight to the outside of the sphere, but still could see what was inside. This was necessary because the subjects had to see the grid lines and the labels indicating the angles in order to indicate the perceived directions.

Now, the steel ring was rotated in order to bring the loudspeakers into horizontal position with respect to the listener. The servo motor which rotated the ring could be heard clearly. Therefore, the ring was moved stepwise with alternating directions to avoid an audible cue to detect the loudspeaker position,. Otherwise, the subject could have guessed according to the duration of the movement. Moreover, since the ring was equipped with more loudspeakers than actually necessary, the subject could not know anyway, which speakers were in operation.

Figure 7.6.1

Test subject within the sphere during the listening tests.

Both test sessions were started with a demonstration of binaural recording examples. All stimuli were presented to the subjects at a listening level of approximately 65 dBA SPL. After the demonstrations, a sequence of 59 virtual images was played; each stimuli of 2 sec duration with a 0,5 sec silence in between. This sequence served as a training and to accustom the subject to their task and to the test signal. According to Figure 7.5.1, the virtual source position was panned around the subject, starting in front (0° azimuth) at the lowest possible elevation (–40°) and moving leftwards. After arriving at the front again, the sound "jumped" upwards to the next elevation (–20°) and moved towards the right around the listener, and so forth until the sound reached the top. Prior to the test session, this training sequence was explained to the subjects and the chart shown in Figure 7.5.1 was handed out. Subjects were asked trying to "follow" the sound, where consulting this chart should help to imagine its moving position in space.

The actual localisation test has been carried out as follows: Each stimulus consisted of a *reference signal* of 3 seconds duration and the actual test signal of 5 seconds with a 3 seconds gap in between. The reference signal was presented at 0° azimuth and 0° elevation, i.e., directly in front of the listener. It should give the subjects prior knowledge of the sound source signal spectrum which is important for the monaural spectral cue. Stimuli, a set of reference and test signals, were repeated when subjects had difficulty in making a judgement.

Subjects were asked to lean their head against the head rest in order to stay in position. They were instructed to look always straight ahead and not to move the head (nor the body) while any sounds were presented. Only after each set of reference and test sound had stopped, subjects were allowed to move in order to look at the perceived direction and to work out the appropriate coordinates. The experimenter, who was always present in a corner of the anechoic chamber in order to operate the experiments, verified head position and stability.

The subject's responses were entered on a data sheet immediately after termination of the stimuli. Thereby, no feedback was given to the subjects. When a sound was heard as coming from more than one direction clearly or ambiguous among multiple directions, subjects were asked to answer all apparent directions, as far as possible. Short breaks with refreshments were given between the sessions. Subjects, who were all paid, were informed that an additional award will be paid as a bonus for those who achieved a high score. Even though it was just a matter of a small amount of money, this little psychological trick was expected to help motivating the subjects.

7.7 Statistical analysis

Before analysing and discussing the results of the experiments, three principle types of errors should be addressed the localisation performance is subject to. These are as follows:

- Systematic errors between the mean judged location and the target location that have the form of a response bias. In free-field listening, these "*localisation errors*"[1] are smallest in azimuth judgements for frontal horizontal targets, and largest in elevation judgements for rear medial targets. In the present experiment, additional errors over free-field conditions are expected due to the systematic variation between the synthesis HRTFs and the listener HRTFs. Furthermore, linear distortions in transmitting the binaural signals to the ears might contribute errors.
- Usually, responses vary around the mean. Blauert [1997] defines the "*localisation blur*"

[1] Term according to Blauert [1997].

to be the amount of displacement of the target that is recognised by 50% of the listeners as a change in judged location-in other words, the just noticeable difference. Rather than using the strictly defined term "localisation blur", these errors will be called "response variation" in this document.

- Front-back and up-down reversals (also called confusions): Errors are attributed to this type, when the target location is confused with the mirror symmetric location obtained by reflecting the target with respect to the frontal plane (for front-back reversals) or the horizontal plane (for up-down reversals). Compared to front-back reversals, which are very common, up-down reversals are less common and difficult to distinguish from other types of errors.

Analysing the results of this sort of localisation experiments is complicated because the stimuli and responses are represented by points in a three-dimensional space. In the present case, points on the surface of a sphere are considered since the distance was constant. For spherically organised data, the usual statistics (mean and variance) are either inappropriate or potentially misleading. For example, using standard spherical coordinates, an azimuth error of 30° for a source on the horizontal plane is much larger in an absolute distance sense than a 30° azimuth error for a point at 60° elevation. Therefore, azimuth judgements were analysed based on a interaural spherical coordinate system. In other words, not the azimuth angles as defined by a standard spherical coordinate system were treated, but the corresponding cones of confusion of target and answer directions were compared. This means is advantageous since the interaural differences (IID and ITD) are clearly represented between different cones of confusion. In the same way as the cones of confusion represent the lateral displacement, cones of constant elevation (as defined in Section 2.2 by a vertical polar coordinate system)[1] give a sense of height. Hence, the performance in terms of elevation localisation was investigated by comparing the elevation angles as they were reported by the subjects.

As a matter of fact, this kind of data analysis is only suitable to evaluate azimuth localisation and elevation localisation, respectively. For example, it is impossible to detect

[1] Note: For the definitions in Section 2.2, the terms "vertical polar" and "interaural polar" coordinate system,

front-back reversals by this means. General statements about the localisation performance in a three-dimensional sense are not possible either. Therefore, following Wightman and Kistler [1989b], the following additional statistics will be used in order to characterise the results:

- ***Average angular error:*** -is defined as the mean unsigned angle, measured on a great circle between each judgement vector and the corresponding vector from the origin to the target position.
- ***Front-back reversals:*** If the angle between the target and the judgement is made smaller by reflecting the judgement about the frontal plane, then the judgement was entered in reflected form, and a counter for the number of front-back reversals was increased by one. In other words, the reversals were counted and resolved before further analysis. Front-to-back (F→B) reversals and back-to-front (B→F) reversals were classified separately. The algorithm for resolving the reversals treats each judgement identically, regardless of target azimuth. Hence, it undoubtedly produces a slight overestimate of confusion rate and an underestimate of error angles for target positions near ±90°.
- ***Correlations:*** -between target and judgement azimuth and between target elevation and judgement elevation angles.

Unlike Wenzel *et al.* [1993], no attempt was made to detect or correct up-down reversals, because (considering own experience) it is believed most elevation judgements that would be classified as up-down reversals are actually the result of localisation errors or localisation blur.

- ***t-test:*** In practice of statistics, the "*t-test*" is usually applied in order to test whether the means of two data series X and Y are significantly different or whether the difference is a coincidence. According to Bronstein and Semendjajew [1996], the t-value is obtained by

$$t = \frac{\bar{x} - \bar{y}}{\sqrt{(n_1 - 1)(\Delta x)^2 + (n_2 - 1)(\Delta y)^2}} \sqrt{\frac{n_1 n_2 (n_1 + n_2 - 2)}{n_1 + n_2}}, \tag{7.7.1}$$

with $\bar{x}$ and $\bar{y}$ denoting the mean values, n_1 and n_2 are the numbers of data points, and Δx and Δy are the *empirical variances* of the data sets X and Y, respectively. With $m = n_1 + n_2 - 1$ and a chosen α*-confidence interval*, the critical t-value $t_{\alpha,m}$ can be found according to a so-called

respectively, were used in stead of "standard spherical" and "interaural spherical" coordiante system.

t-distribution. The means of the two data series are said to be significantly different, if

$$|t| > t_{\alpha,m} \,. \tag{7.7.2}$$

This statement is subject to an error probability of α. For example, for $\alpha = 0{,}05$ (as it was chosen for our tests) and if the test series consist of 100 trials, the obtained result might be wrong five times out of the 100.

Chapter 8
Results and Discussion

8.1 Introduction

In this chapter, results from the subjective experiments are summarized. As outlined in Section 7.7, results have been analysed with respect to various aspects of sound localisation. In principle, a comparison of the 3-way "OSD" system results and the "Stereo Dipole" system results is shown, as far as possible. In order to detect individual differences, results have been generally analysed for each subject separately, and overall mean values were calculated out of them.

In the following, results in terms of azimuth and elevation localisation are summarised as well as precision statistics such as correlation between judgement and target directions or average angular errors. Individual response variations emerge most clearly in the percentage of front-back reversals. A concluding discussion and proposals for potential future work is given in a closing section.

8.2 Azimuth Localisation

Figure 8.2.1 shows the relation between target azimuth and response azimuth for all presented stimuli. Error-free localisation would result in a straight line of responses along the diagonal $y = x$. Data show the overall means across all subjects as well as the individual means for each subject. As explained in Section 7.7, azimuth data were converted into interaural coordinates since the resulting cones of constant azimuth (cones of confusion) are representing the interaural differences. The plots clearly reveal a considerable widening of the range of azimuth judgements for the "OSD" system. As opposed to the "Stereo Dipole", azimuths are widely perceived correctly up to cones of constant azimuth at almost ±80°. However, moderate azimuth angles of ±20° and ±40° were generally perceived further outside. Even for targets at ±60°, the mean judgement is still slightly "pulled" outwards. For both systems, the by far largest response variation between individuals can be recognized for targets at ±80°. Targets on the median plane (cone at 0°) were almost always perceived correctly with both systems. Only a few individuals seemed to feature a slight offset towards either side. In general, responses between subjects disagreed much more with the "Stereo Dipole" system, as can be seen from the wider spread of the individual means at all azimuth angles.

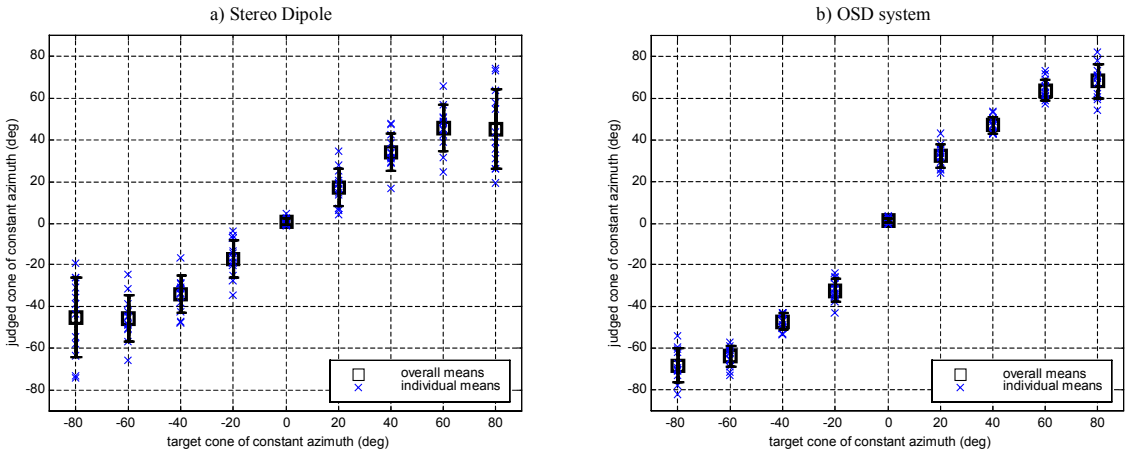

Figure 8.2.1

Mean judged source azimuth versus target source azimuth for all presented locations, regardless target elevation. Means are calculated both for each individual and across all individual subjects. Errorbars denote ± 1 standard deviation.

The above analysis was made for all targets, and hence only azimuth angles were considered

regardless the elevation. Unlike this, Figure 8.2.2 and Figure 8.2.3 show results of the same kind of investigations but analysed separately at four different groups of target elevation. For the sake of clearness, individual means are omitted in these graphs but the standard deviation bars give information about the interindividual response variations. The elevation range was divided in accordance with Table 7.4.1 into the following groups:

- Low: $-40° \leq \delta \leq -20°$
- Middle: $-10° \leq \delta \leq +10°$
- High: $+20° \leq \delta \leq +40°$
- Very high: $+50° \leq \delta \leq +80°$

Generally, results from these charts look fairly similar compared to the overall results given in Figure 8.2.1. The wider azimuth range with the "OSD" system is obtained at all elevations as well as the slightly exaggerated judgements for moderate azimuth targets. Biased azimuth estimations around the median plane, as mentioned above, seem to occur mainly for very high elevated targets. Larger interindividual differences with the "Stereo Dipole", as seen above, emerge here also at all target elevations.

Concluding, it can be stated that with both investigated systems the azimuth localisation performance is generally independent of target elevations. In agreement with the results of the pilot study, it is shown that with the "OSD" system azimuth angles are perceived further outwards. Furthermore, the performance of azimuth judgements with "OSD" is improved not only in terms of the correctly perceived range but also in terms of more reliable estimations, as can be seen from the smaller response variation

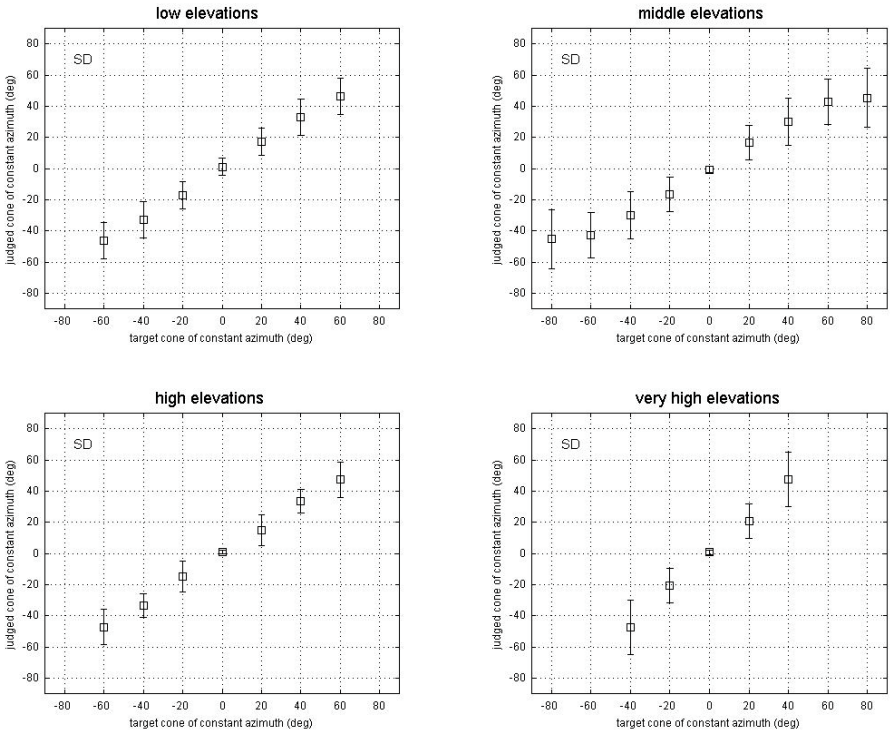

Figure 8.2.2

Mean judged azimuth versus target azimuth (as in Figure 8.2.1) for the "Stereo Dipole" system, analysed at four groups of different target elevations.

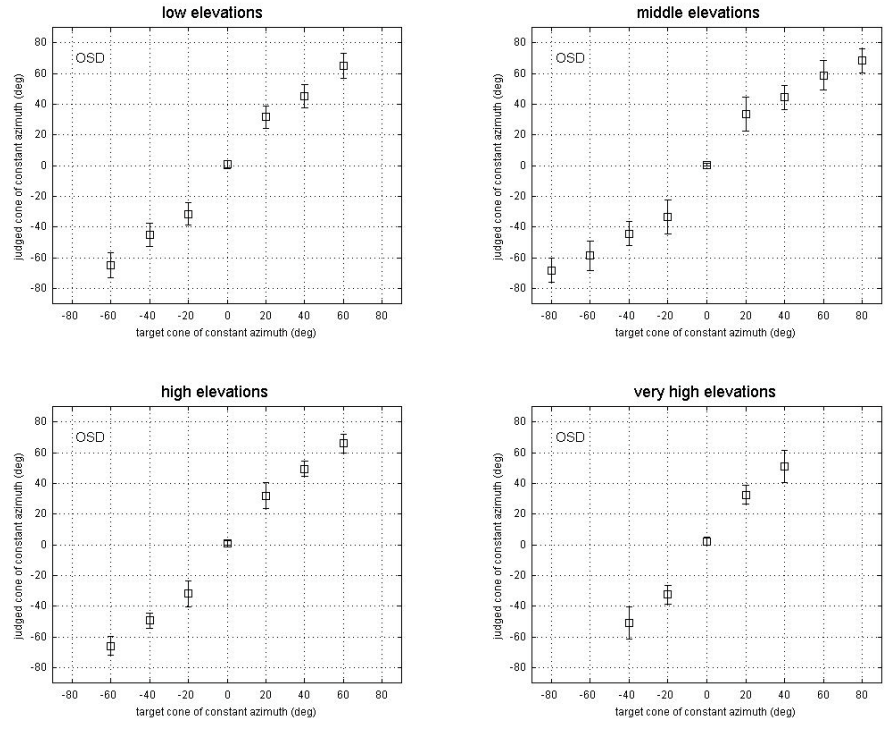

Figure 8.2.3

Same as Figure 8.2.2 but for "OSD" system.

8.3 Elevation localisation

Unlike azimuth judgements, elevation data are analysed according to the coordinate system which was used by the subjects (vertical polar coordinates). Thus, targets can be considered to be situated on several cones of constant elevation between –40° and +80°. From the way the target positions were chosen, as presented in Section 7.4, it resulted that targets situated on elevations ±30°, ±10°, +50°, and +70° were presented each only once per subject, and all of them were located well to the side as seen from the listener. A second response at a time, was merely obtained by mirroring about the median plane. Consequently, averaging of the two corresponding answers results in the single answer value available for each subject. Considering the much larger number of answers which are available at the other elevations, these results from only one answer per subject are insufficient in a statistical sense, and hence they would appear rather randomly distributed as opposed to the other data. Therefore, elevation judgements were analysed only on cones of constant elevation in 20° steps between –40° and +80°. Figure 8.3.1 shows plots of the mean judged elevations as a function of presented elevations for all targets, i.e., regardless target azimuth.

In general, performance with both systems is rather poor and there is a great deal of response variation. Therefore, removing outliers in the analysis[1], made hardly any impact, in particular not on the "Stereo Dipole" data. However, as with azimuth localisation, the mean individual responses seem to agree better for the "OSD" system, which emerges from the smaller deviation bars. Moreover, considering the range of targets between –40° and +40°, a reasonable tendency of desired elevation localisation appears for the mean values, even though the judged range is by far smaller as the target range. Within this region, subjects also seem being able to detect the difference between up and down elevations. In contrast to this, responses with the "Stereo Dipole" generally seem to be biased towards positive elevations. The tendency which can be noticed for the "OSD" data, does not appear that consistently in the "Stereo Dipole" plot. With both systems, targets higher than 40° can not be traced at all. In fact, the mean judged elevation decreases down to horizontal level.

[1] Outliers outside ± 2 standard deviations were removed by the analysis algorithm.

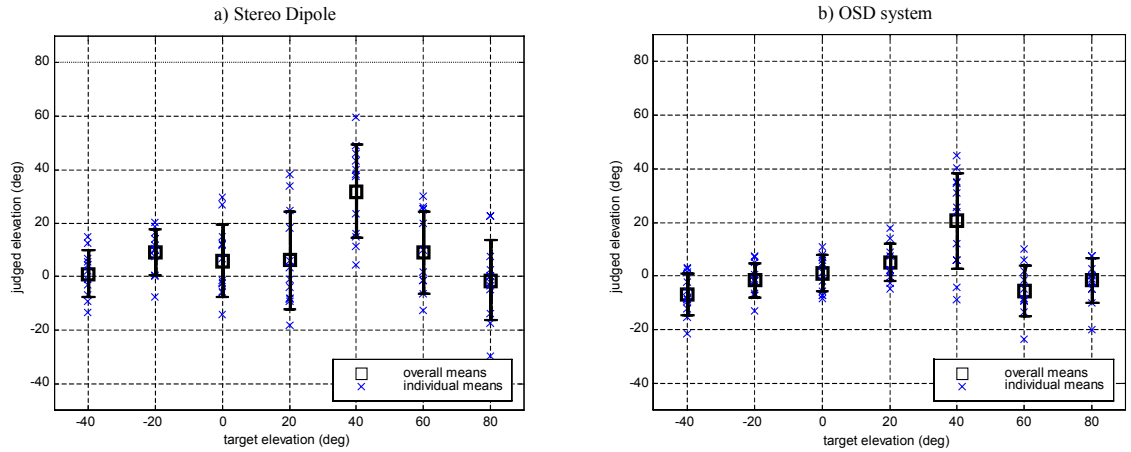

Figure 8.3.1

Mean judged source elevation versus target source elevation for all presented locations, regardless target azimuth. Means are calculated both for each individual and across all individual subjects (outliers outside removed). Errorbars denote ± 1 standard deviation.

This breakpoint at 40° elevation could be the result of the "*pinna notch*" feature disappearing from the HRTF spectrum at higher elevations (see Figure 2.9.2 [b]). Despite the extremely large response variation, it appears that there is a useful elevation cue in the 40° targets that is not present at other elevations. This may explain the exceeding mean judgement compared with the other targets. For some subjects, however, the cue due to the pinna notch might get lost at lower elevations already.

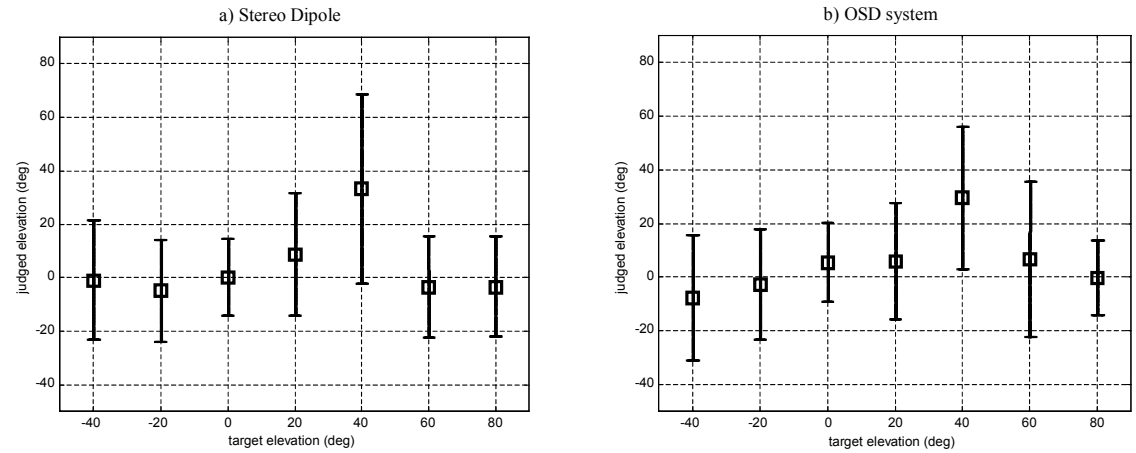

Figure 8.3.2

Mean judged elevation versus target elevation for median plane targets only.

Unlike above, azimuth targets are also taken into account in the following analysis of elevation localisation. Figure 8.3.2 shows the same elevation plots as Figure 8.3.1, but for median target locations only. Because the synthesis HRTFs are perfectly symmetric, medial targets yield identical left and right binaural stimuli. Even though the signals reaching the ears may not be identical because of asymmetries in the transmission paths from the loudspeakers to the ears, medial targets only encode a monophonic spectral cue for elevation localisation. Because there are only two medial locations per elevation (one in the frontal hemisphere and one in the corresponding back), no individual means are shown.

Again, with both systems, the mean judgements seem to be generally clustered near 0° elevations, except for 40° targets. Compared to the above plots, targets at 40° elevation gave even higher judgements. This suggests that the KEMAR HRTFs are more natural in terms of monophonic spectral cues at these targets. The elevation bias with "Stereo Dipole", which appears for the mean judgements, is not seen for medial targets. Hence, apart from judgements at -40° elevation in the left plot, an acceptable tendency for targets up to 40° can be noticed with both systems.

Figure 8.3.3 shows the results where elevation localisation is analysed for side targets exclusively, i.e., left and right targets with azimuth angles between ±45° and ±135°. Positive and negative elevations, respectively, are well distinguished with "OSD", subject to a slight positive bias. Such a bias was already seen for the overall elevation judgements in Figure 8.3.1 with the "Stereo Dipole". Considering the results for median plane targets and side

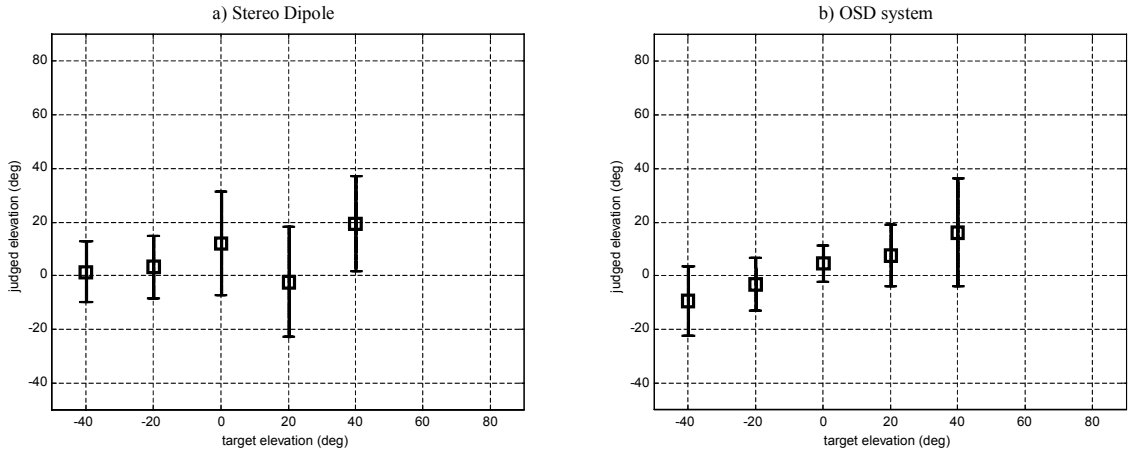

targets, respectively, this bias appears to be attributed to the side targets.

Figure 8.3.3

Mean judged elevation versus target elevation for side targets only ($45° < |\delta| < 135°$).

The plots in Figure 8.3.4 and Figure 8.3.5, respectively, show results from elevation judgements depending on from which hemisphere of the audible space (front or back) the targets were presented. Obviously, the overall performance of elevation localisation is degraded considerably by responses corresponding to targets in the rear hemisphere. Apart from 40° targets, most mean judgements for rear targets are consistently around zero elevation for "OSD". "Stereo Dipole" responses for rear targets below 40° would even suggest the existence of up-down reversals. Exceptionally high judgements at 40° elevation for both frontal and rear targets, are another evidence for superior spectral cues inherent in these targets.

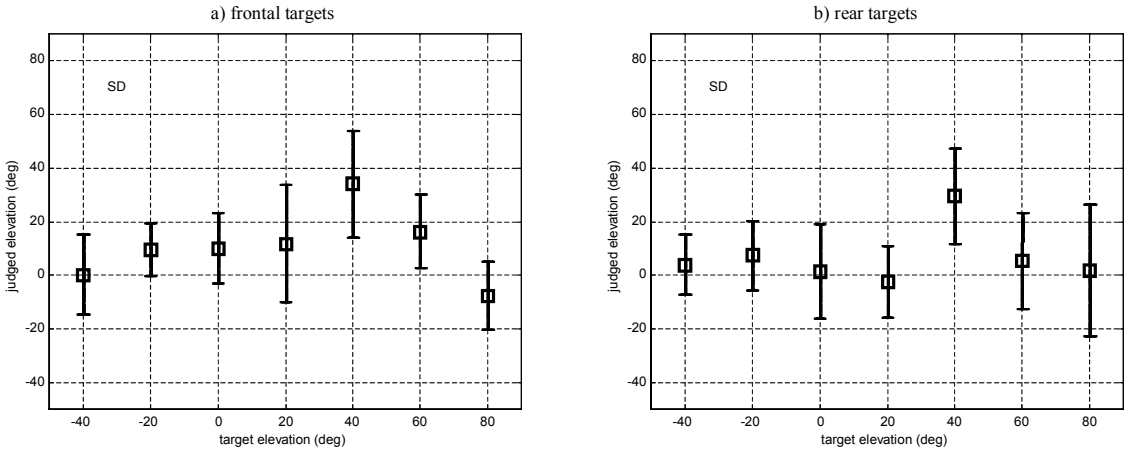

Figure 8.3.4

Mean judged elevation versus target elevations for the "Stereo Dipole" system. Analysed for [a] frontal targets only and [b] for rear targets.

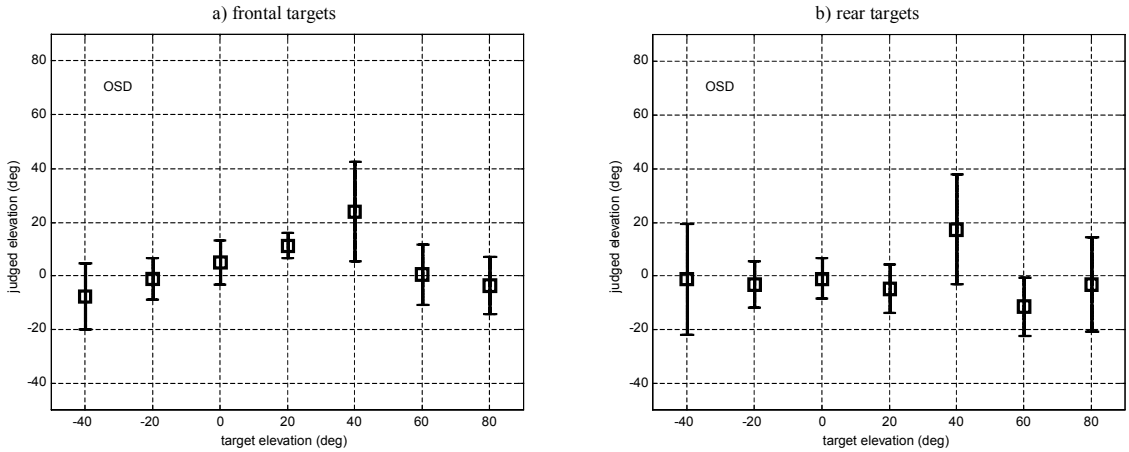

Figure 8.3.5

Same plot as in Figure 8.3.4 but for the "OSD" system.

8.4 Angular Error Statistic

The average angular errors for each individual subject, as defined in Section 7.7, are given in bar chart form in Figure 8.4.1. Clearly, it is shown that the mean error angle is decreased from 37,7° for "Stereo Dipole" to 32,4° for "OSD". Furthermore, this decrease was obtained for all individuals apart from subject 12. The t-test statistics of the data yield the following results:

$$t = 2{,}879 \qquad t_{\alpha,m} = 2{,}074$$

Consequently, the differences between the means of the average angular errors are significant for a $\alpha = 0{,}05$ confidence interval. Note that all following t-tests were made with $\alpha = 0{,}05$.

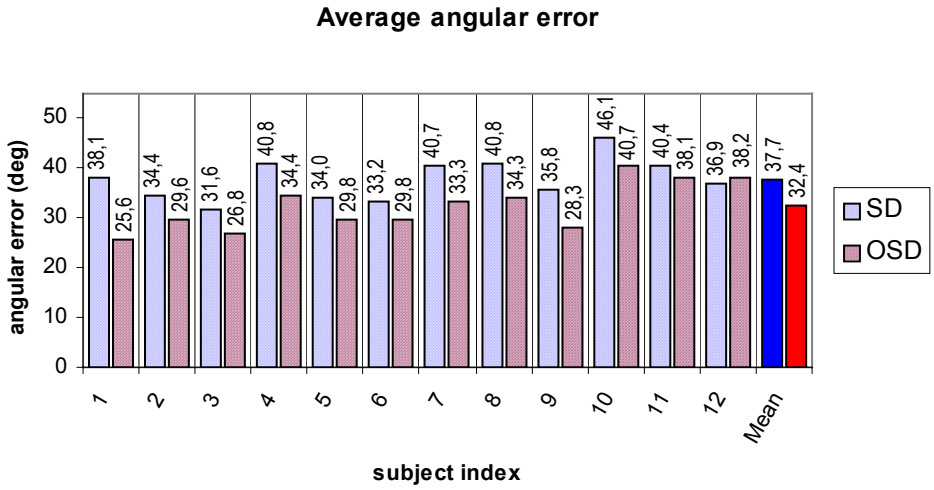

Figure 8.4.1
Global results of the average angular errors.

While above analysis represents the angular error averaged over all presented targets, it's worth having a closer look by analysing the errors for separate regions of auditory space. These regions were defined in accordance with Table 7.4.1: target azimuths were divided into front, side (left and right were combined), and rear quadrants; elevation groups (low, middle, high, and very high) were chosen as shown in Section 8.2. Table 8.4.1 summarises the regional results for the average error angle.

	Subject	Low		Middle		High		Very high	
		SD	OSD	SD	OSD	SD	OSD	SD	OSD
Front	1	35,06	18,45	9,08	13,00	20,47	20,84	61,70	61,44
	2	45,19	33,28	32,59	18,32	31,08	9,58	43,90	65,38
	3	49,73	28,47	25,26	26,59	22,61	18,20	45,11	56,59
	4	24,84	34,43	4,00	26,46	24,69	15,65	61,89	72,72
	5	38,38	30,89	16,44	7,52	20,49	23,76	69,03	71,74
	6	54,11	60,77	32,30	21,38	22,76	13,59	35,30	28,26
	7	53,57	29,91	12,00	11,93	34,15	25,82	43,07	67,03
	8	31,71	30,30	14,91	18,96	21,24	32,95	64,77	63,89
	9	23,37	22,76	16,09	14,39	19,63	16,34	59,28	72,26
	10	41,21	26,73	21,29	23,12	31,80	28,90	58,90	67,64
	11	37,98	27,09	17,65	34,39	27,94	44,23	64,18	76,26
	12	31,86	20,34	25,52	25,63	43,38	50,20	88,66	51,79
	Mean	**38,92**	**30,28**	**18,93**	**20,14**	**26,69**	**25,00**	**57,98**	**62,92**
	t	**2,01**		**0,36**		**0,41**		**0,88**	
	$t_{\alpha,m}$	**2,07**		**2,07**		**2,10**		**2,07**	
Side	1	47,62	27,48	36,77	15,41	38,32	17,99	42,24	29,14
	2	48,99	38,22	32,94	15,53	25,20	19,12	37,48	50,34
	3	56,07	43,54	25,26	8,96	17,90	13,97	23,44	25,49
	4	33,07	26,36	52,98	28,68	42,68	16,49	88,12	38,08
	5	41,53	22,58	29,05	15,26	31,61	31,32	56,64	53,04
	6	36,13	34,43	16,59	18,60	21,97	13,83	38,73	40,15
	7	41,44	38,04	51,19	24,63	26,19	18,01	24,69	58,28
	8	48,67	25,01	47,49	21,90	56,64	38,26	70,83	43,06
	9	43,99	27,14	39,77	24,36	35,18	22,47	73,98	55,38
	10	54,68	33,76	51,10	37,54	57,02	45,09	70,99	82,62
	11	42,93	29,37	53,85	15,21	24,29	39,03	48,24	60,05
	12	27,13	39,45	24,72	25,20	42,33	35,26	61,72	84,19
	Mean	**43,52**	**32,12**	**38,48**	**20,94**	**34,94**	**25,90**	**53,09**	**51,65**
	t	**3,65**		**4,05**		**1,83**		**0,18**	
	$t_{\alpha,m}$	**2,08**		**2,10**		**2,07**		**2,07**	
Back	1	51,77	22,72	19,97	28,26	35,67	28,43	81,49	72,50
	2	22,06	30,31	18,47	16,65	33,21	26,48	47,70	87,60
	3	29,87	20,18	24,88	17,90	17,52	31,59	47,01	70,47
	4	32,43	35,65	53,36	32,97	27,15	36,93	88,81	77,86
	5	35,10	30,85	12,77	15,97	20,54	30,17	75,64	74,01
	6	75,45	55,78	17,72	19,24	19,91	24,44	42,85	36,25
	7	58,52	19,12	11,19	28,58	44,58	40,38	65,25	95,19
	8	26,14	25,50	16,47	25,21	34,67	47,57	69,29	78,36
	9	41,35	38,37	15,64	14,96	33,79	19,20	45,56	54,91
	10	51,40	32,99	22,83	27,32	36,32	46,89	51,14	81,22
	11	59,80	49,72	33,80	39,02	18,99	37,91	73,06	55,80
	12	28,93	26,72	23,11	33,47	34,10	39,27	58,49	68,52
	Mean	**42,74**	**32,33**	**22,52**	**24,96**	**29,70**	**34,10**	**62,19**	**71,06**
	t	**1,80**		**0,61**		**1,23**		**1,38**	
	$t_{\alpha,m}$	**2,09**		**2,09**		**2,07**		**2,07**	

Table 8.4.1

Regional results of the average angular errors (in degrees).

Generally, the errors analysed over all targets appear fairly large because the angular errors are dominated by poor elevation judgements, as seen in the Section 8.3. Consequently, the errors are expected to be smaller at moderate target elevations, which is proven true in Table 8.4.1 by the results for targets in the "middle" elevation regions. In fact, for frontal targets with middle elevations, the result for the "Stereo Dipole" appears smallest (that particular result represents the smallest of all regions), whereas for rear targets the "OSD" result is slightly smaller. However, both differences have not proven significant as seen in the *t*-values. Errors across all side targets are generally seen smaller for the "OSD" system, which has obviously to be attributed to the superior azimuth estimations. For higher elevations on the side, differences in errors appear to be a random result, which is not surprising considering the poor elevation localisation with both systems. For frontal targets, only the "low" elevation region emerges considerable differences, where the OSD yields better results. The same can be observed for rear targets. In both cases, however, differences in the means just do not pass the significance test. At most of the other elevation regions in front and behind, smaller error angles are actually calculated for the "Stereo Dipole" system, but none of these results are significant. Generally, localisation precision appears to be worse for rear targets. With "Stereo Dipole", however, precision is even poorer for side targets because of the confined azimuth performance.

Correlations between target and judged source locations, both in terms of azimuth and elevation, are shown in Figure 8.4.2 and Figure 8.4.3, respectively. The azimuth correlations are fairly good with both systems, but a slight increase with "OSD" can still be detected for most subjects. However, this increase results just not being significant as seen from the t-test analysis:

$$t = 1{,}955 \qquad t_{\alpha,m} = 2{,}074$$

It is remarkable that those subjects in particular who performed rather poor with the "Stereo Dipole" system, improved considerably with the "OSD" system such that their azimuth correlation factors do not differ any more from the majority's.

As expected from the results in Section 8.3, elevation correlation is seen to be very poor for

all subjects even though many improved with "OSD". The t-test results

$$t = 1{,}144 \qquad t_{\alpha,m} = 2{,}074$$

show that this improvement is far from being significant, which is not surprising considering the large response variation for elevation judgements.

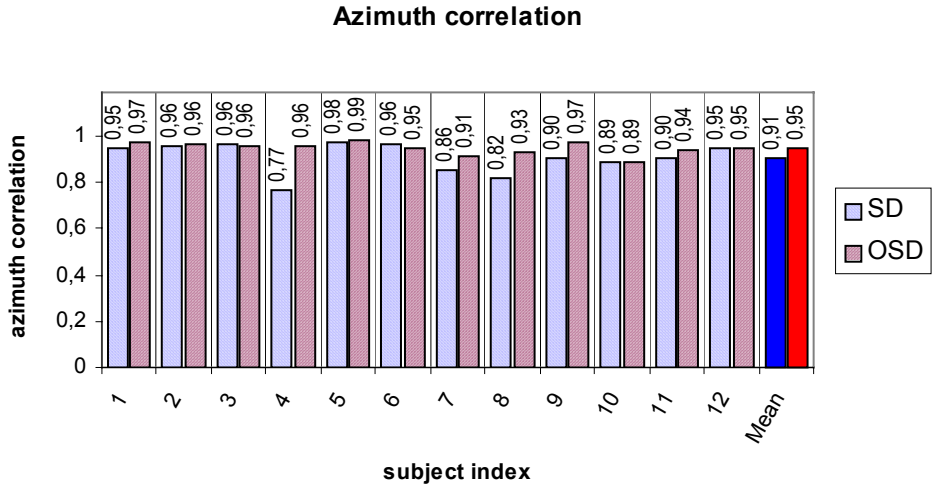

Figure 8.4.2

Individual and mean correlation between judged azimuth angles and target azimuth angles.

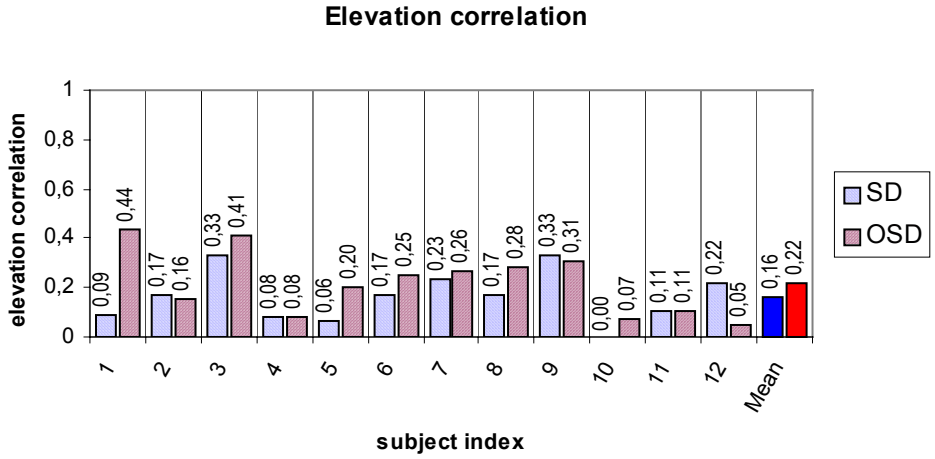

Figure 8.4.3

Individual and mean correlation between judged elevation angles and target elevation angles.

8.5 Front-Back Reversals

Bargraphs of the individual percentages of back → front reversals and front → back reversals for all presented locations are given in Figure 8.5.1 and Figure 8.5.2, respectively. The pattern of the reversals is seen to be very specific to the individual subject. Therefore, both the improvement in terms of back → front reversals with "OSD" as well as better performance for front → back reversals with the “Stereo Dipole” have to be considered not being significant. Results from the corresponding t-tests are:

- back → front reversals: $t = 1{,}387$ $t_{\alpha,m} = 2{,}074$
- front → back reversals: $t = 0{,}635$ $t_{\alpha,m} = 2{,}074$

Subjects No.4, 5, 9, and 11, for example, show very high rates of back → front reversals. On the other hand, these subjects reversed almost never from front to the back, which indicates that they hardly perceived any rear images and therefore reverse practically always to the front. For subjects 4 and 11, this propensity to perceive in the front seems to be disappeared with "OSD", as seen from the significant decrease of back → front reversals while increasing front → back reversals. For subjects 5 and 9, on the other hand, no remarkable change was achieved in terms of reversals. This may be the result of extremely large frequency discrepancies between the HRTFs of these subject's compared to the synthesis HRTFs. Subject No.10 shows a clear preference to perceive in the rear, which was only slightly reduced with "OSD". Subjects No.1, 2,3, 6, 7, and 12 performed always fairly good in terms of reversals to either side. Apart from subject 12, all of them increased their performance in terms of back → front reversals slightly while the front → back reversal rate was decreased with "OSD".

Data summarised in Table 8.5.1 and Table 8.5.2, respectively, are developed from separate counts of reversals for each region of target locations. Reversal percentages to either side are generally seen lower for side targets. This might be explained, considering that interaural differences are larger for side targets. Consequently, the interaural transfer functions for side

targets may provide stronger spectral cues to disambiguate frontal from rear source locations.

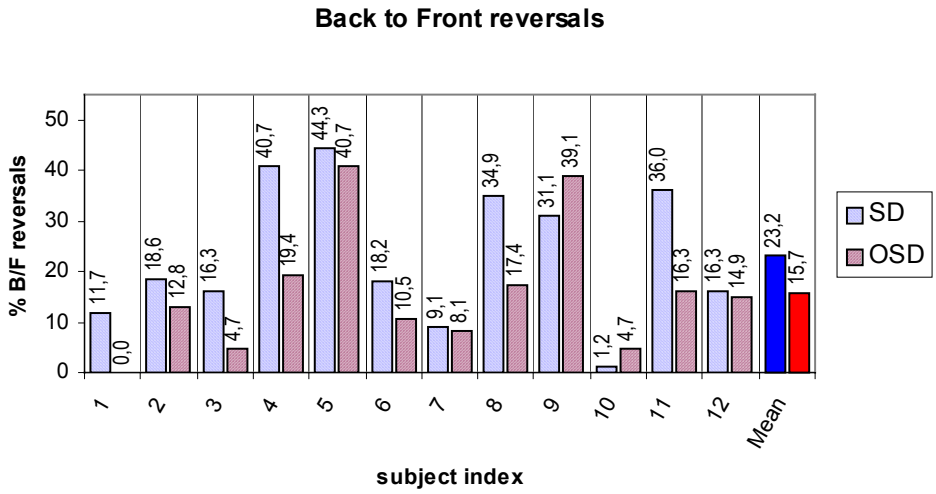

Figure 8.5.1

Percentage of back → front reversal for all presented locations.

	Subject	Low		Middle		High		Very high	
		SD	OSD	SD	OSD	SD	OSD	SD	OSD
Side	1	0	0	11,11	0	40	0	0	0
	2	40	20	16,67	16,67	20	20	0	0
	3	20	20	0	0	20	20	0	0
	4	40	20	33,33	16,67	40	20	0	0
	5	40	40	33,33	16,67	40	40	0	0
	6	20	20	16,67	16,67	16,67	20	0	0
	7	20	0	0	16,67	0	20	0	0
	8	40	20	33,33	33,33	40	40	0	0
	9	40	40	16,67	16,67	40	40	0	0
	10	0	0	0	0	0	0	0	0
	11	20	0	16,67	0	40	0	0	0
	12	20	20	16,67	0	20	20	0	0
	Mean	**25**	**16,67**	**16,2**	**11,11**	**26,39**	**20**	**0**	**0**
Back	1	12,5	0	0	0	50	0	0	0
	2	12,5	50	40	0	25	0	75	25
	3	50	0	40	0	50	0	0	0
	4	87,5	62,5	100	40	87,5	22,22	100	42,86
	5	100	100	100	100	100	100	100	100
	6	50	0	40	40	25	0	50	25
	7	40	25	0	0	25	0	0	25
	8	87,5	0	100	80	50	0	50	25
	9	75	87,5	100	100	33,33	88,89	75	100
	10	12,5	0	0	40	0	25	0	0
	11	100	50	60	60	100	62,5	100	50
	12	50	25	0	40	25	25	50	60
	Mean	**56,46**	**33,33**	**48,33**	**41,67**	**47,57**	**26,97**	**50**	**37,74**

Table 8.5.1

Regional percentage of back → front reversals.

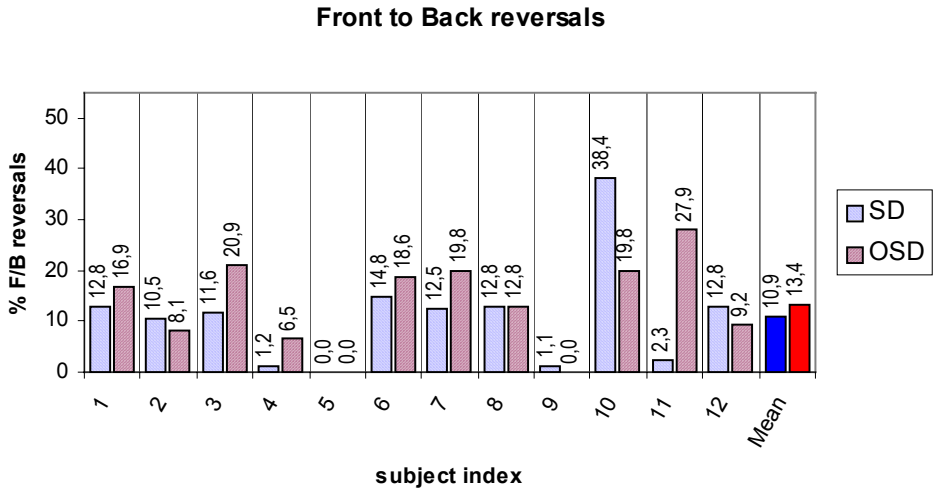

Figure 8.5.2

Percentage of front → back reversal for all presented locations.

	Subject	Low		Middle		High		Very high	
		SD	OSD	SD	OSD	SD	OSD	SD	OSD
Front	1	25	27,27	16,67	40	11,11	0	50	0
	2	37,5	37,5	0	0	25	12,5	0	25
	3	12,5	25	0	40	12,5	50	50	100
	4	0	25	0	0	0	0	25	0
	5	0	0	0	0	0	0	0	0
	6	37,5	37,5	0	0	37,5	50	25	25
	7	12,5	25	0	40	37,5	25	75	75
	8	50	12,5	0	40	50	50	25	100
	9	12,5	0	0	0	0	0	0	0
	10	25	0	40	0	87,5	37,5	100	100
	11	0	50	0	40	0	25	0	50
	12	25	25	40	0	25	25	25	0
	Mean	**19,79**	**22,06**	**8,06**	**16,67**	**23,84**	**22,92**	**31,25**	**39,58**
Side	1	20	40	11,11	16,67	20	20	0	50
	2	20	0	0	0	20	20	0	0
	3	20	20	16,67	16,67	20	20	0	0
	4	0	0	0	16,67	0	20	0	0
	5	0	0	0	0	0	0	0	0
	6	20	20	0	16,67	16,67	20	50	50
	7	20	20	16,67	16,67	0	40	0	0
	8	0	0	0	0	0	0	50	0
	9	0	0	0	0	0	0	0	0
	10	60	20	33,33	16,67	40	40	100	50
	11	0	40	16,67	33,33	0	40	0	50
	12	0	0	16,67	16,67	20	20	0	0
	Mean	**13,33**	**13,33**	**9,26**	**12,50**	**11,39**	**20**	**16,67**	**16,67**

Table 8.5.2

Regional percentage of front → back reversals.

It is remarkable that for very high elevations on the side, none of the subjects reversed to the front while some located frontal targets in the rear. However, considering that only a few targets corresponding to this region were actually presented, this result should be handled with care. With both systems, highest reversal rates resulted for rear targets at all elevations, which were located at the front. Subjects who perceive preferably at the front seem to be more common and they make their judgements more consistently. This is seen from some subjects who show 100% back → front reversals for almost all target elevations around the median plane. Despite some weak indications, due to the large individual variations related to reversals, it is fairly difficult to trace a significant difference between the investigated systems.

8.6 Concluding Remarks

This study has discussed how loudspeaker binaural audio systems can be practically implemented as "multi-way" systems. Such systems are referred to as "Optimal Source Distribution", or "OSD" systems. It was shown that such systems are well-behaving in terms of acoustic transmission path inversion (crosstalk cancellation) over a wide frequency range. As a consequence, "OSD" systems are capable to create very convincing virtual images in a 3D listening space. Results of subjective sound localisation experiments confirmed some remarkable improvements compared to a conventional "Stereo Dipole" system, which uses a pair of closely spaced transducers over the whole reproduced frequency range. The most significant improvement is seen as a respectable widening of the range of perceived azimuth angles towards lateral source locations. While cones of confusions at azimuth angles within approximately ± 45° were recognised reasonably well with the "Stereo Dipole" system, the "OSD" system yielded a range of almost ± 70°.

Moreover, obtained results generally appear more reliable with the "OSD" system, considering the much smaller response variation between subjects. This was also seen for elevation judgements, even though performance in terms of elevation localisation was rather

poor for both systems. In general, elevation localisation is difficult to test due to the large variation in the responses, contrary to azimuth localisation. It is known from experiments with real sound sources that the just noticeable difference (JND) of elevation is relatively large [Blauert, 1997]. Never the less, for target elevations within ± 40°, reasonably consistent results for the "OSD" system still suggest improved accuracy of elevation localisation.

Average angular error calculations can be considered as an analysis of localisation precision in a three-dimensional sense. Over all presented target locations, this performance was significantly improved with the "OSD" system. However, separate investigations for particular regions of the listening space reveal that this improvement is mainly attributed to the better performance for side targets. For targets close to the median plane (frontal and rear), no significant differences in terms of error angles could be found.

The percentage of front-reversals is seen as being very specific to the individual subject. Therefore, significant differences between the two systems must be considered influenced by other factors, such as match of synthesis HRTFs with the subjects HRTFs.

A procedural disadvantage of the localisation tests might be the fact that all target locations were presented only once per subject with each system. As a consequence, response variation was fairly large which makes it difficult in some cases to draw reliable conclusions out of the results. With the hypothesis that interindividual variance is generally larger than intraindividual variance, this lack of reproducibility could have had alleviated. Considering time schedules for the experiments, the experimenter had accept this compromise. Otherwise, less targets had to be presented if one wants to avoid increasing the duration of the test sessions.

Objectives for future work in this area could be to test more practical systems. Since virtual acoustic systems based on binaural reproduction are still fairly sensitive to listener position, a major application of them is in the field of desktop applications, such as computers, video games, or cars. Hence, a 3-way system as it was designed here, (with low-frequency speakers span of 180°) will not be practically for many of those applications. Consequently, systems which require less space appear to be of more interest. This could be realised in 2-way or in 3-way with smaller loudspeaker span for the woofers. According to Takeuchi and Nelson [2000a; 2000b], in theory the woofer span could be considerably reduced without remarkable changes of the low-frequency limit with crosstalk cancellation (see Section 5.8).

Another challenge will be to realise transducers, which in reality change their span as a function of frequency. As proposed by Takeuchi and Nelson [2000a], this might, for example, be realised by exciting a triangular shaped plate whose width varies along its length. The requirement of such a transducer is that a certain frequency of vibration is excited most at a particular position having a certain width such that sound of that frequency is radiated mostly from that position.

Bibliography

AES (1986), edited by Eargle, J.M., *Stereophonic Techniques*, The Audio Engineering Society, New York, 1986.

Atal, B.S., M. Hill, M.R. Schroeder (1966), *Apparent Sound Source Translator*, United States Patent Office, No. 3,236,949 (22 February 1966).

Bauck, J.L., and D.H. Cooper (1996), *Generalised Transaural Stereo and Applications*, J. Audio Eng. Soc., Vol. 44, No. 9, pp. 683-705.

Bauer, B.B. (1961), *Stereophonic Earphones and Binaural Loudspeakers*, J. Audio Eng. Soc., Vol. 9, No.2, pp. 148-151.

Begault, D.R. (1992), *Perceptual Effects of Synthetic Reverberation on Three-Dimensional Audio Systems*, J. Audio Eng. Soc., Vol. 40, pp. 895-904.

Begault, D.R. (1994), *3-D Sound for Virtual Reality and Multimedia*, Academic Press Professional, ISBN 0-12-084735-3.

Berkhout, A.J., D. de Vries, P. Vogel (1993), *Acoustic Control by Wave Field Synthesis*, J. Acoust. Soc. of Am., No. 5, pp. 2764-2778.

Blauert, J. (1997), *Spatial Hearing: The Psychophysics of Human Sound Localisation*, MIT Press, ISBN 0-262-02413-6.

Boone, M.M., E. Verheijen, P. Tol (1995), *Spatial Sound Field Reproduction by Wave Field Synthesis*, J. Audio Eng. Soc., Vol. 43, No. 12, pp. 1003-1012.

Bronstein, I.N., and K.A. Semendjajew (1996), *Teubner-Taschenbuch der Mathematik*, B.G. Teubner, Stuttgart, ISBN 3-8154-2001-6.

Colloms, M., (1997), *High Performance Loudspeakers*, 5th edition, John Wiley & Sons.

Cooper, D.H., and J.L. Bauck (1989), *Prospects for transaural recording*, J. Audio Eng. Soc., Vol. 37, No.1/2, pp. 3-19.

Damaske, P. (1971), *Head-Related Two-Channel Stereophony with Loudspeaker Reproduction*, J. Acoust. Soc. of Am., Vol. 50, No. 4, pp. 1109-1115.

Duda, R.O. (1996), *3-D Audio for Human Computer Interface*, San Jose State University, <http://www-engr.sjsu.edu/~knapp/HCIROD3D/3D_home.htm>.

Gardner, W.G., and K.D. Martin (1994), *HRTF Measurements of a KEMAR Dummy-Head Microphone*, M.I.T. Media Lab, Perceptual Computing Section, Technical Report No. 280. <http://sound.media.mit.edu/KEMAR.html>

Gardner, W.G. (1997), *3-D Audio Using Loudspeakers*, PhD dissertation, M.I.T. Media Lab.

Griesinger, D. (1989), *Equalisation and Spatial Equalisation of Dummy-Head Recordings for Loudspeaker Reproduction*, J. Audio Eng. Soc., Vol. 37, No.1/2, pp. 20-29.

Hartmann, W.M. (1997), *Listening in a Room and the Precedence Effect*, in *Binaural and Spatial Hearing in Real and Virtual Environments*, ed. R.H. Gilkey and T.R. Anderson, Lawrence, Erlbaum Associates, ISBN 0-8058-1654-2.

Heegaard, F.D. (1992), *The Reproduction of Sound in Auditory Perspective and a*

Compatible System of Stereophony, EBU Rev., Pt. A-Technical, No. 50, pp. 2-6 (1958 Dec.); reprinted in J. Audio Eng. Soc., Vol. 40, No. 10, pp. 802-808.

Kirkeby, O., P.A. Nelson, H. Hamada, F. Orduña-Bustamente (1996a), *Fast Deconvolution of Multi-Channel Systems using Regularisation*, ISVR Technical Report, No. 255, Institute of Sound and Vibration Research, University of Southampton.

Kirkeby, O., P.A. Nelson, H. Hamada (1996b), *"Stereo Dipole"*, British Patent Application, No. 9603236.2

Kirkeby, O., P.A. Nelson, H. Hamada (1997), *The "Stereo Dipole" - Binaural Sound Reproduction using two closely spaced Loudspeakers*, presented at the 102nd Audio Engineering Society Convention, 22-25 March 1997, Munich, Germany, AES preprint 4463 (I6). Also published in J. Audio Eng. Soc., Vol. 46, No. 5, pp. 387-395 (1998).

Kirkeby, O., and P.A. Nelson (1997), *Virtual Source Imaging using the "Stereo Dipole"*, presented at the 103rd Audio Engineering Society Convention, 26-29 September 1997, New York, AES preprint 4574 (J10).

Kirkeby, O., P.A. Nelson, H. Hamada (1998), *Local Sound Field Reproduction using two closely spaced Loudspeakers*, J. Acoust. Soc. of Am., Vol. 104, No. 4, pp. 1973-1981.

Kleiner, M. (1978), *Problems in the design and use of "dummy heads"*, Acustica, Vol. 41, pp. 183-193.

Kreyszig, E. (1983), *Advanced Engineering Mathematics*, John Wiley and Sons.

Møller, H. (1989), *Reproduction of Artificial-Head Recordings through Loudspeakers*, J. Audio Eng. Soc., Vol. 37, No.1/2, pp. 30-33.

Møller, H. (1992), *Fundamentals of Binaural Technology*, Applied Acoustics, Vol. 36, 1992, pp. 171-218

Møller, H., C.B. Jensen, D. Hammershøi, M.F. Sørensen (1997), *Evaluation of artificial heads in listening tests*, presented at the 102nd Audio Engineering Society Convention, 22-25 March 1997, Munich, Germany, AES preprint 4404 (A1).

Nelson, P.A., and S.J. Elliott (1992), *Active Control of Sound*, Academic Press, London, ISBN 0-12-515426-7.

Nelson, P.A., H. Hamada, S.J. Elliott (1992), *Adaptive Inverse Filters for Stereophonic Sound Reproduction*, IEEE Trans. Signal Process., Vol. 40, No. 7, pp. 1621-1632.

Nelson, P.A., F. Orduña-Bustamente, H. Hamada (1995), *Inverse Filter Design and Equalisation Zones in Multi-Channel Sound Reproduction*, IEEE Trans. Speech Audio Process., Vol. 3, No. 3, pp. 185-192.

Nelson, P.A., and F. Orduña-Bustamente (1996), *Multi-Channel Signal Processing Techniques in the Reproduction of Sound*, J. Audio Eng. Soc. Vol. 44, pp. 973-989.

Nelson, P.A., O. Kirkeby, T. Takeuchi, H. Hamada (1997), *Sound Fields for the Production of Virtual Acoustic Images*, J. Sound. Vib., Vol. 204, No. 2, pp. 386-396.

Oppenheim A.V., and R.W. Schafer (1975), *Digital Signal Processing*, Prentice-Hall Inc., Englewood Cliffs, NJ, ISBN 0-13-214635-5.

Pierce, A.D. (1981), *Acoustics. An Introduction to its Physical Principles and Applications*, McGraw-Hill, New York.

Press, W.H., S.A. Teukolsky, W.T. Vetterling, B.P. Flannery (1992), *Numerical Recipes in C*, Second edition, Cambridge University Press.

Proakis, J.G., and D.G. Manolakis (1996), *Digital Signal Processing-Principles, Algorithms, and Applications*, 3rd ed. Prentice-Hall Inc., Englewood Cliffs, NJ, ISBN 0-13-394289-9.

Pulkki, V. (1997), *Virtual Sound Source Positioning Using Vector Base Amplitude Panning*, J. Audio Eng. Soc., Vol. 45, No. 6, pp. 944-951.

Rife, D.D., and J.Vanderkooy (1989), *Transfer-Function Measurements using Maximum Length Sequences*, J. Audio Eng. Soc., Vol. 37, No. 6, pp. 419-444.

Rife, D.D. (1994), *Maximum Length Sequence System Analyser (MLSSA), Reference Manual, Version 9.0*, DRA Laboratories.

Schroeder, M.R., and B.S. Atal (1963), *Computer Simulation of Sound Transmission in Rooms*, IEEE Int. Conv. Record, 7, pp. 150-155.

Schroeder, M.R. (1975), *Models of Hearing*, Proceedings of the IEEE, Vol. 63, No. 9, pp. 1332-1352.

Takeuchi, T., P.A. Nelson, O. Kirkeby, H. Hamada (1997), *Robustness of the performance of the "Stereo Dipole" to misalignment of head position*, presented at the 102nd Audio Engineering Society Convention, 22-25 March 1997, Munich, Germany, AES preprint 4464 (I7).

Takeuchi, T., P.A. Nelson, O. Kirkeby, H. Hamada (1998), *Influence of Individual Head Related Transfer Functions on the Performance of Virtual Acoustic Imaging Systems*, 104th Audio Engineering Society Convention, AES preprint 4700 (P4-3).

Takeuchi, T., and P.A. Nelson (2000a), *Optimal Source Distribution for Virtual Acoustic Imaging*, British Patent application, No. 0015419.5

Takeuchi, T., and P.A. Nelson (2000b), *Optimal Source Distribution for Virtual Acoustic Imaging*, ISVR Technical Report, No. 288, Institute of Sound and Vibration Research, University of Southampton.

Vanderkooy, J. (1994), *Aspects of MLS Measuring Systems*, J. Audio Eng. Soc., Vol. 42, No. 4, pp. 219-231.

Wenzel, E.M., M. Arruda, D. Kistler, F.L. Wightman (1993), *Localisation using nonindividualised Head-Related Transfer Functions*. Prentice-Hall Inc., J. Acoust. Soc. of Am., Vol. 94, No. 1, pp. 111-123.

Widrow, B., and S.D. Stearns (1985), *Adaptive Signal Processing*. Prentice-Hall Inc., Englewood Cliffs, NJ, ISBN 0-13-004029-0.

Wiener, N. (1949), *Extrapolation, Interpolation and Smoothing of Stationary Time Series with Engineering Applications*. Wiley, New York.

Wightman, F.L., and D.J. Kistler (1989a), *Headphone Simulation of Free-Field Listening, I: Stimulus Synthesis*, J. Acoust. Soc. of Am., Vol. 85, No. 2, pp. 858-867.

Wightman, F.L., and D.J. Kistler (1989b), *Headphone Simulation of Free-Field Listening, II: Psychophysical Validation*, J. Acoust. Soc. of Am., Vol. 85, No. 2, pp. 868-878.

Wilkinson, J.H. (1965), *The Algebraic Eigenvalue Problem*, Oxford University Press.